Spring 2017

Channel Bar Morphology, Distribution, And Mining-Related Geochemistry In The Big River, St. Francois County, Missouri: Implications For Geomorphic Recovery

Lindsay Marie Olson
Missouri State University

CHANNEL BAR MORPHOLOGY, DISTRIBUTION, AND MINING-RELATED GEOCHEMISTRY IN THE BIG RIVER, ST. FRANCOIS COUNTY, MISSOURI: IMPLICATIONS FOR GEOMORPHIC RECOVERY

A Masters Thesis

Presented to

The Graduate College of

Missouri State University

In Partial Fulfillment

Of the Requirements for the Degree

Master of Science, Geospatial Sciences in Geography, Geology, and Planning

By

Lindsay Marie Olson

May, 2017

CHANNEL BAR MORPHOLOGY, DISTRIBUTION, AND MINING-RELATED GEOCHEMISTRY IN THE BIG RIVER, ST. FRANCOIS COUNTY, MISSOURI: IMPLICATIONS FOR GEOMORPHIC RECOVERY

Geography, Geology, and Planning

Missouri State University, May, 2017

Master of Science

Lindsay Marie Olson

ABSTRACT

Tailings releases associated with large-scale historical Pb mining in St. Francois County, Missouri resulted in system-wide contamination of Pb and excess sediment in the Big River. Previous studies have addressed basin and segment scale variability of the contaminants; however, little is known about reach and bar scale variability. This study addresses how mining sediment inputs influence bar form and geochemistry across a range of scales. Bar sediment samples were collected at 21 reaches and analyzed for particle size and geochemistry, while air photo analysis was used to evaluate channel morphology, bar type, and area. Bar area is initially low in the upper mining region but increases with distance downstream. Bars near mining inputs are highly contaminated with Pb and decrease in contamination with distance downstream. While chat-sized mining sediment has not moved more than 60 km downstream, having attenuated or dispersed locally by moving into storage in bars or young floodplains, Pb contamination is transported further with fine sediment and is found throughout the study area. Bar sediments are well-mixed vertically; the bar head contains more Pb than the tail near mining sites. Signs of geomorphic recovery indicate that the channel is in the process of returning to equilibrium; however geochemical recovery will likely not occur for centuries. Further, if increasing trends in flooding continue, bar formation and mobility may increase in the future.

KEYWORDS: fluvial geomorphology, Missouri, lead, mining, sediment transport

This abstract is approved as to form and content

_____

Robert Pavlowsky
Chairperson, Advisory Committee
Missouri State University

CHANNEL BAR MORPHOLOGY, DISTRIBUTION, AND MINING-RELATED GEOCHEMISTRY IN THE BIG RIVER, ST. FRANCOIS COUNTY, MISSOURI: IMPLICATIONS FOR GEOMORPHIC RECOVERY

By

Lindsay Marie Olson

A Masters Thesis
Submitted to the Graduate College
Of Missouri State University
In Partial Fulfillment of the Requirements
For the Degree of Master of Science, Geospatial Sciences in Geography, Geology, and Planning

May, 2017

Approved:

_____
Robert Pavlowsky, PhD

_____
Xiaomin Qiu, PhD

_____
Jun Luo, PhD

_____
Julie Masterson, PhD: Dean, Graduate College

ACKNOWLEDGEMENTS

I would like to extend my deepest gratitude to my advisor, Dr. Bob Pavlowsky, for his guidance and support in helping me succeed in this endeavor. None of this would have been possible without you. Thanks also to my committee members, Dr. Xiaomin Qiu and Dr. Jun Luo, who offered helpful insight and ideas to expand my research and improve my writing. I am very grateful to my classmates at MSU who assisted with field data collection, particularly Megan Harrington, Anna Larkin, Andrew DeWitt, Andrea Mayus, Daniel Williams, and David Dickson. Ozarks Environmental and Water Resources Institute assistant director Marc Owen is deserving of a special thank you for continually offering insight, wisdom, guidance, and humor throughout my graduate work.

I am also very appreciative of the United States Fish and Wildlife Service for funding my field data collection and graduate research position at OEWRI through CESU Task # 301819T002, entitled "Big River Sediment Assessment Project". I also want to thank the MSU Graduate School for providing additional financial support for data collection. This research would not have been possible without your assistance.

My family and friends back in Wisconsin were a critical support system for me in accomplishing this feat. Much love and thanks goes out to Mom and Dad for having confidence in me and supporting me in many ways. I sincerely appreciate my boyfriend, Cory, who provided endless love and support as I pursued my dream while he patiently waited for me 650 miles away. Lastly, this work would not have been possible without the love and patience of my beloved feline companion, Walter, who spent countless hours warming my lap while I studied and wrote. Although he is no longer here to sit by me as I finish, I couldn't have made it this far without him.

TABLE OF CONTENTS

Chapter 1: Introduction 1

Chapter 2: Background 4
- Stream Response to Disturbance and the Recovery Process 5
- Sediment Transportation Processes 13
- Mining Sediment Impacts on Stream Morphology 20

Chapter 3: Study Area 22
- Physical Characteristics 22
- Channel and Valley Morphology 26
- Historical Land Use 28

Chapter 4: Methods 32
- Location and Description of Field Sites 32
- Field Methods 36
- Laboratory Methods 39
- Geospatial Methods 41

Chapter 5: Results and Discussion 52
- Characterization of Gravel Bars 52
- Downstream Bar Texture and Geochemical Variability 66
- Within-Bar Texture and Geochemical Variability 75
- Evidence of Geomorphic Recovery 91

Chapter 6: Conclusions 97

Literature Cited 101

Appendices 108
- Appendix A: Field Site Details 108
- Appendix B. Bar Sediment Sample Descriptions 109
- Appendix C. Pebble Count Data 112
- Appendix D. Channel Recovery Assessments 113
- Appendix E. Bar Sediment Sample Analysis 128
- Appendix F. GIS 500 m Channel Cell Analysis 133
- Appendix G. GIS 500 m Valley Cell Analysis 142

LIST OF TABLES

Table 1. Characteristics of USGS gages on the Big River. 26

Table 2. Size fractionation of metals in tailings materials. 31

Table 3. Description of the study area segments. 35

Table 4. Characteristics of aerial photographs used in the study. 42

Table 5. Digitized channel features. 45

Table 6. Characteristics of USGS gauges used for air photo corrections. 47

Table 7. Bar quantities, area, and spacing in the study area. 54

Table 8. Characteristics of gravel bars by segment. 55

Table 9. Channel bar sediment sample size distribution by segment. 78

Table 10. Distribution of fine (<2 mm) sediment by sample depth. 84

Table 11. Channel bar variation of Pb by broad segment. 88

LIST OF FIGURES

Figure 1. The five stages of channel evolution. 10

Figure 2. Simon's six-stage channel evolution model. 11

Figure 3. Comparison of 5-stage CEM to the dimensionless stability diagram. 12

Figure 4. Hjulström curve of sediment erosion, transport, and deposition velocities. 14

Figure 5. Longitudinal profile view of wave translation and dispersion. 16

Figure 6. Channel positions of common bar types in alluvial rivers. 20

Figure 7. Location of the study area within the Big River watershed. 23

Figure 8. Federal mill and mine tailings pile, ca. 1940. 29

Figure 9. Field site locations in the Big River. 33

Figure 10. Segment drainage area by river kilometer. 35

Figure 11. Bar head, middle, and tail positions of a typical point bar. 36

Figure 12. Gravelometer used in pebble counts. 37

Figure 13. Channel centerline, digitized for all photo years. 44

Figure 14. Bar, island, shelf, and channel features digitized in air photo analysis. 44

Figure 15. Relationship of active channel width to specific discharge. 48

Figure 16 Relationship of channel bar width to specific discharge. 49

Figure 17. Location and type of individual bar units. 53

Figure 18. Total bar area in each 500 m channel cell. 57

Figure 19. Side bar area in each 500 m channel cell. 57

Figure 20. Center bar area in each 500 m channel cell. 58

Figure 21. Point bar area in each 500 m channel cell. 58

Figure 22. Average valley width. 59

Figure 23. Relationship of 2007 bar width and 2007 valley width. 60

Figure 24. Relationship of 2007 bar width and historical active width. 60
Figure 25. Relationship of 2007 bar width and 2007 active channel width. 60
Figure 26. Bar area changes over time, shown as a three-point moving average. 62
Figure 27. Historical mean bar area by segment, 1937-2007. 63
Figure 28. Channel sinuosity by segment. 65
Figure 29. Bar Ca concentrations in the sand-sized (<2 mm) fraction by site average. ... 68
Figure 30. Scatter plot of bar Ca concentrations in the fine size fraction..... 68
Figure 31. Bar Pb concentrations in the fine size fraction by site average. 69
Figure 32. Scatter plot of bar Pb concentrations in the fine size fraction. 69
Figure 33. Bar Zn concentrations in the sand-sized (<2 mm) fraction by site average. ... 71
Figure 34. Scatter plot of bar Zn concentrations in the fine size fraction. 71
Figure 35. Pb:Zn ratio in the sand-sized fraction (<2 mm) of bars by site average..... 72
Figure 36. Pb:Ca ratio in the sand-sized fraction (<2 mm) of bars by site average..... 72
Figure 37. Distribution of sediment size fractions as a percent of total sample mass. 74
Figure 38. Distribution of fines by bar position. 76
Figure 39. Chat-sized sediment (4-16 mm) as a percent of sample mass. 76
Figure 40. Coarse gravel (>32 mm) as a percent of sample mass. 77
Figure 41. Average D_{16} distribution by bar position in pebble county surveys. 80
Figure 42. Average D_{50} distribution by bar position in pebble county surveys. 80
Figure 43. Average D_{84} distribution by bar position in pebble county surveys. 81
Figure 44. Percent fines (<2 mm) in surface and subsurface samples. 82
Figure 45. Percent chat-sized sediment (4-16 mm) in surface and subsurface samples... 83
Figure 46. Percent coarse sediment (>32 mm) in surface and subsurface samples. 83
Figure 47. Distribution of lead (ppm) by sample bar position. 85
Figure 48. Distribution of zinc (ppm) by sample bar position. 86

Figure 49. Distribution of calcium (ppm) by sample bar position. 87
Figure 50. Lead content (ppm) in surface and subsurface samples. 89
Figure 51. Zinc content (ppm) in surface and subsurface samples. 89
Figure 52. Calcium content (ppm) in surface and subsurface samples. 90
Figure 53. Depth to probe refusal at thalweg. 92
Figure 54. Average depth to probe refusal by channel position. 93
Figure 55. Depth to probe refusal at thalweg compared to adjacent bar type. 94
Figure 56. Presence of recovery factors at rapid channel recovery assessment sites. 95
Figure 57. Comparison of current and historical channel width and percent bar area. 96

CHAPTER 1: INTRODUCTION

Large-scale historical mining activities in the "Old Lead Belt" region of southeastern Missouri resulted in excess sediment releases to the Big River in the form of gravelly chat and sandy tailings (MDNR, 2004; NewFields, 2007; Pavlowsky et al., 2010; Owen et al., 2012). These inputs changed the overall mineral and geochemical composition of the channel substrate (Smith and Schumacher, 1991, 1993; Roberts et al., 2009; Pavlowsky et al., 2010) and resulted in overall fining of bars and bed sediment within segments of the Big River below the mining area (Pavlowsky et. al., 2010). Mining sediments also resulted in the contamination of channel and floodplain deposits with lead (Pb) and other metals along 171 kilometers of the Big River from the city of Leadwood to the Meramec River (MDNR, 2004; Pavlowsky et al., 2010).

In October of 1992, a 285 sq km area of the Old Lead Belt containing six mine waste sites was listed on the Environmental Protection Agency's (EPA) National Priority List as a Superfund Site (Asberry, 1997; Gunter, 2011). Since then, 145 km of the Big River have also been listed as impaired under section 303(d) of the Clean Water Act due to excessive fine sediment deposition and heavy metal concentrations (MDNR, 2004). As a result of the contamination and excess sedimentation, the United States Fish and Wildlife Service (USFWS) is concerned about the health of fish and invertebrate populations including freshwater mussels in the Big River (Meneau, 1997). Metal contamination in fish also poses a risk to humans if consumed. These concerns have led to several studies by the Missouri Department of Natural Resources (MDNR), the USFWS, the EPA, educational institutions, and other professionals to examine the effects

of sedimentation and metal contamination in the Big River (Smith and Schumacher, 1991, 1993; Gale et al., 2004; MDNR, 2004, 2007; NewFields 2006; Roberts et al., 2009; Pavlowsky et al., 2010; Young, 2011; Owen et al., 2012).

Sediment in the Big River has been contaminated with Pb concentrations above the probable effects concentration (PEC) of 128 parts per million (ppm) and is toxic to sediment-dwelling organisms (Meneau, 1997; MacDonald et al., 2000; MDNR, 2004; Roberts et al., 2009). Another harmful condition for fish and invertebrate species that is caused by mining activities is the fining of bed sediment, which causes siltation, riffle embeddedness, and channel instability (MDNR, 2004). Reduced population and diversity in freshwater mussels within and below mining segments have already been reported in the Big River (MDNR, 2004). These observations give way to rising concern for the vitality of these species and highlight the need to further study sediment characteristics within the Big River.

Gravel bars in the Big River in the core mining area in St. Francois County are contaminated with Pb in both fine (<2 mm) and "chat" sized fractions (4-16 mm) (Pavlowsky et. al., 2010). Excess sediment produced by historical land disturbance has been reported to migrate downstream in a wave-like fashion in Ozarks streams (Jacobson and Primm, 1997; Jacobson and Gran, 1999). In the case of the Big River this could mean the transportation of Pb contaminated sediment further downstream and the degradation of fragile habitat by contaminated sediment (MDNR, 2004). The potential for habitat destruction and remobilization of Pb contaminated sediment are important reasons to study the geochemical and physical characteristics of Pb-contaminated gravel bars with respect to spatial distribution.

While watershed-scale patterns of sediment contamination and storage have been previously described in the Big River (Schmitt and Finger, 1982; Smith and Schumacher, 1991; Roberts et al., 2009; Pavlowsky et al., 2010, Young, 2011), an analysis of sediment characteristics and contamination trends in bar forms is needed to better understand the extent and distribution of mining sediment in the Big River at the reach-scale. The purpose of this study is to address how mining sediment is distributed in channel bar forms across a range of scale. The associated implications for management are also discussed. The objectives of this study are to i) determine reach and bar scale variability of Pb content and sediment size; ii) relate bar form, sediment size, and contaminants to mine locations, long-term sediment transport trends, and channel conditions/morphology; and iii) evaluate the potential for both natural channel and sediment recovery and management-based applications. The results could be used by resource managers to evaluate remediation plan effectiveness, determine the potential for remobilization of contaminated sediment, and assess sediment transportation patterns in comparable rivers systems (Bunte and Abt, 2001; Hooke and Yorke, 2011).

CHAPTER 2: BACKGROUND

Fluvial geomorphology is the study of river processes and forms. The processes that control fluvial geomorphology should be thought of as a system of input supply (sediment source), transportation, and deposition (Schumm, 1977). There are three main components in the study of fluvial geomorphology. They are (i) the study of river form, such as the analysis of channel geometry and the location and distribution of in-channel features; (ii) channel history, or the processes that formed the present-day channel; and (iii) the study of those factors which have an impact on river shape and form, including climate, geology, and land use (Charlton, 2008).

Channel form (morphology) is influenced by a variety of factors which begin with the characteristics of the watershed. Topographic relief, geology, hydrology, valley form, and land use are primary factors of channel form (Schumm, 1977). Channel form is described by three dimensional characteristics: planform, longitudinal profile or slope, and cross-sectional shape (Rosgen, 1996; Charlton, 2008). Channel form characteristics are influenced by the fluvial processes of erosion, transportation, and deposition (Schumm, 1977).

The land use history of a fluvial system can have long-term effects on its geomorphology (Jacobson, 1995; Jacobson and Primm, 1997; Knighton, 1989; Saucier, 1983). For example, in mined watersheds there may be an increase in sediment supply, change in average particle size, or a change to the geochemistry and mineralogy of the sediment supply. Excess sediment may disrupt channel processes and can cause flooding, bank erosion, or initiate an aggradation-degradation cycle (Knighton, 1989; James, 2010).

Geographic location also plays a role; for example, the effects of hydraulic gold mining on the mountainous rivers in the Sierra Nevada are different than the effects of sub-surface lead-zinc (Pb-Zn) mining near Ozarks highland gravel-cobble rivers (Gilbert, 1917; NewFields, 2007; Pavlowsky et. al., 2010). Thus, local geography, geology, and land use of the watershed of interest should be considered when analyzing geomorphic change in river systems.

Stream Response to Disturbance and the Recovery Process

Stream disturbance and response is the result of a complex set of action-reaction processes related to a river's tendency toward equilibrium. Channel evolution models describe these processes and aid in forecasting a system's geomorphic response to disturbance (Schumm et al., 1984; Simon, 1989). Stream response to disturbance and associated recovery processes have been the subject of many studies in over the past century. These studies assessed channel disturbance due to channelization (Hupp, 1992; Hupp and Simon, 1991; Simon and Hupp, 1987), mining (Gilbert, 1917; James, 1989, 2006; Knighton, 1989; Pavlowsky et al., 2010), and other land use (Jacobson, 1995; Jacobson and Primm, 1997; Jacobson and Gran, 1999, Owen et al., 2011). Several models have been developed to predict processes and timescales of channel recovery from disturbance, both natural and introduced, and are known as channel evolution models (CEMs).

Assessment Methods. A common method for identifying disturbance at the reach scale is through aerial photograph analysis (De Rose and Basher, 2010; Downward et al., 1994). Parameters that can be derived from historical photo analysis include channel

sinuosity, channel width, historical planform change, and erosion rates (Hughes et al., 2006). Georeferencing images can introduce error into analysis because algorithms must be applied to the photos to "warp" the two-dimensional image to fit the three-dimensional surface of Earth. For this reason, care must be taken to ensure that error from georeferencing is measured and taken into consideration during analysis (Downward et al., 1994; Hughes et al, 2005; De Rose and Basher, 2010). A variety of techniques have been devised to assess the level of error, and the results of the error assessment should be reported in any research relying on aerial photograph analysis.

Field surveys yield local-scale data. For example, a simple cross section provides information about bankfull width, channel depth, entrenchment ratio, and area and can be used to calculate discharge and velocity at varying stream flows (Rosgen, 1996). Other field data important to analyzing disturbance, particularly in systems disturbed by excess sediment, is depth to probe refusal and bar cores (Pavlowsky et al., 2010). Further, longitudinal profiles provide stream slope, which can be an indicator of bed elevation and degradation or aggradation from stable levels (James, 2006; Knighton, 1989). Characteristics of vegetation, or lack thereof, indicates bank condition (Hupp and Simon, 1991).

Reconnaissance surveys, sometimes called rapid assessments, are visual observation and interpretation of conditions by trained scientists. The reliability of reconnaissance surveys has been debated but they are generally thought to provide a good over-arching assessment of the channel condition in a reach before commencing detailed field data collection (Downs and Thorne, 1996). There has been some attempt to devise a standard survey form; however, none has achieved wide popularity. This is partially

because uses for these surveys vary so greatly that the surveys are often better customized (Downs and Thorne, 1996). These surveys are qualitative nature, and provide a method for describing channel condition changes between reaches.

Geomorphic Disturbance. Disturbances to rivers are caused by many sources and can have a wide variety of impacts on the channel and bank morphology, bar form and size, water quality, and vegetation. Effects of disturbance on the river morphology can include channel widening, channel degradation (incision), aggradation, and planform adjustments (Jacobson, 1995). Causes can be natural or human induced, with land use changes being a primary driver in the late 1800s and early 1900s (Jacobson, 1995; Jacobson and Primm, 1997). Effects of disturbance can be assessed at a variety of scales, from the basin-scale to the reach scale to individual channel positions (Bunte and Abt, 2001; Schumm, 1985). To understand how disturbance affects a channel, the variables of stream morphology must be examined.

The primary variables in stream morphology are sediment and stream flow. This relationship is explained by Lane (1955) in the formula $Q_s*D_{50} = Q*S$, where Q_s is the rate of sediment discharge, D_{50} is the median sediment size, Q is the rate of stream discharge, and S is the slope of the channel bed (Lane, 1955). A channel is maintained in a state of equilibrium when the equation is balanced, while changes in sediment load and size must be compensated for by changes in discharge or slope to maintain equilibrium (Schumm, 1977; Lane, 1955; Rosgen, 1996). As the primary control on channel shape, significant change in sediment load or size can exceed geomorphic thresholds and cause channel morphology changes in the form of both channel cross-sectional shape and slope (Schumm, 1977; Knighton, 1989).

Geomorphic Recovery. Geomorphic recovery is achieved when the river returns to a state of equilibrium, or quasi-equilibrium, after disturbance from its original balanced state. This occurs after a series of planform adjustments along with complementary changes in stream discharge/velocity and degradation or down-cutting of the bed (Charlton, 2008). The time and amount of channel adjustment required to reach this state varies by river type, cause of disturbance, and many other variables (Morisawa, 1985; Simon, 1989; Martin and Pavlowsky, 2011; Owen et al, 2011). Additionally, the time required for recovery also varies by scale; recovery at the basin-scale may never fully be realized, while individual reaches may adjust in only a few decades (Charlton, 2008).

Lateral widening is one indicator of geomorphic recovery. As Schumm et al. (1984) outline, bed aggradation (widening) and bank erosion are a recovery indicator as channel planform adjusts, bar stabilize, and new floodplains form as the channel returns to equilibrium. While degradation during initial disturbance can lead to narrow, incised channels and increased slope (Charlton, 2008), aggradation causes lateral widening, an indicator of recovery (Chang, 1984; Schumm et al., 1984). Channel disturbance from excessive sedimentation will also cause channel widening and increased width-to-depth ratio as the river's slope and velocity, by extension, adjust to the increased bed load (Schumm, 1977).

A link also exits between bed aggradation, bank accretion and the appearance of woody vegetation on low and mid-banks. As bars and new floodplains stabilize, vegetation becomes established and serves as another indicator of recovery (Hupp, 1992; Simon and Hupp, 1987). In the Ozarks, field observations by Martin et al. (2016) found bank erosion to be the primary recruitment of large woody debris (LWD). When

associated with lateral widening, this bank erosion and LWD presence may also indicate recovery processes are taking place.

Fluvial geomorphologists use a variety of methods to determine the stage of recovery a disturbed channel is in. One of the best starting points to assessing recovery is to conduct a field reconnaissance survey of conditions assessing characteristics such as bank conditions and vegetation. Thorne and Downs (1996) argue that visual field reconnaissance is "the only viable source of relevant geomorphological data…" and point out that the use of stream reconnaissance surveys is also addressed by Simons et al., (1982), as the "Level 1 Geomorphic Analysis" and again by Schumm et al. (1984) as "Reconnaissance Level Analysis." Reconnaissance surveys can be used to determine the stage of recovery a channel is in according to channel evolution models, described in the next section. As valuable as reconnaissance surveys are, they best used as a precursor or in addition to more technical field surveys that provide quantitative measures of the qualitative reconnaissance findings. These include measurements of bank angle, cross sections, particle size distribution, and channel slope (Thorne and Downs, 1996).

Channel Evolution Models. There have been numerous models developed to determine rates and processes associated with geomorphic river recovery in disturbed rivers. The most commonly cited model today is Schumm's 1984 CEM (Figure 1), which has been modified by others in the years following (Simon, 1989; Doyle and Shields, 2000; Watson et al., 2002). Schumm's model describes a five-stage process of river evolution beginning with the stable channel, interim stages of disturbance, and finally the channel's return to stabilization (Schumm et al., 1984). Following Schumm, Simon (1989) presents a modified version which includes the addition of a threshold stage

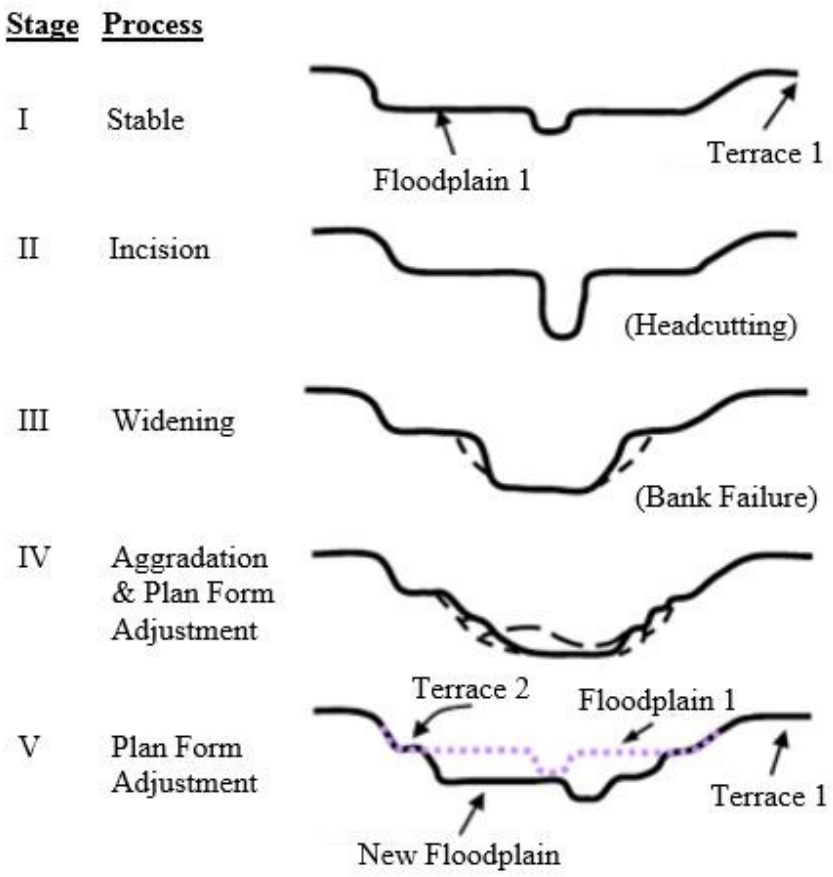

Figure 1. The five stages of channel evolution (after Schumm et al., 1984).

(Figure 2) and models recovery of rivers which have been specifically subjected to anthropogenic dredging and channelization. This CEM follows a six-stage model of bank-slope development, which is highly correlated to overall channel evolution (Simon and Hupp, 1986). Inputs to Simon's model are limited to channel width, bank condition, and bed slope, making this a universal and easily employable model (Doyle and Shields, 2000; Simon, 1989).

While Schumm and Simon's models are the most well-known, others are also worth mentioning. Doyle and Shields (2000) take Simon's model a step further by incorporating sediment characteristics into the model using Lane's 1955 formula for

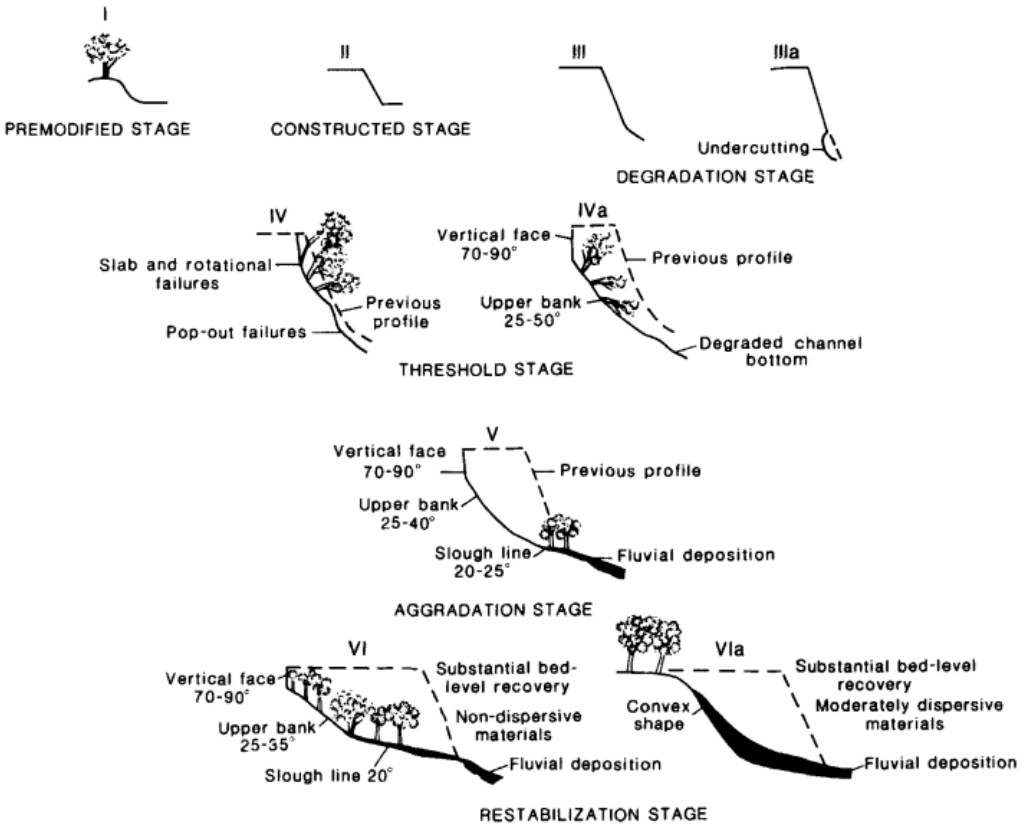

Figure 2. Simon's six-stage channel evolution model (from Simon, 1989).

stream equilibrium. Doyle and Shields (2000) hypothesized that grain size would increase in stages IV and V if a supply of coarse material is available in channel banks, bed, or fluvially. They also evaluated whether fining would occur in the later stage V and stage VI. Their results supported the coarsening of grain size in stags IV and V on a natural, un-straightened river, but not the fining later. They concluded that grain size in incising channels is as variable as other geomorphic measures such as slope, channel width, etc., and that due to this variability, CEMs provided only limited usefulness in predicting grain size changes.

Watson et al. (2002) formulated a CEM featuring two dimensionless measures of bank stability and sediment continuity. The first is bank stability (N_g), a ratio between

existing bank height and angle and critical bank height and existing angle. The second is hydraulic stability (N_h), which is the ratio between sediment transport capacity and sediment supply. The authors go on to show the association between the CEM and the dimensionless stability diagram (DSD), with N_g on the vertical axis and N_h on the horizontal (Figure 3). When both N_g and N_h are greater than 1 (unstable) they correspond with CEM phase III, the most dynamic phase of channel recovery (Watson et al., 2002). When N_g and N_h are computed correctly and examined in the context of the DSD, the model provides an understanding of a river's evolution and allows resource managers to select appropriate rehabilitation measures.

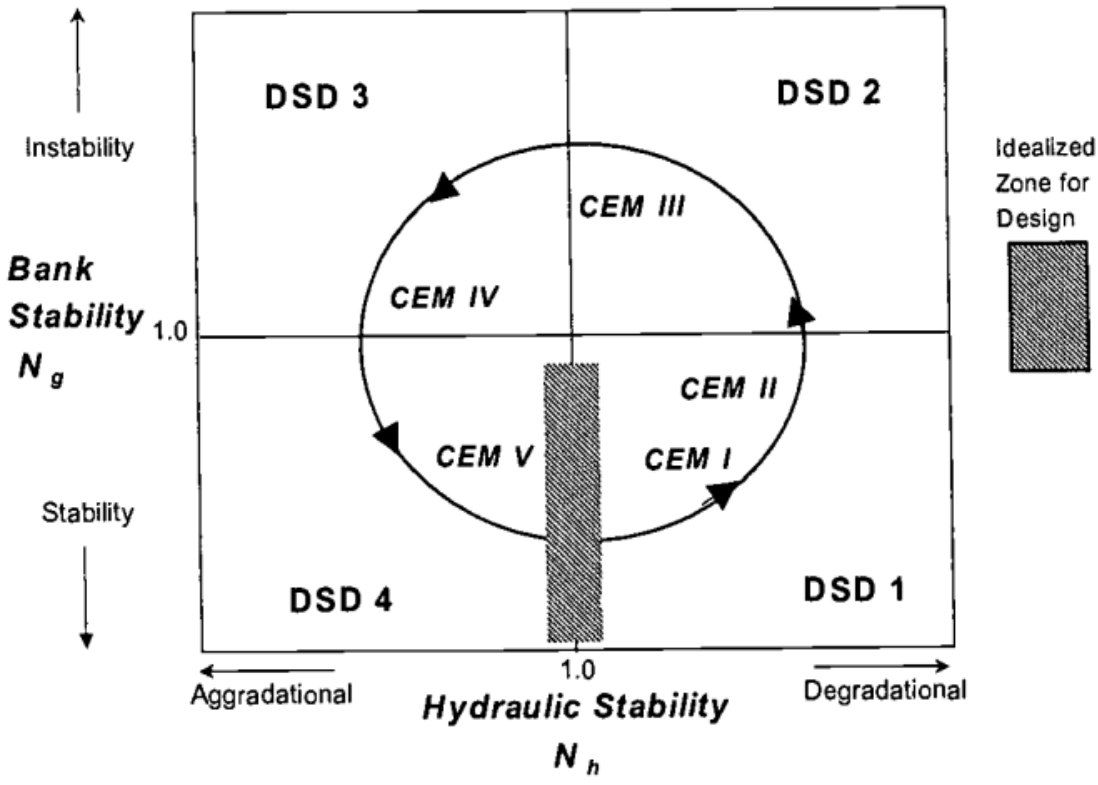

Figure 3. Comparison of 5-stage CEM to the dimensionless stability diagram.

Sediment Transportation Processes

The movement of sediment through the fluvial system is one of the most complex and least understood components in the study of fluvial geomorphology (Lisle et al., 1997). Termed sediment routing, it is the combined processes of sediment erosion, transport, and deposition (Jacobson and Gran, 1999). The channel bed load is composed of sediment of sand-size and larger and makes up most the channel bed (Schumm, 1977). While fine sediments of clay and silt size are also found in bed material, they are more difficult to erode than sand-sized particles, which are readily eroded and transported during flood events and deposited as flow wanes (Hjulström, 1939; Schumm, 1977). However, silt and clay sized particles may be suspended and transported over a longer period once mobilized. Many factors affect how sediment is transported through a system including stream discharge, flood events, size and composition of the sediment, and watershed disturbance factors such as land use.

Sediment Analysis. The importance of sediment size analysis for geomorphic assessment is well explained by Stephenson (1970). In his article, graphs comparing fluvial, marine, and terrace grain size show various ways the "four moments" of sediment frequency (mean, standard deviation, skewness, and kurtosis) can be presented to emphasize sediment distribution in a study area. He stresses that grain size is the most important factor to consider. Stephenson's examples provide compelling evidence for the importance of comprehensive sediment analysis by showing the striking differences in the graphs between the different sediments and explaining the significance of these differences.

Sediment size fractionations are transported and deposited at varying velocities relating to their particle size. This relationship is best explained by the Hjulström Curve, as show in Figure 4 (Hjulström, 1939). When stream velocity falls below transport capacity for a given sediment size, the sediment particle is deposited and stored in the active channel as bed or bar. Thus, gravel bar formation is closely tied to stream competence and is a driving factor in geomorphology and the development and location of channel meanders (Knighton, 1989). The maximum sediment grain size that a given stream can transport is proportional to the velocity of flow and is called stream competence (Morisawa, 1985).

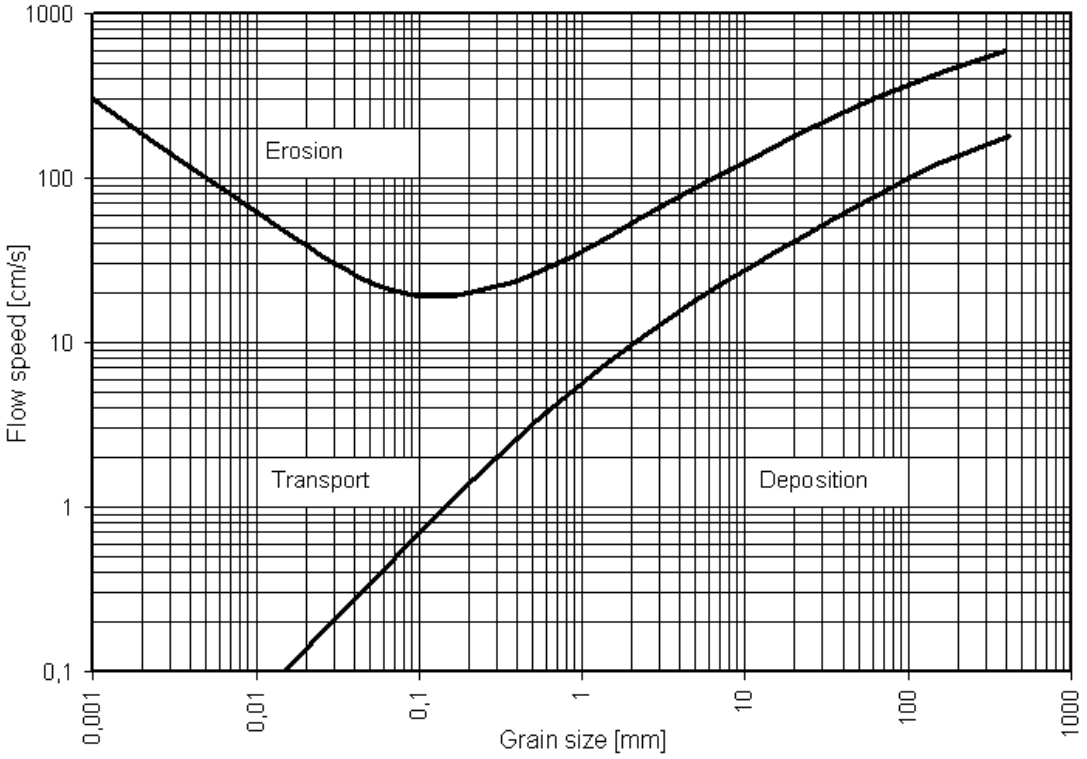

Figure 4. Hjulström curve of sediment erosion, transport, and deposition velocities (from Hjulström, 1939).

Sediment Waves. Sediment waves are the result of excessive sedimentation to a river over a short period of time, which behave like a wave moving through the river system as a single unit (Gilbert, 1917; James, 1989, 2006, 2010; Bartley and Rutherfurd, 2005). Also referred to as sediment waves, sediment slugs, sediment pulses, bed-load sheets, or gravel waves, the study of sediment traveling in a bed wave has been an increasingly popular topic over the past century (James, 2010). While the term sediment wave is used to describe sediment flux due to large sediment input into a river, bed waves describe changes in bed elevation as it responds to the sediment (James, 2010). Sediment waves can vary in size, with smaller waves resulting from land clearing and removal of mining. It should also be noted that the wave model is not appropriate for describing the recovery process in all streams (Bartley and Rutherfurd, 2005).

The popularity of studies about sediment waves can be traced back to late 1800s studies on the effects of sediment from hydraulic gold mining in California (Gilbert, 1917; James, 2010). The first commonly referenced intensive study on this topic is Gilbert's 1917 model of sediment wave behavior. Gilbert's model indicates that an excessively large, unnatural sediment load introduced to a stream system is transported directly and in a relatively short period of time, with little left behind. This model has been disputed by various scientists and is now considered to be an over-simplified description of sediment/bed wave behavior (James, 1989, 1991, 2006, 2010; Knighton, 1989; Bartley and Rutherfurd, 2005). Key scientists in the study of sediment wave transport now tend to agree that transport occurs in a more asymmetrical method: when excess sediment is input over a short period of time, some is transported, while some is

stored only to be later remobilized (James, 1989, 2006, 2010; Knighton, 1989; Bartley and Rutherfurd, 2005; Young, 2011).

The term for bed wave movement downstream is known as translation, while the widening of the wave is known as dispersion (James, 2006). It is important to understand the difference in these as both cause a rise and fall in bed elevation at a specific cross-section over time, yet the actual wave behavior is quite different when viewed from a longitudinal profile view (Figure 5). Dispersion results in degradation of the bed wave peak with aggradation occurring away from it, while translation results in degradation upstream of the wave and deposition ahead of the wave as the wave progresses downstream. These can be thought of as lateral (translation) and vertical (dispersion) movements and they describe the two characteristic ways in which bed waves behave.

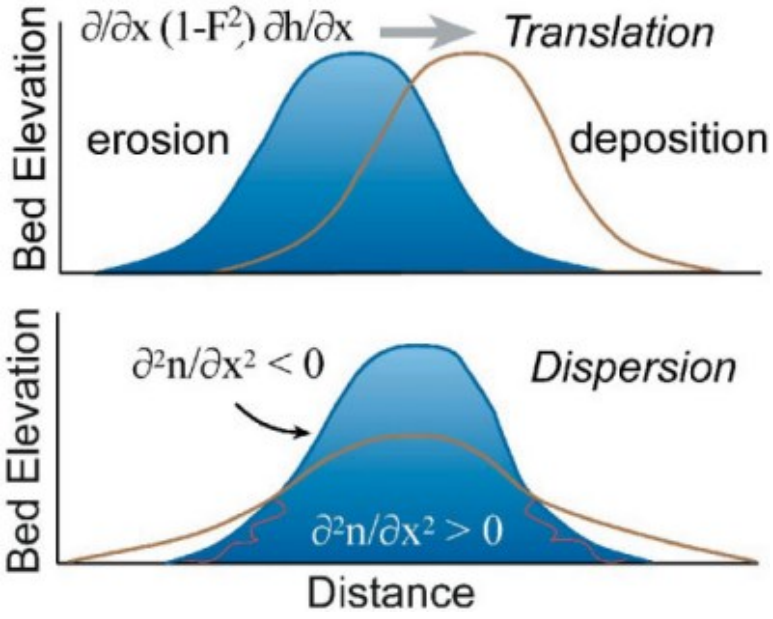

Figure 5. Longitudinal profile view of wave translation and dispersion (from James, 2006).

James describes an alternative way in which bed waves can move, which is through alteration of stream slope (2006). In this process, the bed first aggrades as sediment is input into the channel. As sediment supply slows or stops, a process of degradation occurs. For non-headwater input points, degradation first occurs upstream of the input point and follows as the wave moves downstream. It is generally agreed upon that bed waves attenuate, or reduce in intensity, over time (Jacobson, 1995; Jacobson and Gran, 1999; James, 2006). James (2006) examined the status of hydraulic gold mining sediment in the Bear River, California and applied Gilbert's model of sediment wave transport. He found that the volume and percent of sediment in storage was far greater than originally estimated. As with others, James disputes Gilbert's model of symmetrical wave transport as characteristic of all sediment waves. From his findings, James identified an asymmetrical model of sediment transport/storage in the Bear River.

Because of the asymmetrical movement of bed waves, their interaction with riverine systems is complex and not well predicted. Bartley and Rutherfurd (2005) assessed geomorphic variables in three reach types (unaffected by sediment, affected, and recovering) in three rivers. Though the sediment input was similar in each river, the recovery responses varied greatly. Only one river's recovery followed Gilbert's model of sediment wave recovery. The result of the research is the author's attempt to define yet another model of channel recovery which combines Gilbert's model with geomorphic variability.

Channel Sediment Transport and Deposition. Channel bed sediment can be classified as bed, bar, and high or stable bar. Bar deposits are active bed sediment that is exposed above the wetted channel during periods of mean or low flow and are

accumulations of channel bed materials. They occur where the sediment load is greater than the transport velocity of the stream (Kellerhals, 1989). Channel sediment is mobilized during flood events and deposited as flow wanes or when there is a local decrease in sediment transport capacity. Sediment is first deposited in areas of flow separation and is also affected by changes in slope, channel width, and/or local velocity (Brierley and Fryirs, 2005).

Ozarks streams are characterized by a meandering thalweg with alternating bar forms at the segment scale, with periodic disturbance and stable reaches at the basin scale (Panfil and Jacobson, 2001). Alternating bars are formed alongside the riffle, where the channel steepens locally. Riffles exhibit a localized increase in velocity and decreased flow resistance, which is caused due to decreased turbulence because of diminishing sediment in motion, decreasing the rate of energy loss (Leopold et al., 1964). As the near-bottom flow moves diagonally away from the thalweg towards the bank the shallow flow depth combined with decreasing flow velocity results in deposition of coarse sediment at the bar head during high flow events (Bunte and Abt, 2001). At the downstream end of a bar, surface flow is directed diagonally away from the thalweg and up the bar slope towards the channel bank, resulting in fine sediment deposition at the bar tail. This trend is also true laterally across a bar, with coarser sediment found near the wetted channel and increased fining towards the bank.

In additon to alternate bars, meandering streams are also characterized by point bars, mid-channel or center bars, and delta bars (Rice et al., 2009; Hooke and Yorke, 2011). Point bars are a depositional feature located on the insides of meander bends. In these meanders, flow is concentrated on the outside of the bend; sediment is deposited on

the inside of the bend where flow velocity is lower, and banks on the outside of the bend are eroded. Mid-channel, or center bars, are unattached to the floodplain and migrate through the channel (Rice et al., 2009; Hooke and Yorke, 2011). These bars are more common in aggrading streams or those with excess sediment loads. Bars grow when flow is diverted away from the bar; however, if flow continues to be diverted, bars may become stablized by fine sediment and vegetation and begin to form new floodplain (Rice et al., 2009; Hooke and Yorke, 2011).

In Ozarks streams, aggradation due to the influx of sediment leads to the development of large, sweeping gravel bars, often found on the inside of meander bends (Jacobson and Primm, 1997). Side bars and occasional center bars are common, and many of these have stabilized with vegetation since the initial sediment influx due to human land clearing and settlement (Saucier, 1983). In mined watersheds such as the Big River, excess sediment input related to mine tailings led to stream instability, aggradation, and rapidly changing morphology of bar forms (Jacobson, 1995).

Figure 6 shows four of the common bar types and found in Ozarks streams and their approximate channel location. The study of bar forms provides important information about sedimentation patterns and landscape history and has become more feasible in recent years with the advancement of photogrametric technologies (Rice et al., 2009). The general trend in gravel-bed streams is increasing bar area with distance downstream; however, in disturbed channels this is trend is disrupted and segments of larger bar areas may be found upstream of smaller bar areas (Jacobson and Gran, 1999).

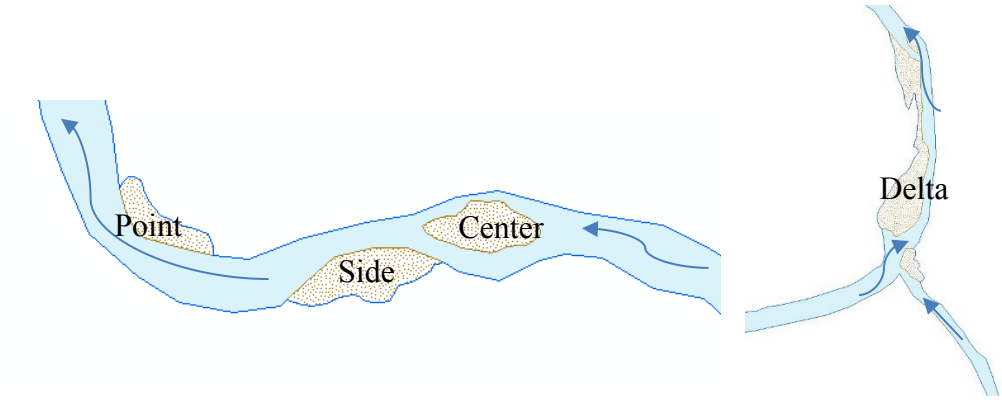

Figure 6. Channel positions of common bar types in alluvial rivers. Arrows indicate direction of flow.

Mining Sediment Impacts on Stream Morphology

The study of mining impacts on stream morphology stemmed from interest in understanding the effects of hydraulic gold mining in California (Gilbert, 1917; James, 1989). These studies focus on the effects of the excess sediment input from mine tailings but also consider other problems associated with mining in a river's watershed, such as heavy metal contamination. They have opened the door to a better understanding of the geomorphic processes driving sediment transport in fluvial systems and the variables that play a role in transport, storage, and channel recovery.

In addition, Knighton's 1989 study analyzes the impacts of tin mining on the Ringarooma River in Tasmania. The study shows that channel aggradation was most extreme near mining sediment input points and decreased in intensity downstream. Up to a 300 percent increase in channel width was also observed (Knighton, 1989). As degradation began in the upper reaches of the river to account for the excess sediment, aggradation continued downstream. This indicates an asymmetrical process of sediment

transport. Knighton hypothesizes the river will return to a "normal" state 50 years from when his article was published, around 2039.

The geomorphology of a fluvial system plays an important role in the transport of mining sediment. For example, Macklin et al (2006) compare the effects of tailings dam failures on two unrelated river systems. They find that four factors contribute to the effects of tailings on river channels: 1) quantity of input, 2) concentration of contamination, 3) rate of input, and 4) effectiveness of cleanup efforts, if any. The results show that local geomorphic variables must be taken into consideration when estimating the extent of damage caused by mining sediment.

While initial studies expressed that excess mining sediment is transmitted downstream in a direct, wave-like fashion (Gilbert, 1917), others have found this to be inaccurate (James, 1989; Knighton, 1989). James concludes in his research that the mining sediment persists in and affects fluvial systems for far longer than initially thought. Knighton's research points to a more a-symmetrical dispersion with sediment attenuation and storage effects, rather than consistent bed wave transport (Knight, 1989).

It is essential to understand grain size when examining the impacts of mining sediment transportation through a river system. In two Norwegian rivers. Langedal (1997) found that mining sediment tended to be stored in low-gradient reaches that acted as a sediment trap under normal flow conditions but could be remobilized by major flood events. By understanding sediment grain size and transport capacity of the river, resource managers can make better informed decisions regarding dispersion control of contaminated sediment (Langedal, 1997).

CHAPTER 3: STUDY AREA

The Big River watershed (Figure 7) is in southeastern Missouri and lies on the Salem Plateau of the Ozark Highlands physiographic region. The watershed drains about 2,500 km^2. Elevations of the Big River range from 530 m above sea level (masl) at the headwaters in the St. Francois Mountains to 124 masl at its confluence with the Meramec River at Eureka, MO (Pavlowsky et al., 2010). The general direction of flow is north and the length of the Big River is approximately 222 km (Meneau, 1997). The largest tributary is Mineral Fork, which drains 490 km^2. The Big River flows through Washington, St. Francois, and Jefferson Counties. This this study focuses on an 80 km segment of the river located entirely within St. Francois County, which flows through what is known as the Old Lead Belt Mining District. The northern and most downstream portion of the study area is the county line between Jefferson and St. Francois Counties.

Physical Characteristics

The study segment is located within the well-dissected Salem Plateau where the topography is deeply incised along the river with steep hill slopes (Brown, 1981). The study area is predominately underlain by the Bonne Terre Formation, a dolomite unit of Cambrian age which is the primary host-rock of the Zn and Pb mineralization that has been historically mined in this region (Smith and Schumacher, 1993; MDNR, 2011). There are some minor limestone and shale units present as well as sandstone outcrops, which are visible in some areas (Brown, 1981). The downstream portion of the study area

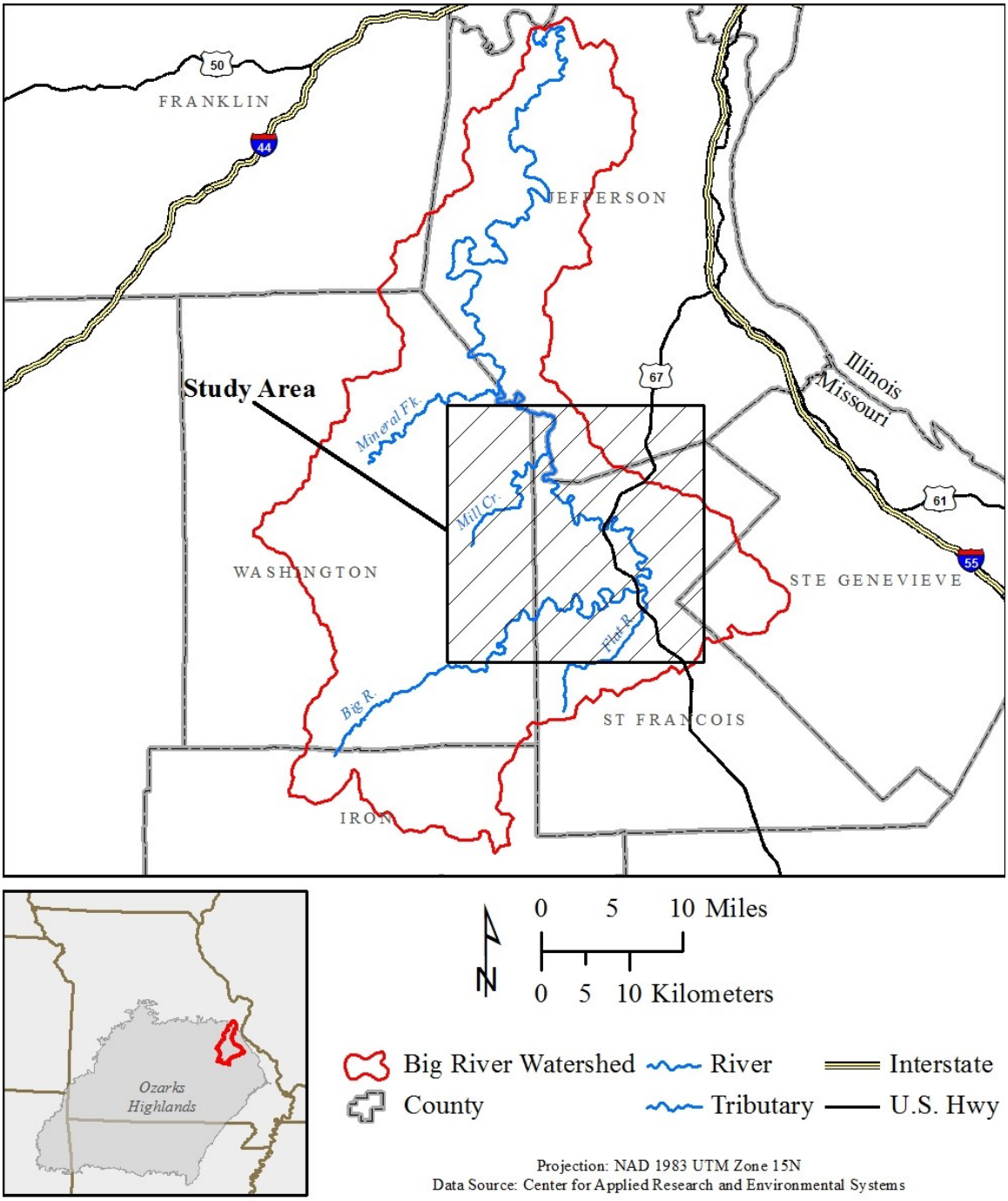

Figure 7. Location of the study area within the Big River watershed.

is underlain by the Eminence and Potosi Formations, also of Cambrian age (MDNR, 2011).

Soils in the study area are generally formed in Pleistocene glacial loess over cherty or non-cherty residuum formed from dolomite, limestone, and shale. Upland hill slopes are composed of soil formed in cherty red clay residuum from limestone and dolostone and contain large concentrations of coarse chert fragments throughout the solum. They are overlain by 0.5 - 1.0 m of loess (Brown, 1981). Upland soils in this region consist primarily of the moderately to excessively well-drained Caneyville-Crider-Gasconade association formed in loess and clayey materials. Slopes range from 2 to 35 percent and these soils range in depth from 33 to 79 cm. They are underlain by hard dolomite (Brown, 1981). Crider soils are commonly found on ridge tops and Caneyville soils are found on gentle to steep slopes at elevations higher than the Gasconade soils found on side slopes. Deep, cherty Goss soils and well-drained Hildebrecht soils are also found on uplands in this area. Goss soils feature a cherty silt-loam texture and depth to bedrock ranging from 150 cm to greater than 250 cm (Brown, 1981).

Floodplains in the study area are mainly composed of well drained Haymond and Kaintuck soils and moderately drained Wilbur soils (Brown, 1981; Skaer, 2000). These frequently flooded soils range from fine sandy loam to silt loam. Most the floodplain in the study area is Haymond while the occurrence of the Kaintuck series increases downstream. The Wilber series is a poorly drained floodplain soil that is generally found in back swamp locations at the base of terraces and paleo-channel fills. Terraces and benches are composed of Auxvasse soils and Horsecreek soils (Brown, 1981). Within the study area the Big River valley is composed of 32 percent Haymond soils, 11 percent

Caneyville soils, 8 percent Crider soils, 6 percent Horsecreek soils, 5 percent Kaintuck soils. The remaining 62 percent is distributed between 38 other minor soil types.

The Big River watershed has a humid continental climate that is annually variable. The average annual temperature ranges from 15-18 ºC with extremes ranging from as high as 38 ºC to as low as -26 ºC (Jacobson and Primm, 1997; Rafferty, 1980). The climate is primarily driven by moist Gulf Coast air masses and east-moving storm systems, along with occasional polar fronts. Relative humidity is around 60 percent in midafternoon, increasing overnight to an average of 80 percent at dawn (Brown, 1981). Average annual rainfall in the Big River watershed is approximately 74 cm, commonly peaking in May, while the lowest period of precipitation is in February. Annual runoff is about 33 cm (Meneau, 1997). Snowfall accounts for an additional average precipitation of 35 cm (NewFields, 2007).

Three permanent USGS gage stations exist on the main stem of the Big River. They are located at Irondale, Richwoods, and Byrnesville, Missouri (Table 1). Mean annual flow ranges from 5 m^3/s at the Irondale gage, which has a drainage area of 453 km^2, to 25 m^3/s at the Byrnesville gage, which drains 2,375 km^2 and is located 23 km upstream of the Big River's confluence with the Meramec River (USGS, 2012a, 2012b, 2012c). Elevation change between the Irondale gage and the Byrnesville gage is 97.4m over a river distance of 168.3 km. The peak flood event for all three gages occurred in the fall of 1993; however, peak flow at the Irondale gage occurred in a separate storm event than the Richwoods and Byrnesville gages downstream of it. The Byrnesville gage, with the longest record, shows a trend of increasing flood frequency, with four of the top five

Table 1. Characteristics of USGS gages on the Big River (USGS, 2012a, 2012b, 2012c).

USGS Station Number	USGS Station Name	Record Length	Drainage Area (km^2)	Datum (masl)	Mean Annual Q (m^3/s)	Maximum Peak Flow (m^3/s)	Date of Max Flow
07017200	Big River at Irondale, MO	1965-2011	453	229.60	5	1,390	11/14/1993
07018100	Big River near Richwoods, MO	1949-2011	1,904	159.41	20	1,693	9/23/1993
07018500	Big River at Byrnesville, MO	1922-2011	2,375	132.19	25	1,801	9/25/1993

largest maximum annual peaks having occurred in the past 25 years in 1993, 1994, 2008, and 1986, respectively (Young, 2011).

Channel and Valley Morphology

Streams in the Ozarks are characterized by chert gravel-cobble beds along wide, flat valley bottoms with thick alluvial deposits (Jacobson, 1995). Sinuosity in Ozarks streams is low due to frequent long, straight stable reaches which alternate with disturbance reaches characterized by rapidly changing planform (Jacobson, 1995). These disturbance reaches are referred to as sedimentation zones in Saucier (1983) and as active reaches in Martin and Pavlowsky (2011). Stable reaches have generally trapezoidal cross-sections and lack significant gravel deposition (Jacobson, 1995). They are usually bordered on one side by the valley wall and by broad valley on the other, indicating that bedrock is not a constraint of stable reaches (Jacobson, 1995; Panfil and Jacobson, 2001).

Erosion and deposition activities are widespread in disturbance reaches, and it is in these zones that sediment storage and remobilization most frequently occurs in Ozarks streams (Jacobson, 1995; Panfil and Jacobson, 2001). Disturbance reaches are driven by hydraulic interactions between the channel and its valley, effected by variables of constrictions, expansions, and areas of flow separation (Jacobson, 1995; Panfil and Jacobson, 2001). Rapid lateral channel migration is another characteristic of disturbance reaches. Sinuosity in Ozarks streams is approximately 1.1 but may be as high as 1.5 in disturbance reaches (Jacobson, 1995). It is thought by Jacobson (1995) that the alternating pattern of stable and disturbance reaches is a natural characteristic of Ozarks streams and is not the result of human disturbance.

While the pattern of stream sediment transport may not have changed, historical land use did lead to notable changes in sediment quantity and channel planform in Ozarks streams (Saucier, 1983; Jacobson, 1995; Jacobson and Gran, 1999). Land clearing caused the residual soils of the uplands to erode, releasing excess sediment to Ozarks tributaries, ultimately leading to an increase in gravel bars on main channel rivers. These bars have since been stabilized by vegetation, as evidenced by aerial photography since the 1930s (Saucier, 1983; Jacobson and Primm, 1997). In a study on the Current River in southeast Missouri, Jacobson and Gran (1999) found that the excess sediment from land use change is traveling in a wave-like fashion with anomalies occurring at tributary junctions and disturbance reaches. Using a sediment transport model, they determine that the spatial distribution of gravel is related to previous land disturbances in a time-lagged fashion; present day activities do not affect sediment transport to the same extent.

Historical Land Use

Prior to settlement, Ozarks uplands were composed of oak savannah, while lowlands and hill slopes were mainly forested with deciduous and pine stands (Brown, 1981; Saucier, 1983). Initially part of the Louisiana Purchase, settlement in the St. Francois County began in the early 1800s and initiated a period of deforestation to make way for agricultural and grazing land that was most intense after 1850 (Brown, 1981; Jacobson and Primm, 1997). In the Big River watershed corn, row crop, dairy, and pork industries predominated through the 1920s. Most land cover is currently forest or woodland (48%) and pasture land (26%) (Meneau, 1997). Urban areas make up 9 percent of the land use in the watershed.

Lead Mining. Lead mining has been on-going in the Old Lead Belt District since its discovery in the area around 1700. Missouri has been a leading producer of Pb for the United States since 1920 (Meneau, 1997). Early Pb mines were primarily in Washington and St. Francois Counties and consisted of shallow open pits mined for large surficial galena crystal deposits (Pavlowsky et al., 2010; Smith and Schumacher, 1993). Open pit mining began around 1864 in Bonne Terre by St. Joseph Lead Company, and expanded after diamond-bit borings indicated presence of lead ore throughout the area (Gunter, 2011; NewFields, 2006; Smith and Schumacher, 1993). A maximum of 15 mining companies operated around Bonne Terre, Flat River, Leadwood, Desloge, and Elvins in the late 1800s and early 1900s; however, by 1933 the St. Joseph Lead Company had acquired all companies and mining properties (Smith and Schumacher, 1991 and 1993).

Up until the 1930s mining was conducted via gravity milling. Gravity milling produced sediment ranging from 4-16 mm in size, known as chat. Introduced in 1917,

froth flotation produced fine-sand sized tailings of less than 0.25 mm and quickly became the dominant Pb recovery technique (NewFields, 2007). The chat was stored in tailings piles (Figure 8) while the finer waste material was transported to slurries called slime ponds in dammed valleys (Smith and Schumacher, 1991 and 1993; Pavlowsky, et al., 2010).

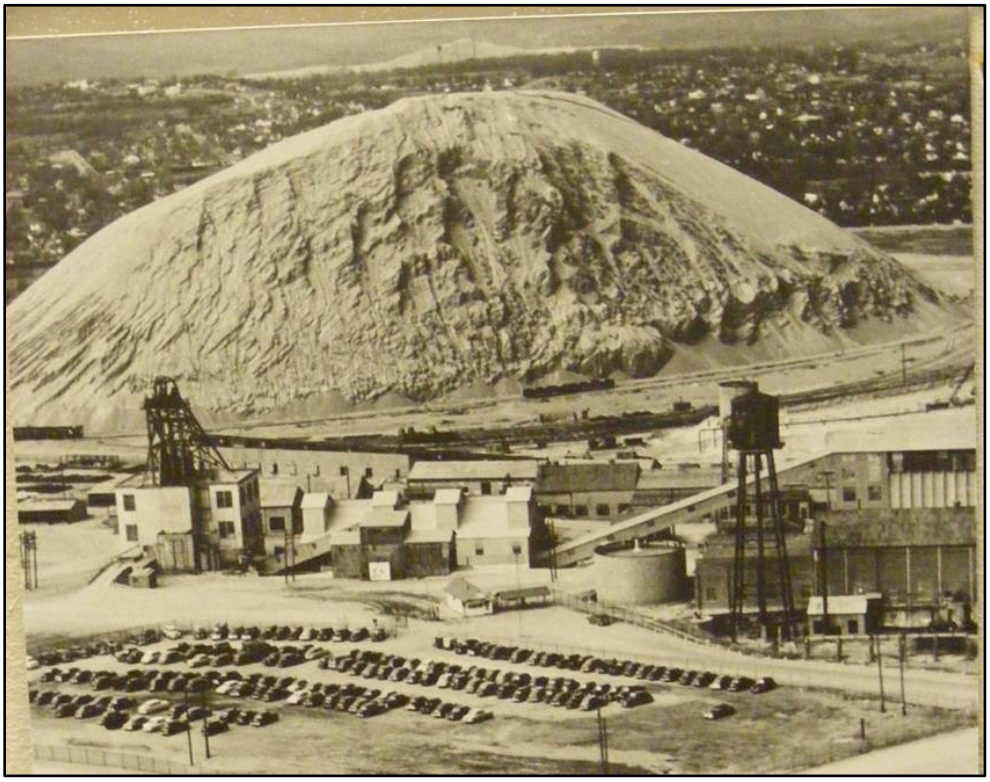

Figure 8. Federal mill and mine tailings pile, ca. 1940 (source unknown).

Mining in the Old Lead Belt peaked in 1942 with an estimated production of 197,430 tons of lead; however, rapid decline followed as mining resources became depleted and production expanded in the Viburnum Trend area southwest of the Old Lead Belt. St. Joseph closed its last mine in 1972 (Gunter, 2011; Smith and Schumacher,

1993). Today six major tailings piles covering 3,000 acres of land hold approximately 23 percent of the 227 million megagrams (Mg) of tailings produced during the mining of the Old Lead Belt District (NewFields, 2006; Smith and Schumacher, 1993).

Tailings stored in these piles are high in lead content. Pavlowsky, et al (2010) analyzed the geochemistry of various size fractions of chat and tailings from the Leadwood pile along the Eaton Branch and the National pile along Flat River Creek (Table 2). Lead content was highest in the finest (< 63 μm) and coarsest (1-8 mm) size fractions tested, as the milling process is more efficient in recovering Pb and Zn in the middle range fractions (Taggart, 1945). Pb content in the Leadwood pile ranged from 1,291 ppm to 5,380 ppm, while Pb content in the National pile was as high as 9,902 ppm in the chat-sized fraction of 4-8 mm.

Effects of Mining in the Big River. Pavlowsky et al. (2010) found Pb contamination to be present in some form throughout the entire main stem of the Big River. Glide and bar samples were found to contain Pb levels greater than the PEC of 128 along the entire 171 km length of the Big River from the upstream-most mining influence to the confluence with the Meramec River. However, some samples were below the PEC starting at 30 km upstream of the confluence (Pavlowsky et al, 2010). A segment between 6 and 38 km downstream of initial mining inputs contains the highest concentrations of Pb at more than five times the PEC.

The study noted that mining sediment has been sorted gradationally with distance downstream from mining. Sediment in the 4-8 mm range were found as far as 34 km downstream, while coarse sand (<2 mm) was found as far as 56 km downstream of mining and fines of <250 μm were found as far as 72 km downstream (Pavlowsky et al.,

Table 2. Size fractionation of metals in tailings materials (from Pavlowsky et al., 2010).

Size Fraction	Pb (ppm)	Zn (ppm)	Ca (%)	Pb:Zn (ratio)
Leadwood Pile				
<63 µm	5,380	9,720	21.8	0.6
<250 µm	1,291	4,210	22.3	0.3
1-2 mm	1,556	1,687	21.6	0.9
1-2 mm cr[a]	4,191	3,560	21.5	1.2
4-8 mm cr	3,362	1,178	21.1	2.9
<2 mm	1,329	5,164	21.8	0.3
National Pile				
<63 µm	5,156	676	21.7	7.6
<250 µm	1,452	287	22.7	5.1
1-2 mm	2,193	162	21.7	13.5
1-2 mm cr	2,224	185	22.9	12.0
4-8 mm cr	9,902	307	25.2	32.3
<2 mm	1,385	275	24.1	5.0

[a] Samples with the suffix "cr" were prepared for analysis with ball mill crushing.

2010). It was concluded that chat sediment must be stored in bed and bank deposits, likely within 20 km of its input point. Finally, they concluded that while 63 percent of the estimated 3,700,000 m^3 of contaminated sediment in stored in downstream Jefferson County, 73 percent of mining sediment is stored within St. Francois County (Pavlowsky et al., 2010).

CHAPTER 4: METHODS

A combination of field, laboratory, and GIS methods were used to identify the characteristics and spatial extent of gravel bars in the Big River, evaluate the distribution of mining sediment in bar deposits, and to assess whether characteristics of geomorphic recovery are present. These methods assess the geospatial characteristics of bar and bed sediment in the Big River at scales ranging from segments of 10 to 18 km to the small-scale variability of an individual gravel bars.

Aerial photographs were interpreted to assess morphology and location of gravel bars in the Big River and how their spatial patterns relate to valley form, bluff control, channel planform, and mining sources. Rapid geomorphic assessments were conducted at a subset of sites to identify presence or absence of geomorphic recovery indicators. Sediment samples geochemical analysis was used to determine where mining sediment is being stored within the Big River and what the contribution of mining sediment is to the chat (4-16 mm) and fine (<2 mm) size fractions in bed and bar deposits. At the channel or bar-scale, pebble counts and sediment "grab" samples were used to determine how texture and geochemistry vary within and between bars from the same river segment.

Location and Description of Field Sites

Twenty-one river reaches were studied, including 4 upstream control sites and 17 study sites below mining influence (Figure 9). Each study reach is made up of three sub-reaches of 10-12 bankfull widths in size. The sites were chosen based on location and accessibility. Most sites are located near a public fishing access or upstream of a road

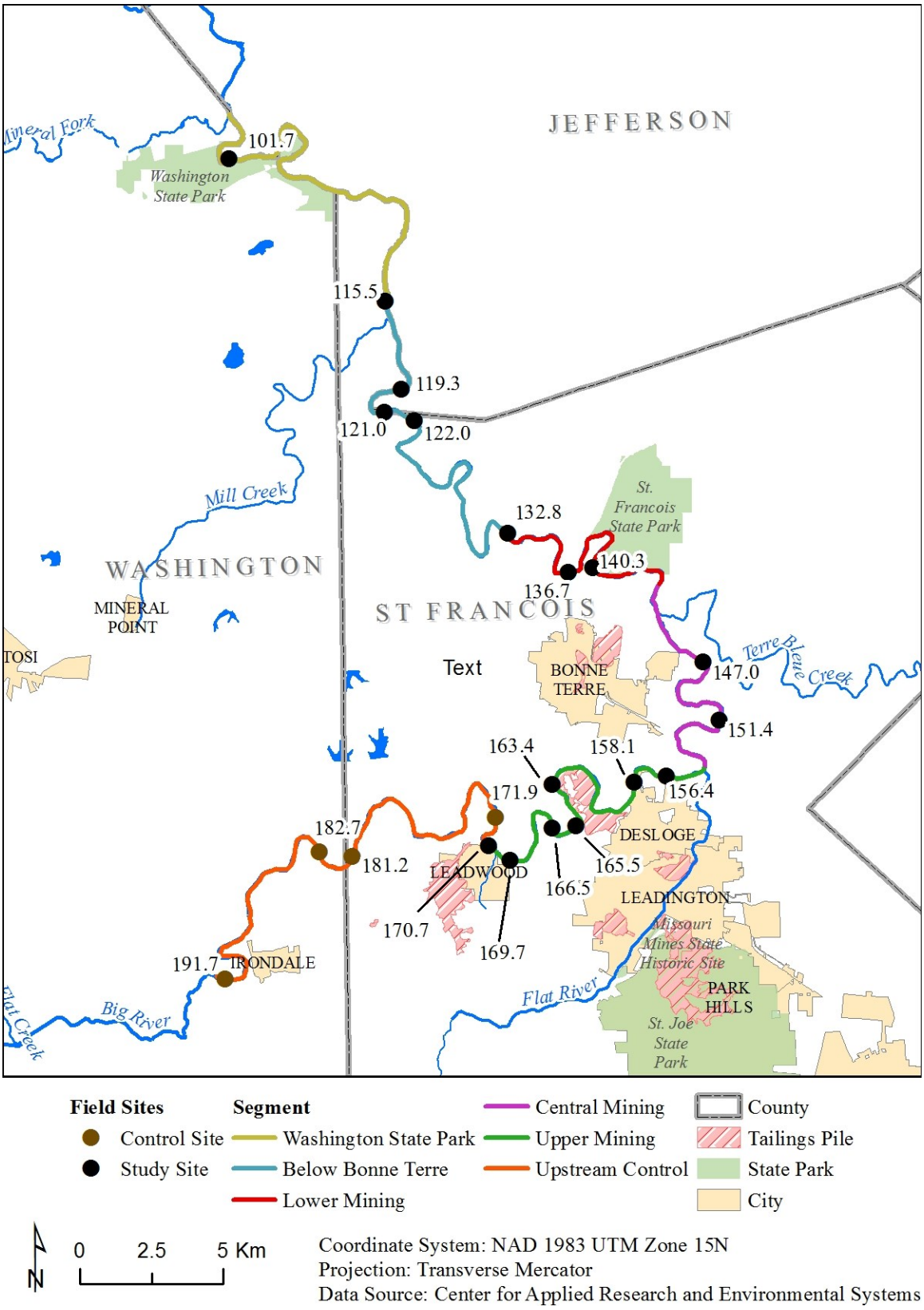

Figure 9. Field site locations in the Big River.

crossing, and two sites are in Missouri state parks. The sites are identified by their river kilometer (R-km), which is the distance upstream from the mouth of the Big River at its confluence with the Meramec River, where R-km = 0.0. The R-km locations were first assigned by Pavlowsky et al (2010) and occur along the centerline of the Big River, which was digitized from 2007 air photos in a geographic information system (GIS). While the mining district is contained entirely within St. Francois County, the control sites extend into Washington County. The sites are located between river kilometers (R-km) 191.7 at the Irondale USGS gage site to R-km 101.7 in Washington State Park along the Jefferson-St. Francois County line. Each site, or reach, was composed of three riffle-pool sequences. One riffle-pool sequence within a reach referred to as a sub-reach in this study. Appendix A gives more detail about the study reaches including their coordinates, drainage area, and descriptive name.

Six segments, each containing at minimum of two study reaches, were defined based on characteristics including uniform drainage area and land use (Figure 10). The six segments are the control segment, starting at R-km 183.5 and running to just above Eaton Branch near Leadwood at R-km 171.5, which is the most upstream point of mining sediment input to the Big River; the upper mining segment from Eaton Branch to just above the Flat River Creek confluence at R-km 155 near Park Hills; the central mining segment from the Flat River Creek to Terre Bleue Creek at R-km 144.5; the lower mining segment between Terre Bleue Creek to Highway E near Bonne Terre at R-km 133; below Bonne Terre from Highway E to just above Mill Creek at R-km 115.5; and the final segment, which runs through Washington State Park to just above Mineral Fork at R-km 99 (Table 3).

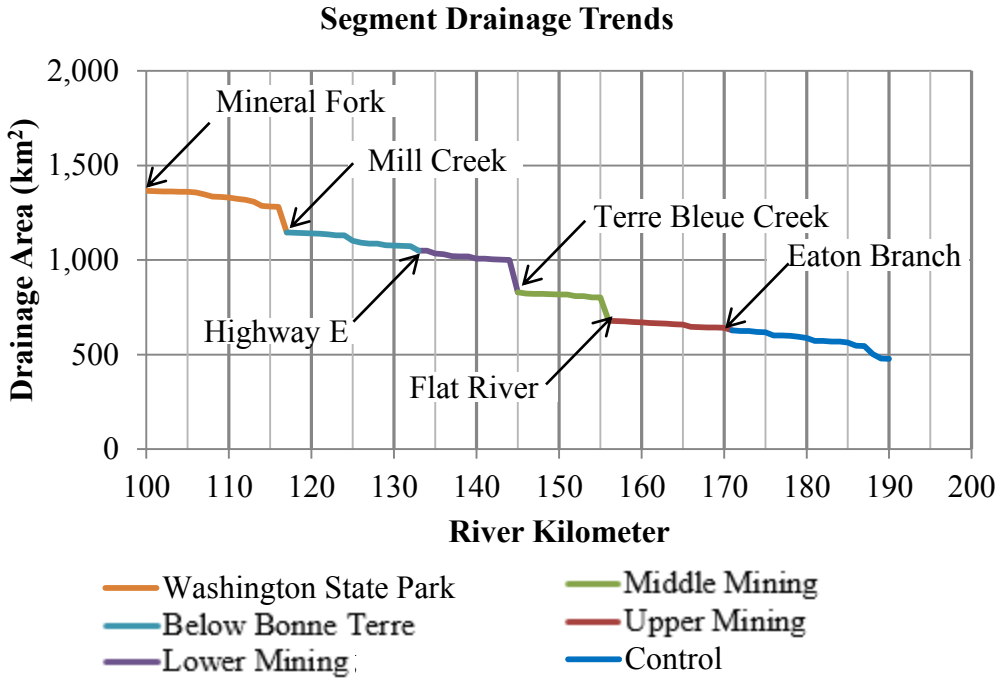

Figure 10. Segment drainage area by river kilometer.

Table 3. Description of the study area segments.

Segment	Length (km)	R-km	Description
Upstream Control	13.0	183.5-170.5	Control to Eaton Cr.
Upper Mining	15.5	170.5-155.0	Eaton Cr. to Flat River Cr.
Central Mining	10.5	155.0-144.5	Flat River Cr. To Terre Bleue Cr.
Lower Mining	11.5	144.5-133.0	Terre Bleue Cr. to Hwy E
Below Bonne Terre	17.5	133.0-115.6	Hwy E to Mill Cr
Washington State Park	16.5	115.6-99.0	Mill Cr. to Mineral Fork

Field Methods

Sediment Sampling. Gravel bar sediment "grab" samples were collected at 17 sites downstream of mining inputs and 3 upstream control sites (Appendix B). Gravel bars were sampled at the surface and subsurface of the bar head, middle, or tail. Surface samples were collected to a depth of 0-15 cm, and sub-surface samples collected at a depth of 15-30 cm. Each bar head, middle, and tail sample was collected at the center of the respective bar position (Figure 11). Materials used to collect the samples were a shovel, gallon zipper bags, and a permanent marker for labeling bags. The location of each sample was recorded with a Trimble GeoXH hand-held global positioning system (GPS) and later imported into an ArcGIS geodatabase.

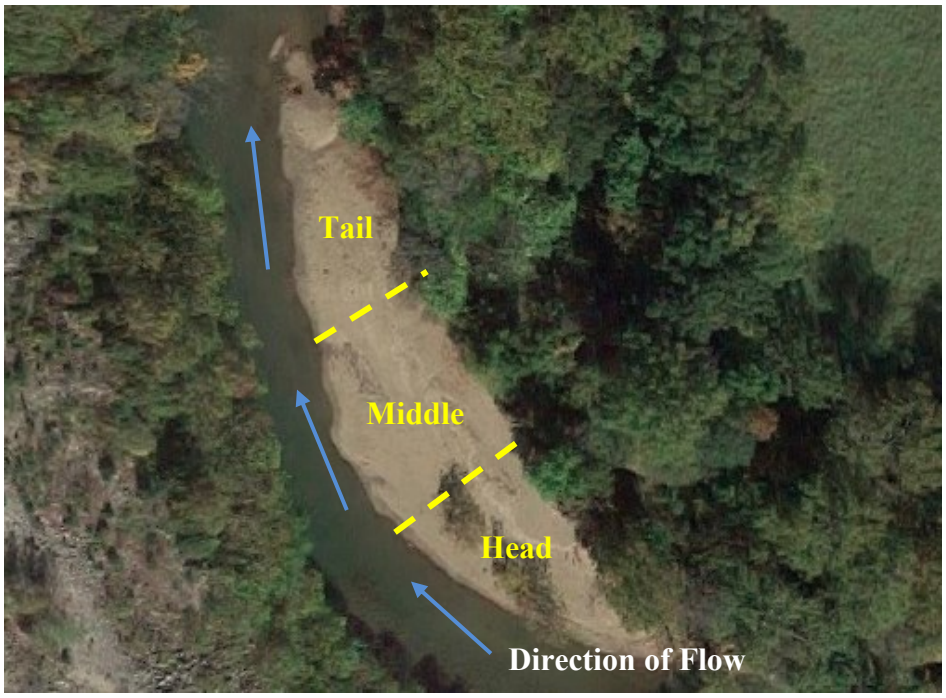

Figure 11. Bar head, middle, and tail positions of a typical point bar.

Pebble Counts. Pebble counts were to determine surface texture of bar deposits. The pebble counts were performed at the bar, if present, of each of the three site sub-reaches using the Wolman method (1954). The equipment used was a standard square-hole gravelometer (Figure 12), a folding ruler, and a paper recording sheet. Following the standard set forth in Bunte and Abt (2001), 30 measurements were taken at each bar head, middle, and tail using a blind-touch method and an average grid spacing of 1-2 m by 1-2 m. The gravelometer was used to determine the sample clast size, which was noted on the recording sheet. In addition to the 30 blind-touch samples, the 10 largest clasts on the bar middle were also measured and noted. Following field collection, the pebble count data was entered into a Microsoft© Excel table for further analysis. Results of the pebble counts are given in Appendix C.

Figure 12. Gravelometer used in pebble counts.

Geomorphic Recovery Assessment. Visual assessments are a useful method for evaluating overall channel condition and evidence for geomorphic recovery (Downs and Thorne, 1996). In this study, a customized qualitative visual assessment was used to measure channel recovery. For every 50 m in a reach the following variables were noted

- GPS location
- Channel bed form characteristics: channel unit, water depth, depth to probe refusal
- Gravel bar characteristics: primary type, high and low bar surface area as a percent of the active channel
- Floodplain characteristics: type and width; bank conditions including angle, presence of under cutting, presence of slumping; presence of islands
- Quantity of large woody debris in channel
- Presence of recovery indicators: lateral widening, bank recession, and floodplain recovery

When assessing recovery factors, each right and left bank pair was assessed on a scale from 0 to 2, with 0 meaning there was no presence of the recovery indicator, 1 meaning it was somewhat present, and 2 meaning it was present. Half numbers were given if the recover indicator was somewhat present (0.5) or present (1.5) on only one side of the river. This information was gathered at an average of 10 points within each study reach along with a photo record of each survey point. The data was then entered into a spreadsheet in Microsoft Excel© and analyzed from upstream to downstream for identification of trends and patterns of degradation and recovery. The full results of the channel recovery assessments are given in Appendix D 1-4.

Probe Depth/Depth to Refusal. In-channel tile probe depth to refusal was first used in the Big River by NewFields (2007) and later by Pavlowsky et al (2010) to

calculate the volume of sediment stored in the channel. In this research, the average probe depth is used to identify spatial patterns of recent bed deposits as evidence for where mining sediment is stored and potential aggradation in the Big River. Depth to probe refusal, that is, the layer at which a resistant layer is detected by inserting a tile probe, can indicate a lag surface representing historical river beds and serve as a good measure of deposition of new/loosely packed sediment on the channel bed. This procedure was performed as a part of the geomorphic recovery assessment every 50 m in each study reach for an average of 10 probes per reach. The equipment used for this procedure was a 1 cm diameter metal tile probe. At each point, the probe was inserted at the thalweg and pushed down as far as possible (to refusal) and both the probe and water depth were measured and recorded.

Cross-Sectional Surveys. A minimum of one cross-section was collected at selected field site using a Topcon auto level, stadia rod, and field book for recording. A metric measuring tape was run from one bank top to the other and points were collected at 10-20 m intervals along the tape. The cross sections were collected at the transition zone between the glide and riffle channel positions, where the channel is typically the most geomorphically stable (Panfil and Jacobson, 2001). These surveys were used to develop a relationship between flow and channel and bar width for air photo correction, described later in this section.

Laboratory Methods

Sample Preparation. Following field collection, samples were brought back to Missouri State University's Department of Geography, Geology, and Planning's

Sediment Analysis Laboratory. Sample bags were opened and thoroughly dried in a 60 ºC oven. Once dry, the samples were disaggregated by manually sieving in standard 1-phi intervals. A mortar and pestle were used to break apart any soil clods. The mass of each size fraction was recorded on a data sheet for later analysis in Microsoft Excel©. After sieving, each sample was divided into sediment larger or smaller than 2 mm. Sediment that was larger than 2 mm was transferred into a labeled gallon bag and moved into storage. Sediment less than 2 mm was placed into a metal-free bag labeled by sample number for geochemical analysis.

Geochemical Analysis. An X-MET3000TXS+ Handheld X-Ray Florescence Analyzer (XRF) was used to perform geochemical analysis of 2 mm or smaller sediment from each sample site (OEWRI, 2007). The XRF is based on energy dispersive X-ray fluorescence technology and uses an X-ray tube as the source of X-rays. It is designed for fast and accurate soil analyses in the field or laboratory. The XRF determines geochemistry using energy dispersive X-ray florescence.

X-rays produced by the instrument bombard the atoms of the target sample. Photons collide with electron shells and electrons move. The movement of the electrons decreases the atom's energy and an X-ray photon is emitted. The energy of the X-ray photon is approximately equal to the decrease in the atom's energy and the X-ray's fluorescence. Each element produces uniquely defined energy changes and the quantities of electrons in various shells are proportional to the number of atoms of the element in the sample. The detector measures the fluorescent X-rays and their produced energies. The net intensities of the X-rays are then converted into element concentrations using

empirical coefficients and linear polynomial multi-parameter regressions derived from the Universal Soils Fundamental Parameters calibration standards.

Samples in this study were measured for a time of 90 seconds. The XRF collects data about 24 common alloying elements and three of these, Pb, Zn, and calcium (Ca), were analyzed in this study. The detection limit for Pb is 15 ppm and for Zn is 8 ppm. As such, it cannot be stated that no Pb or Zn is found in samples with no detection, only that it was below the detection limit. This is indicated in Appendix E as "ND," for not detected.

Geospatial Methods

To assess historical channel bar and planform change, GIS was used to analyze alluvial features over a period of seven decades. Channel banks and bars were digitized from 86 aerial photographs for the years 1937, 1954, 1976-1978, 1990, and 2007. The 1937, 1954, 1970s, and 1990 photographs were collected from the United States Geological Survey (USGS). The 1937 and 1954 photos were provided on a disc by the USGS while the 70s and the 1990 photos were manually scanned in at 600 dots per inch. The 2007 2 ft resolution digital orthophotograph quarter quadrangle (DOQQs) aerials photos were previously georeferenced and were acquired from the Missouri Spatial Data Information Service (MSDIS, 2009). Table 4 summarizes the characteristics of the photographs used in this study.

Rectification Error. It is important to note the error associated with the rectification process in order to validate analyses made from air photo analysis (Mount and Louis, 2005; Hughes et al., 2006). Known points called ground control points (GCPs)

Table 4. Characteristics of aerial photographs used in the study.

Photo Year/Date	Number of Photos	Source	Notes	Resolution (m)	RMSE Range (m)	Mean Point to Point Error (m)
1937, July 23	15	USGS	Black and White Geotiff	0.9	0.2 - 0.9	7.6
1937, July 27	8	USGS	Black and White Geotiff	0.9	0.4 - 0.9	4.1
1937, Aug. 14-15	10	USGS	Black and White Geotiff	0.9	0.9 - 2.3	6.5
1937, Aug. 24	3	USGS	Black and White Geotiff	0.9	0.5 - 0.9	8.6
1954, Oct. 17-18	11	USGS	Black and White Geotiff	1.3	0.4 - 0.9	2.8
1954, Nov. 13-16	11	USGS	Black and White Geotiff	1.3	0.3 - 2.7	4.7
1976, Feb. 23	3	USGS	Black and White Geotiff	0.8	0.3 – 0.9	4.0
1978, Oct. 21	8	USGS	Black and White Geotiff	0.9	0.6 – 0.9	3.7
1990, Feb. 20	7	USGS	Black and White DOQ Geotiff	1.0	0.7 - 1.0	5.8
2007, Mar 8-10	10	MSDIS	True color MrSID leaf-off DOQQ	0.6	Reference Images	

are used to register the image to the earth. The distribution of these points can affect the accuracy of the rectification; if possible they should be evenly spread across the photo area to reduce error (Mount and Louis, 2005; Hughes et al., 2006). During the rectification process, the root-mean-square error (RMSE) was calculated for the rectified photo. The RMSE, based on the Pythagorean Theorem, is calculated for difference between the location of each pair of known and transformed GCP coordinates and is one measure of the error associated with air photo analysis (Hughes et al, 2006). For consistency during the rectification process, the RMSE was kept below 1.0 m where possible, however due to poor resolution of the older photos, some were above this guideline.

A secondary measure of photo rectification accuracy was a point-to-point (P2P) measurement, taken for various points in each air photo to a GCP in the 2007 base-year photo (Hughes et al., 2006). The P2P error is the measured distance between a GCP and the coordinates of the GCP on the rectified photo (Hughes et al, 2006). The average P2P error was 5.02 m. Table 4 shows the mean measured P2P error for each set of photos by date.

Feature Digitization. After rectifying all photographs, alluvial features were digitized using ArcGIS 10.0 in a heads-up digitization method (Figure 13, Figure 14, and Table 5). Digitized channel bars were classified as point, side, center, or delta, as described by Rice et al. (2009). Islands were classified separately from bar forms based on vegetation presence and locational permanence between the various photograph years. To analyze patterns of channel and bar width by river location, channel and valley "cells" were created to summarize the data. After first digitizing the 2007 left and right banks, a

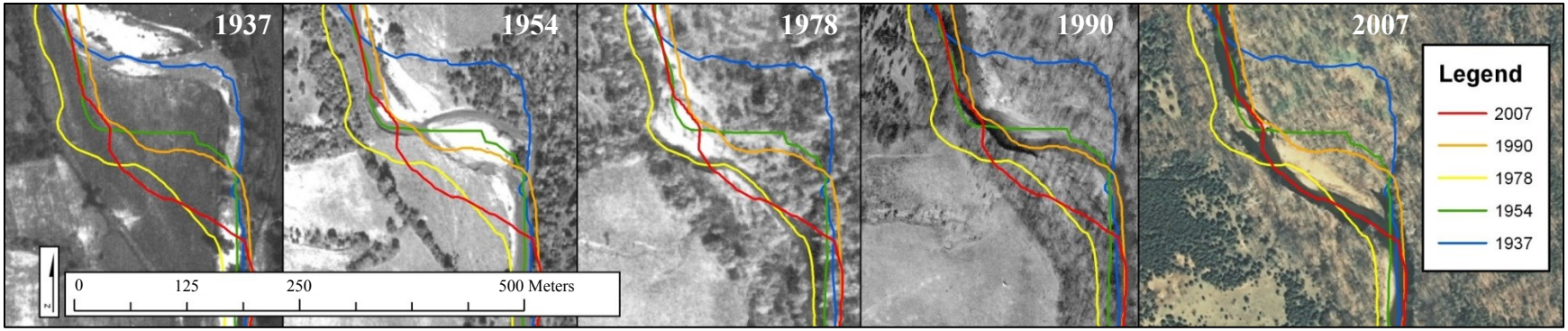

Figure 13. Channel centerline, digitized for all photo years.

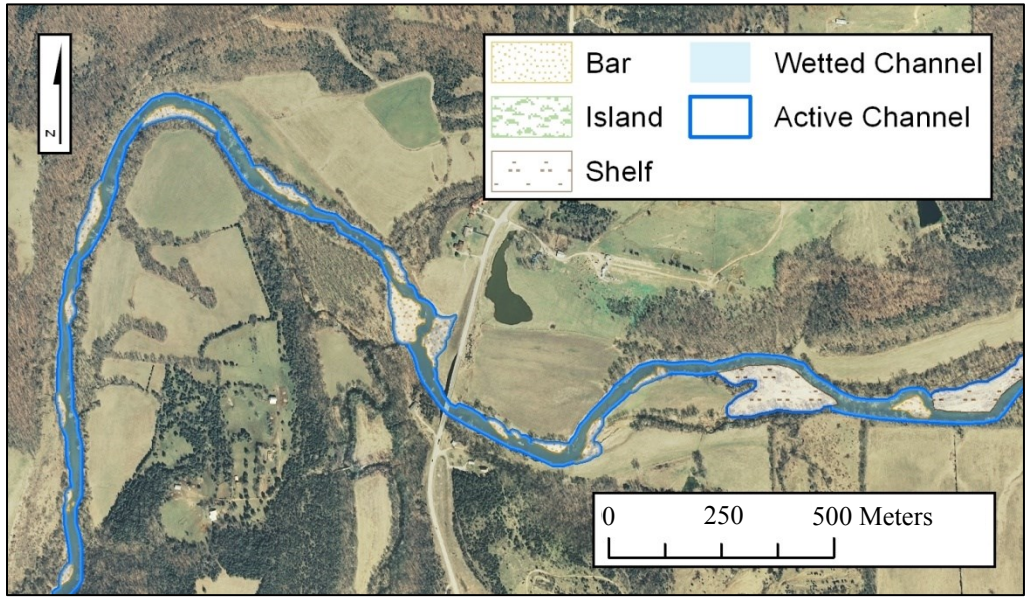

Figure 14. Bar, island, shelf, and channel features digitized in air photo analysis.

Table 5. Digitized channel features.

Name	Type	Description
Left Bank & Right Bank	Line	Edge of banks
Centerline	Line	Centerline of active channel
Active Channel	Polygon	Active area of channel (bars plus wetted)
Wetted Channel	Polygon	Wetted area of channel
Bars	Polygon	Gravel bars, shelves and islands within channel

centerline was created by collapsing the two bank lines into one center line. Points spaced 500 m apart were added along the centerline of the 2007 base year to provide reference locations. The centerline was then buffered by 250 m on each side and channel cells measuring 500 m in length were then created by "cutting" the buffered centerline perpendicular to the centerline at each 500 m point. Results of the 500 m channel cell feature analysis are given in Appendix F. A similar layer for the river valley was created by first determining the valley extent based on topography and hydric soils from the Natural Resource Conservation Service (NRCS) soils GIS data (NRCS, 2011), and then cutting the valley into 500 m cells along the valley centerline. Results of the 500 m valley cell feature analysis are given in Appendix G. Areas of bluff control were noted by comparing the valley and channel locations. Bluff control was noted and considered to be a factor where the historical planform did not vary greatly and where the valley wall was adjacent to the channel for five or more continuous channel cells (2,500 m).

Air Photo Correction. The aerial photographs used in this study vary in location and time and the features digitized from them cannot be compared directly without first

addressing variation in stream discharge (Q) on photo day (Table 6). As stream Q rises, a greater cross-sectional area of the stream is filled with water, causing greater visible channel width and lower visible bar width when viewed in an aerial photograph. The opposite is true during periods of low flow. To account for this error, the GIS-measured channel and bar widths were corrected based on photo day Q and stage.

Cross sections were collected at nine sites in the Big River and Q on the date of collection, corrected for drainage area, was noted for each cross section. The response of bar and channel width for varying Q and stage levels, based on the nearest gage station and corrected for area of drainage, were determined for each cross section. The results were graphed as bar or channel width vs. specific discharge (l/s/km2) and a mean logarithmic equation explaining bar and channel width relative to flow was developed for each (Figure 15 and Figure 16).

The correction was applied to the R-kms covered by each unique air photo using the specific discharge on that date based on the gage nearest the R-kms covered by the air photo. The equations were applied assuming 3.5 m average bar width (that is, how each particular Q would affect a bar of 3.5 m wide) and an average active channel width of 44.35 m (that is, how each particular Q would affect an active channel width of 44.34 m. These averages were derived from cross sectional site average bar and active channel width. For example, a specific discharge of 1.22 l/s/km^2 would result in an expected increase in active channel width from the measured air photo width by 4.53 m based on the equation for active channel width (Figure 15, 44.35-(2.7954*LN(1.22)+39.26) = 4.53). This value was then added to the measured active width in each channel cell covered by that air photo to make the correction. Using this method, the active channel

Table 6. Stage and discharge characteristics of USGS gauges used for air photo corrections.

Discharge and Stage at USGS Gage Stations for Aerial Photo Dates and Selected Flows		Big River at Irondale (R-km drains 453 km^2)		Big River near Richwoods (drains 1,904 km^2)	
		Q (m3/s)	Stage (m)	Q (m3/s)	Stage (m)
90 Percent Exceeds		0.28	0.40	2.86	0.70
Annual Mean		5.32	0.82	20.13	1.47
10 Percent Exceeds		10.39	0.97	37.38	1.86
Photo Year/Date	River kms				
2007 - Mar 8-12	0-186	2.91	0.71	10.40	1.15
1990 - Feb. 20	57-188	6.80	0.87	27.35	1.65
1976 - Feb. 23	64-117	3.06	0.72	10.45	1.15
1978 - Oct. 21	118-189	0.31	0.41	2.52	0.67
1954 - Nov. 13-16	0-131	n/a	n/a	2.44	0.66
1954 - Oct. 17-18	132-184	n/a	n/a	2.89	0.71
1937 - Aug. 14-15	0-136	n/a	n/a	n/a	n/a
1937 - July 27	138-158	n/a	n/a	n/a	n/a
1937 - Aug. 24	159-172	n/a	n/a	n/a	n/a
1937 - July 23	173-186	n/a	n/a	n/a	n/a

and channel bar widths were adjusted for each 500 m cell for all data digitized from photos prior to 2007 (the base year) based on Q on the date of the aerial photo from which the feature was digitized.

The importance of addressing these flow corrections is substantiated by the relative percent difference between the field measurements and the 2007 air photo

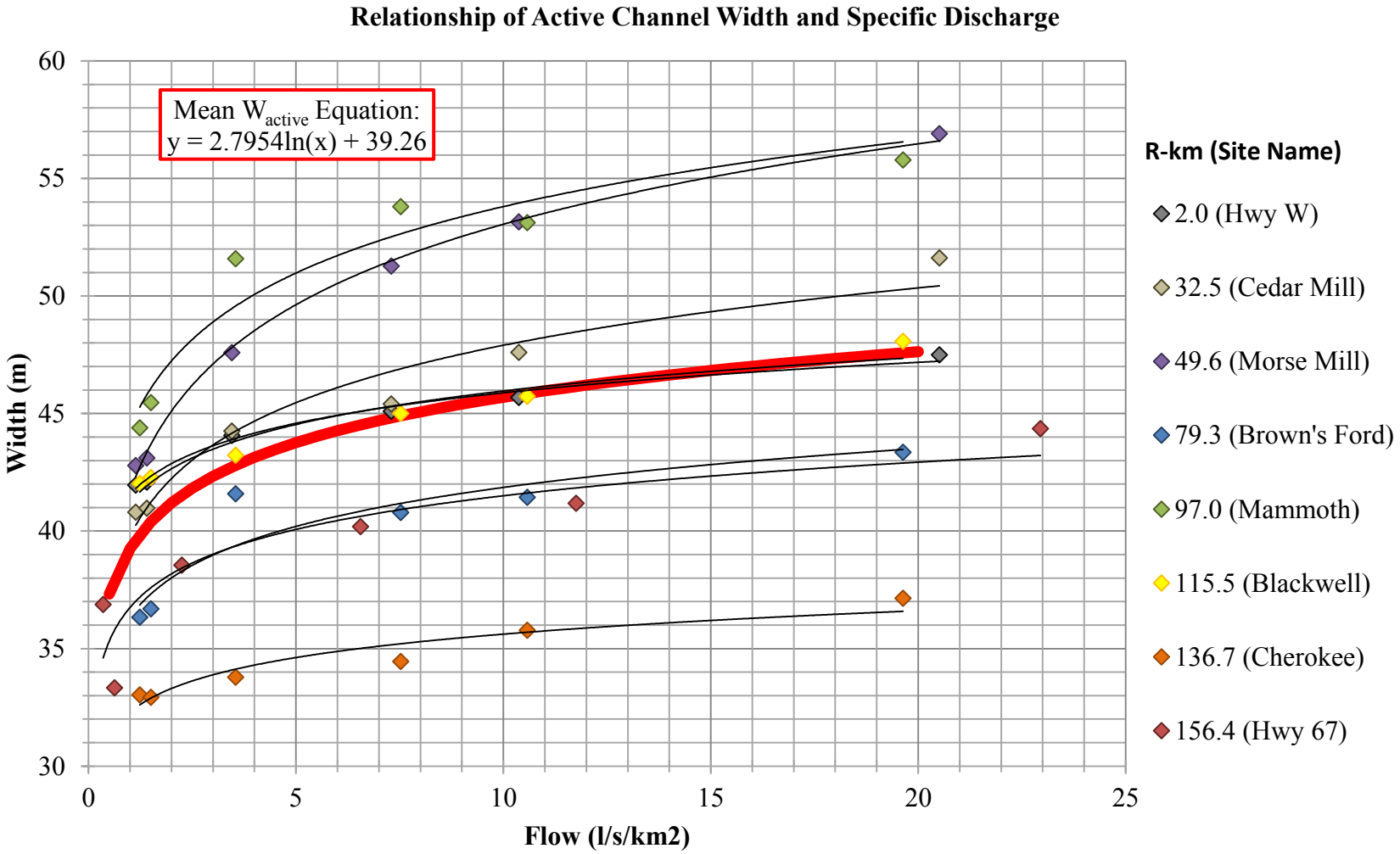

Figure 15. Relationship of active channel width to specific discharge at field cross sections.

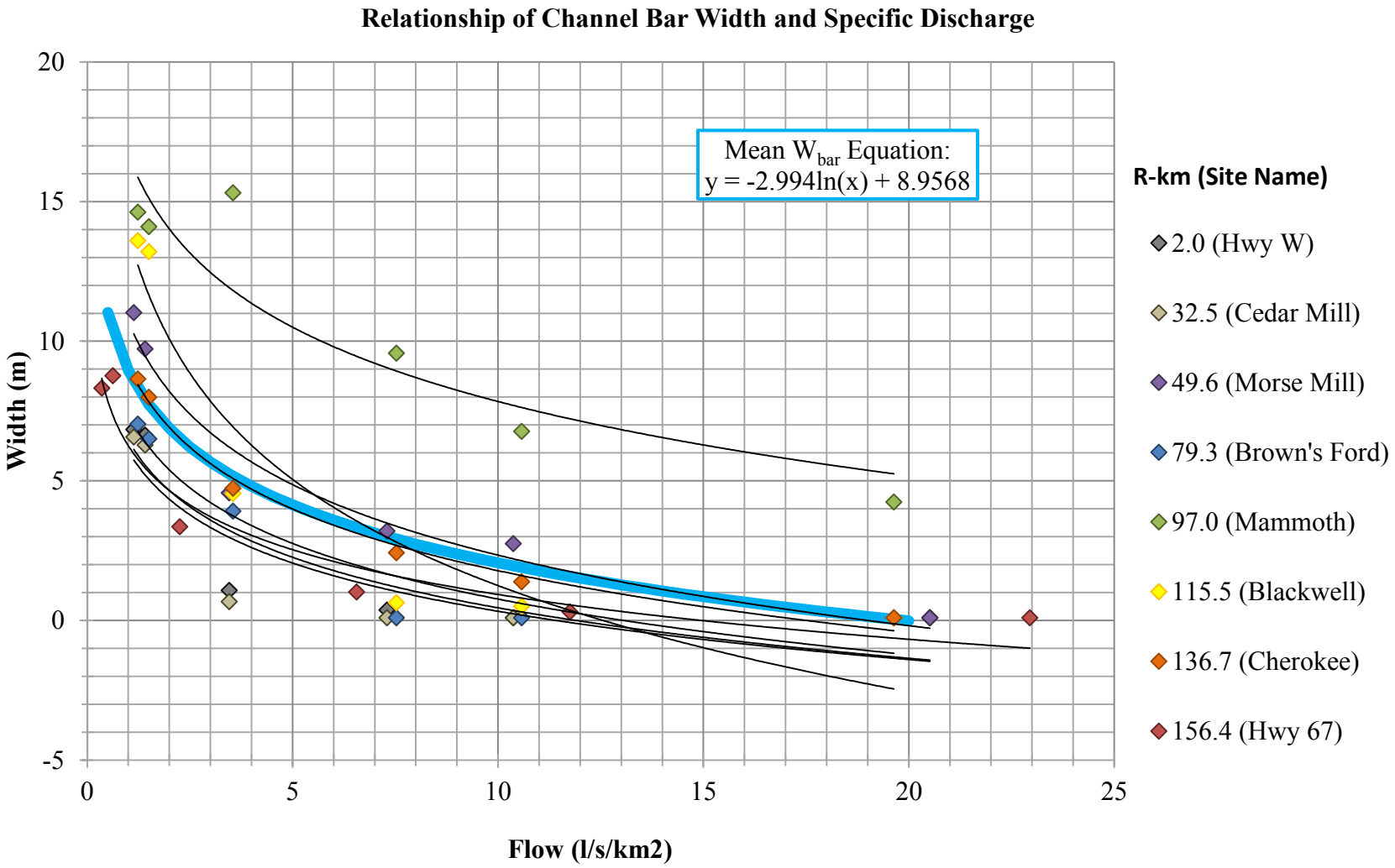

Figure 16 Relationship of channel bar width to specific discharge at field cross sections.

measured bar and channel width at those sites. The difference in measured active width of the field and air photo measurements at a site ranged from as little as 1 percent to as high as 85 percent with an average of 16 percent. Relative percent difference in bar widths between field and photo measurements ranged from 0.1 to 27 percent, with an average of 5.8 percent. When field measurements were corrected to the 2007 photo day Q, the relative percent difference for active channel and bar width was reduced to an average of 9.7 percent and 5.3 percent, respectively.

Changes in Hydrology. Yet another consideration in geospatial analysis for this study was to examine the changes in hydrology between the most recent air photo and the time that sediment grab samples were collected. The most recent photo used in the air photo analysis was dated March 10, 2007, while sediment grab samples were collected between October 2008 and December 2011. It is important to look at the trend in hydrology during this "gap" period to assess how sediment sample analysis results may be related to the 2007 bar geospatial analysis.

The USGS gage stations at Irondale and Richwoods were examined for hydrological trends during the gap period (USGS, 2012a, 2012b, 2012c). At both gages, flow during the gap period was within normal parameters when compared with the total record of each gage. At Irondale, 12 percent of days in the gap period had Q greater than the 10 percent exceedance based on the historical record (1965-2011), with four days having Q greater than bankfull (defined as the 1.5 year recurrence flood). No days exceeded the 5-yr flood Q. At the Richwoods gage, 12 percent of flows were greater than the 10 percent exceedance (1949-2011), with 10 days having greater than bankfull Q and 1 day having greater than the 10-year flood Q. Notable high flow events occurred at both

gages in March and April 2008, May and October 2009, and April 2011. During bankfull floods only about 20-30 percent of the bed is actively transporting sediment, while during the 5 year or greater flood up to 100 percent of the bed may be transporting material (Ashmore, 2011; Wilcock et al., 2009). This indicates that while hydrology in the gap period may have mobilized some sediment, the channel should not have experienced a significant reworking of bar and bed forms.

CHAPTER 5: RESULTS AND DISCUSSION

The objectives of this study are to determine reach and bar scale variability of Pb content and sediment size; relate bar form, sediment size, and contaminants to mine locations, long-term sediment transport trends, and channel morphology; and to evaluate the potential for both natural channel and sediment recovery. To meet these objectives, current and historical sediment conditions were examined. Aerial photographs were used to analyze present-day and historical active channel and bar width. Sediment samples were analyzed to determine variability of geochemistry by grain size, location downstream of mining, and location on the gravel bar. Patterns in sediment at the sub-bar scale will help to identify segment scale variations and the distribution of mining sediment within them. This information, along with an in-channel qualitative geomorphic assessment, will aid in the determination of whether there is evidence for geomorphic recovery and what the management implications are for long-term restoration of in-channel sediment.

Characterization of Gravel Bars

Bars in the Big River range in size and shape and are affected by several variables including sediment size and volume, tributary inputs, location relative to mining, and valley and bluff control. Figure 17 shows the downstream patterns of bar types in relationship to each other, valley width, bedrock control, and tributary inputs. Side or alternate bars are the most common in the Big River, while delta bars, which are only present at tributary inputs, occur less frequently. Point bars tend to occur in areas where

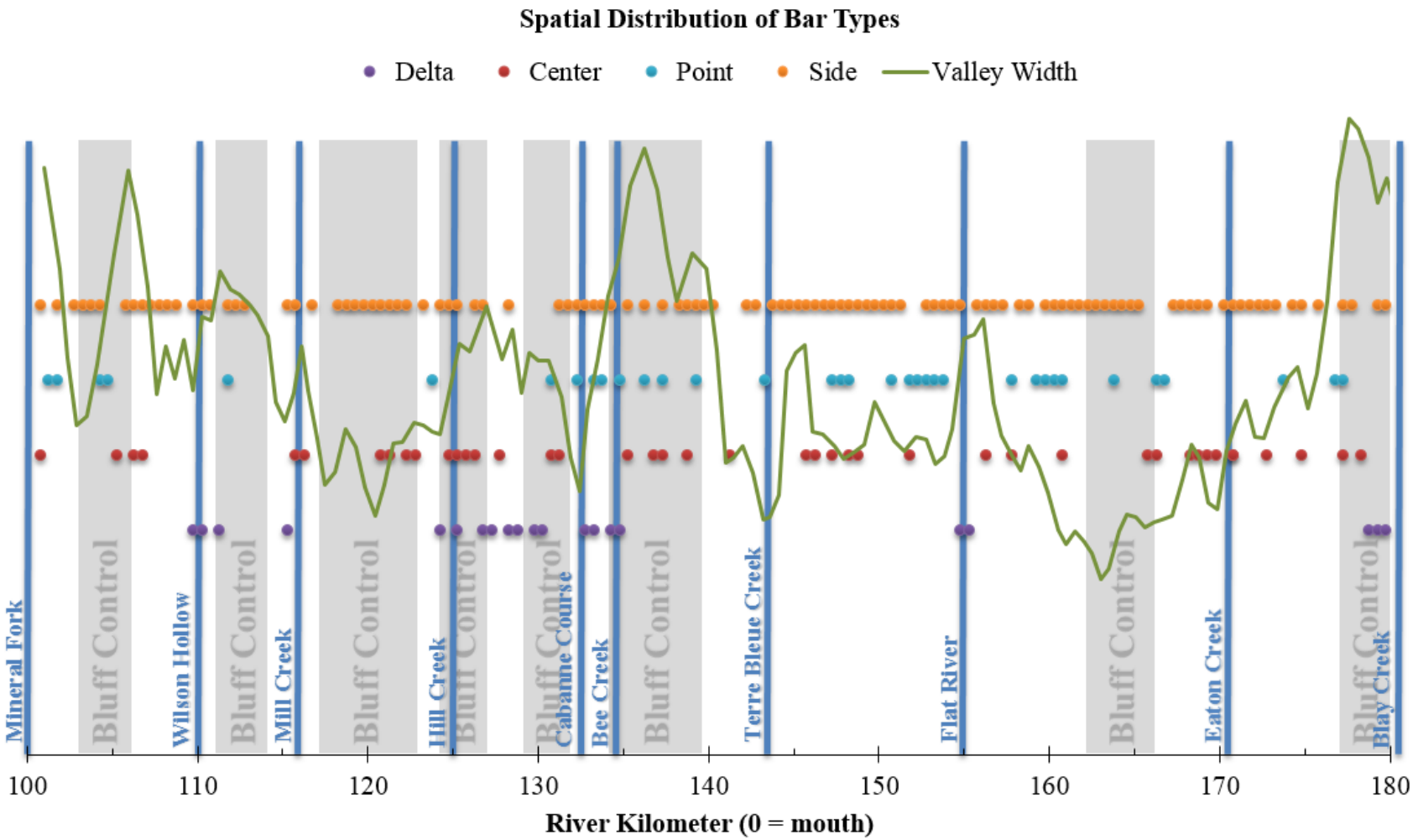

Figure 17. Location and type of individual bar units relative to valley width, bedrock control, and stream tributaries in the Big River.

the valley is wide, sinuous, and there is little bluff control, primarily upstream of R-km 130. Center bars are well-distributed throughout the study area.

The quantity, total and average size, and spacing of each bar type is detailed in Table 7. Side bars are the most common by more than two times the next common bar type in the Big River. Side bars also have the closest unit spacing at an average of 1,798 m between side bar units. Center bars are half as common as side bars and significantly smaller in unit size than all other bar types at an average of 920 m^2. Delta bars, which indicate sediment inputs from tributaries into the Big River, are the most uncommon, yet are the second largest in unit size.

Table 7. Bar quantities, area, and spacing in the study area.

Bar Type	Count	Total area (m2)	Average Bar Size (m^2)	Average Spacing (m)
Side	123	391,692	3,184	717
Center	48	44,147	920	1,798
Point	37	94,487	2,554	2,347
Delta	27	143,035	5,298	3,288
Totals	235	673,361	2,989	2,038

Bar patterns by segment are shown in Table 8. The control segment has the highest total and average bar area and highest bar density, although the number of individual bars per kilometer is lower than in central mining. Interestingly, while the central mining segment has the highest density of bars per km and the lowest spacing

Table 8. Characteristics of gravel bars by segment.

Segment	Segment Length (km)	Total # of Bars	# of Side Bars	# of Center Bars	# of Point Bars	# of Delta Bars	Density of Bars (bars/km)	Average Bar Spacing (m)	Total Bar Area (m^2)	Average Bar Area (m^2)	Bar Area per km (m^2/km)
Washington State Park	14.5	40	23	6	6	5	2.8	449	116,055	2,901	8,004
Below Bonne Terre	17.5	48	23	13	3	9	2.7	372	114,699	2,390	6,554
Lower Mining	11.5	30	15	5	7	3	2.6	379	106,495	3,550	9,260
Central Mining	10.5	35	19	6	9	1	3.3	294	60,642	1,733	5,775
Upper Mining	15.5	42	24	9	8	1	2.7	366	130,421	3,105	8,414
Control	14.5	40	19	9	4	8	2.8	372	145,049	3,626	10,003
Total	84.0	235	123	48	37	27	2.8	372	673,361	2,884	8,016

between bars, it has the lowest total and average bar area. Low average bar area but high density indicates that the central mining segment contains frequent but small gravel bars.

Downstream Pattern of Bar Area. Figure 18 shows 2007 total bar area as a three-point moving average, that is, each point is an average of bar area over three consecutive 500 km channel cells. The segments with the lowest average bar area occur in the upper (R-km 183.5 - 155) and central mining (R-km 155-145.5) segments. Higher peaks in average bar area are noticeable both in the control region above R-km 170.5 and in the lower mining and downstream segments below R-km 145.5. Bar area decreases below Flat River (R-km 155) before increasing again just above Hwy E north of Bonne Terre. In addition to influencing bar type, tributary input also plays a role in bar area as they carry upland sediment into the main stem of the Big River. Historically Eaton Branch carried in sediment from the Leadwood tailings pile, while Flat River Creek carried mining sediment from the National, Federal, and Elvins piles. The Desloge pile is located inside a large meander between R-km 165-160. The Bonne Terre pile drains to the Big River from several points between R-km 145 and Turkey Creek at R-km 136

The downstream trends of different bar types were also examined. Side bars tend to fluctuate throughout the study area, with no one area peaking or dipping significantly from others (Figure 19). Alternating side bars are a common feature of Ozarks streams (Jacobson, 2005). Center bars, while much less common, are also evenly distributed throughout the study area, with no one reach having a significant increase or decrease over others (Figure 20). Recall that center bars can be evidence of channel aggradation due to excess sediment (Hooke and Yorke, 2011). Point bars have a larger area in the upper reaches and decrease with distance downstream (Figure 21).

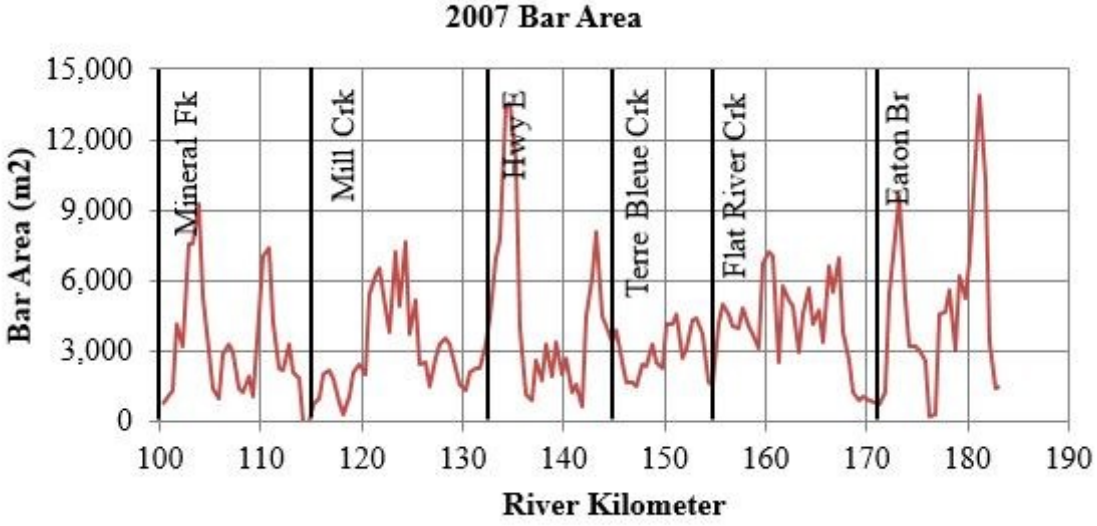

Figure 18. Total bar area in each 500 m channel cell, shown as a three-point moving average.

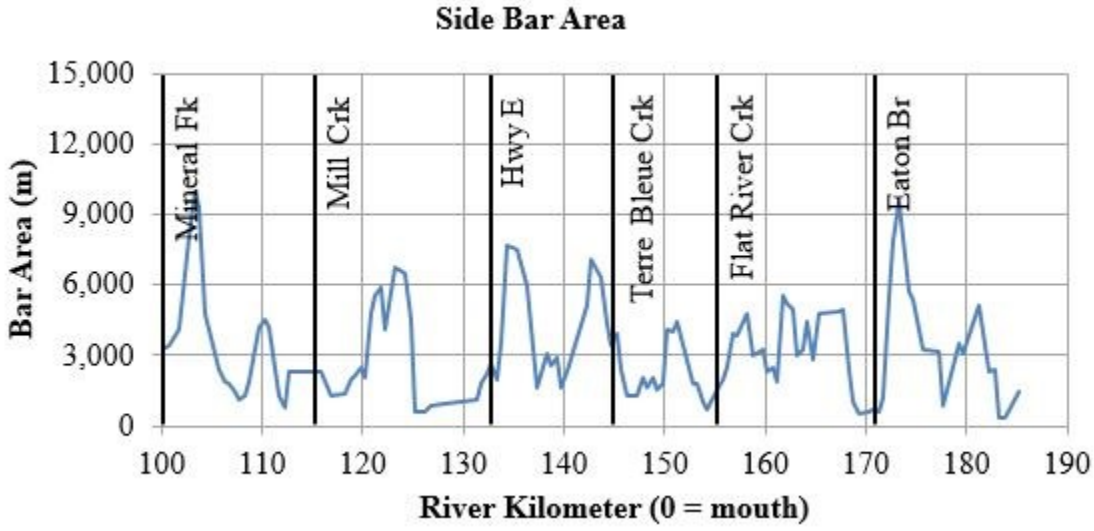

Figure 19. Side bar area in each 500 m channel cell, shown as a three-point moving average.

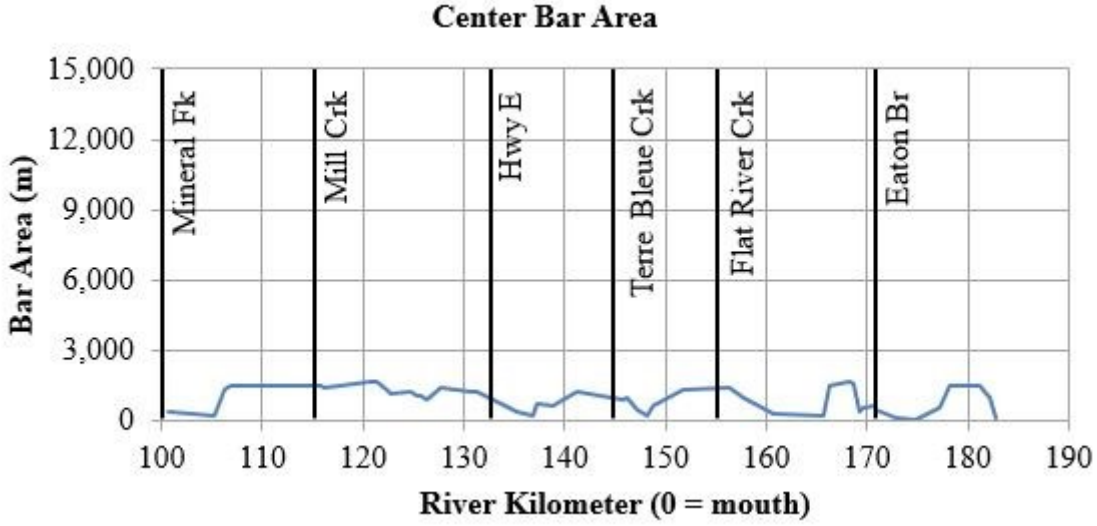

Figure 20. Center bar area in each 500 m channel cell, shown as a three-point moving average.

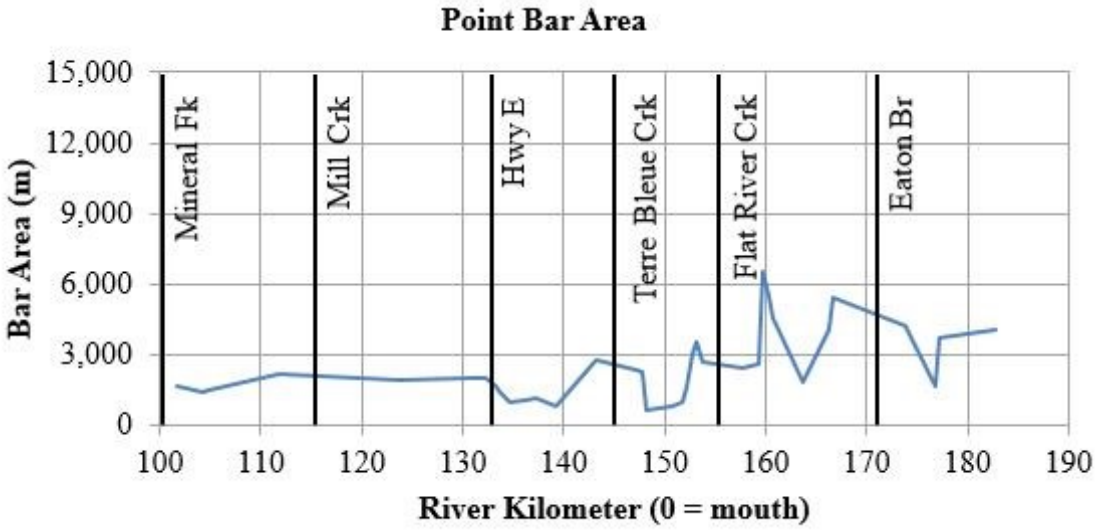

Figure 21. Point bar area in each 500 m channel cell, shown as a three-point moving average.

Relationship of Bar Width and Channel Morphology. Average bar width is particularly high between R-km 130 and 140 (Figure 18), which coincides with a wider average valley width than above and below that range (Figure 22). To examine the relationship between bar area and valley width further, bar width was compared with current and historical valley width within each 500 m channel cell for both current and historical data (Figures 23-25). Where bar area is smallest, valley width tends to be relatively narrow. There is a slight positive correlation between bar width and present-day valley width (Figure 23).

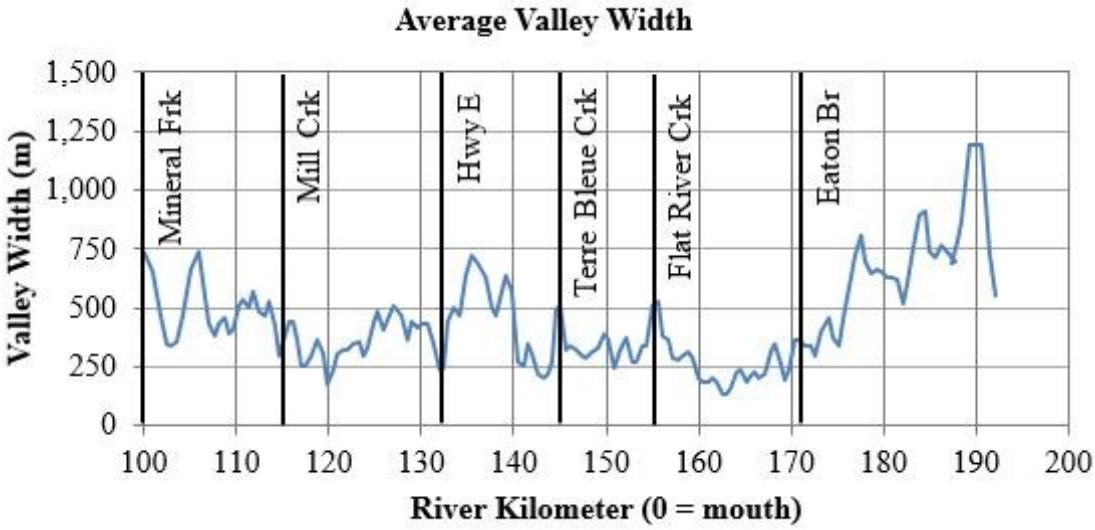

Figure 22. Average valley width, shown as a 3-point moving average.

When compared with historical active width, the relationship becomes stronger, although the r^2 value is still quite low (Figure 24). Historical active width is the area the active channel has meandered within between 1937 and 2007 based on air photo digitization of the channel. Areas where the historical active width is wide indicate

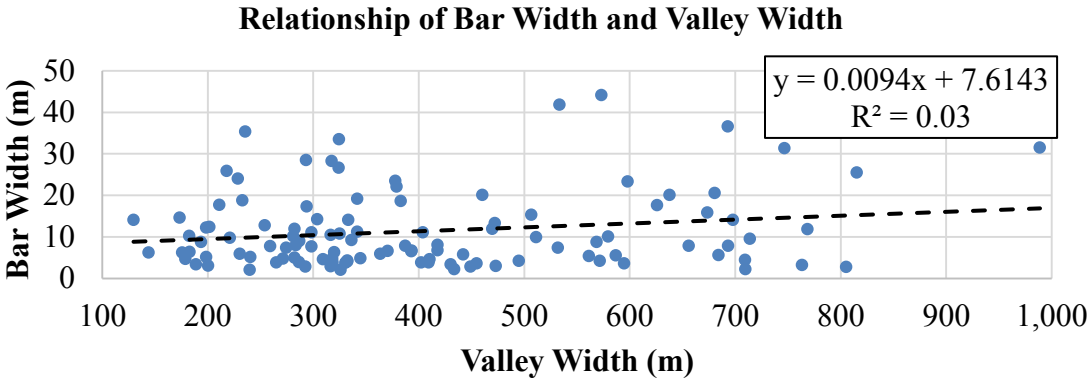

Figure 23. Relationship of 2007 bar width and 2007 valley width, cells with no bars removed.

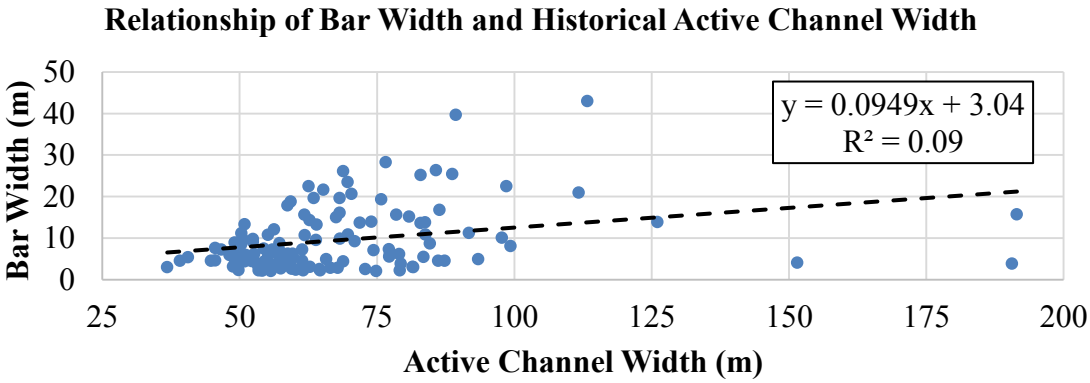

Figure 24. Relationship of 2007 bar width and historical active width.

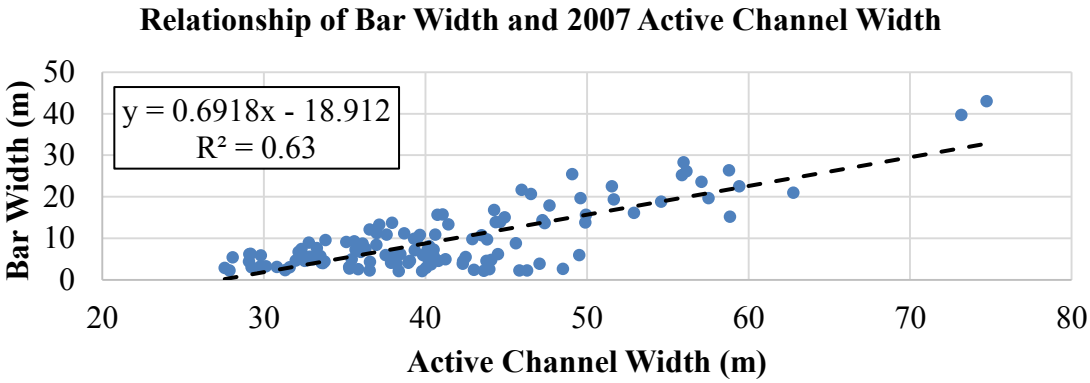

Figure 25. Relationship of 2007 bar width and 2007 active channel width.

dynamic channel planform changes over the 70-year period. Those reaches where the historical channel is narrow have remained stable; lateral channel migration is limited and depositional area is reduced in these reaches. A few channel cells have experienced significant channel migration, and removing those outliers increases the relationship between historical channel widths and current bar width to an r^2 of 0.22.

As expected, bar width in the Big River is most closely associated with active channel width, with which it has a positive correlation and r^2 value of 0.63 (Figure 25). This is expected, as wider channels where bed slope and flow velocity decrease and sedimentation and bar formation increase compared to narrow channels (Panfil and Jacobson, 2001). The relationship of 2007 bar area to historical active channel width is much weaker than the relationship between 2007 bar area and 2007 channel width, suggesting that present-day bar area is closely tied to present-day channel morphology rather than historical trends.

Historical Trends in Bar Size & Distribution. While average bar area varies downstream, the general location of bar area peaks and scarcities has remained relatively consistent over the 70-year study period (Figure 26). These patterns suggest that persistent geomorphic variables such as local geology, valley width, and hydrology control over-all bar area over long-term periods. Above the Highway E bridge there is a persistent peak in bar area, and a deficit downstream of the bridge. Structures such as bridges can cause constraints in hydraulic patterns and affect channel changes (Jacobson, 1995), and that is likely the case at Highway E.

Bar area in the Big River has fluctuated over the past 70 years (Figure 27). Bar area tended to decrease between 1937 and the 1970s. This was consistent across all

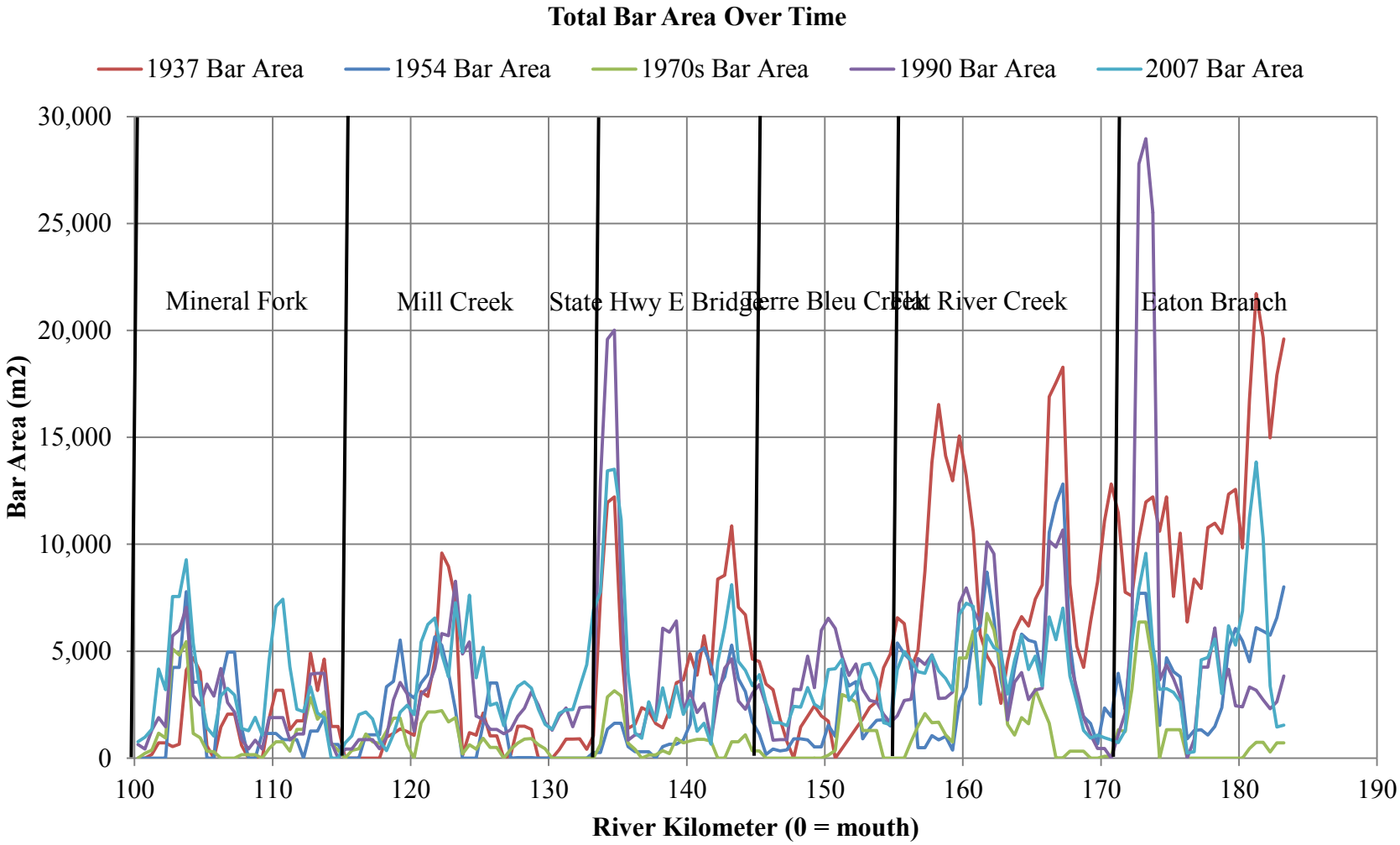

Figure 26. Bar area changes over time, shown as a three-point moving average.

segments of the river but is most pronounced in the upstream control and upper mining segments. Notably, bar area for the two most downstream segments remained relative stable from 1937 to 1954. Both decreased by the 1970s. For all segments, bar areas increased in 1990 and remained relatively stable through 2007. Bar area in the upper mining and upstream control is remarkably high in 1937 and stabilizes after a significant decrease between 1937 and 1954. These segments may have been influenced by other erosion-causing land use activities, such as the clearing of uplands.

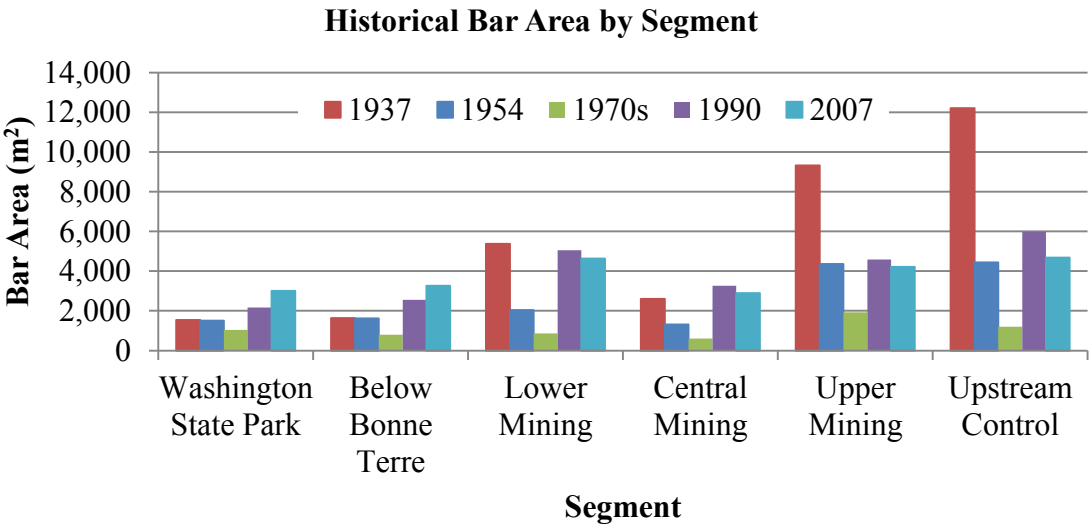

Figure 27. Historical mean bar area by segment, 1937-2007.

Bar area is highest in the upper reaches of the Big River in most years, peaking above mining in control sites and decreasing with distance downstream. However, distribution of bar area changed throughout the 1900s. While bar area remained high in upper reaches, increases in bar area can be seen in the central and lower mining segments by the 1990. The lowest segment, between R-km 100 and 133 (Washington State Park

and Below Bonne Terre) show an increase in bar area between 1990 and 2007, while all other segments show a decrease.

Implications of current and historical bar area trends. Historical aerial photograph analysis in this study revealed that bar width is most closely tied to current-day channel width; where the active channel is wide, the bar area is also wide. Bar area is much lower in the central mining segment with smaller, more frequent bars than other areas. Recall that Ozark streams are comprised of alternating stretches of straight stable reaches and sinuous active reaches (Jacobson, 1995; Martin and Pavlowsky, 2011). In the upper mining segment, sinuosity is the lowest of any other segment, while the downstream central mining segment is slightly higher in sinuosity (Figure 28). This suggests that these segments may be characteristic Ozarks stable segments, which tends to transport sediment rather than store it in large complex bar formations. It is known that mining in the Big River watershed has altered the sediment supply of the Big River (NewFields, 2007; Pavlowsky et al. 2010). This study confirmed those findings, showing that historical bar area peaked in 1937. This coincides with the end of mining techniques that resulted in mining chat of 4-16 mm in size. Chat sized tailings were no longer being produced and would only be mobilized by flood events thereafter.

Following this initial sediment influx, bar area decreased in all segments between 1937 and the 1970s. This may be due to the initial sediment wave attenuating and stabilizing, moving into storage in floodplains and becoming vegetated, where bars would not appear to be active bar in air photo analysis. By the 1990s bar areas were on the rise again. One possible contributor to this event is described in NewFields (2006), who noted that a large flood event in 1977 caused the release of over 50,000 m^3 of

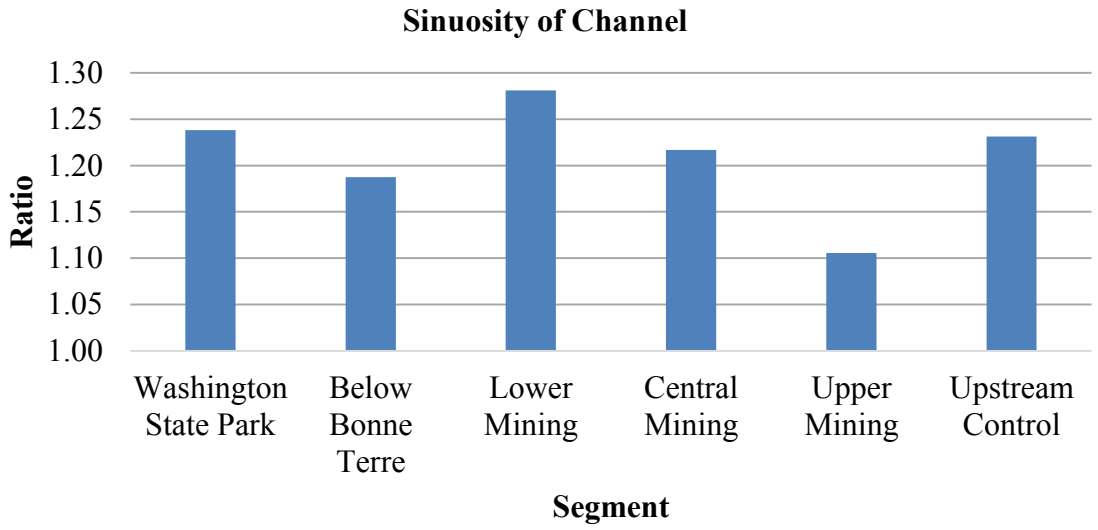

Figure 28. Channel sinuosity by segment.

mining sediment from the Desloge pile to the Big River. Large flood events in 1973 and 1986 would have also mobilized a large volume of bed sediment. The increase was greatest in the central and lower mining segments (refer back to Figure 26 and Figure 27). The largest storm event in the history of the Irondale and Richwoods gages occurred in the fall of 1993, and a period of lower annual peak flows followed through the 2007 photo year. Altogether bar area in 2007 is smaller than in 1937 with the exception of the most downstream segments, suggesting that the sediment wave sediment may be beginning to migrating downstream.

Increased flood frequency in the Ozarks due to climate change may reactivate stored bar sediment and bank materials and increased bar area as sediment is mobilized for transport. Studies have found that precipitation events have been increasing over the past 30 years in the Midwest (Winkler et al., 2012; Mallakpour and Villarini, 2015). Coupled with increasing average temperature, flood frequency is also increasing in the

Midwest (Mallakpour and Villarini, 2015). While flood peaks are within historic norms, the increasing frequency of flood events would cause more frequent bed sediment mobilization and transport. This may account for the upswing in bar area between the 1970s and 2007.

Downstream Bar Texture and Geochemical Variability

During this study, 95 bar samples were collected and analyzed for particle size and geochemistry, specifically Pb, Zn, and Ca content (Appendix E). The samples were composed of 22 surface samples at a depth of 0-15 cm and 73 subsurface samples at a depth of 15-30 cm. There were 21 samples taken from the bar head position, 39 from the bar middle, and 35 from the bar tail. The full results of the analysis for each sample are given in Appendix E.

Sediment Mineralogy Trends. The sediment in the Big River is from a combination of natural and mining sources (Pavlowsky et. al., 2010). The distribution of these sources may vary with sediment size since finer sediments are more mobile than chat-sized and larger sediment (Hjulström, 1939). In addition, the chemical makeup in the various sediment size fractions can indicate the quantity of sediment that is derived from lead mine tailings. Observations by Pavlowsky et al (2010) determined that sediments in the 4 – 8 mm size fraction at control sites were greater than 95 percent naturally sourced weathered chert and feldspar grains. Further, no dolomite was present in the channel bed in control sites. Conversely, laboratory tests indicate that 100 percent of mine tailings sampled from the Leadwood, Federal, and National tailings piles were composed of dolomite (NewFields, 2006). Levels of Pb and Zn are well below the PEC at

control sites, yet sediment from tailings piles contains from 1,200 to 9,900 ppm Pb (Pavlowsky et al., 2010). This indicates that the Pb and Zn concentrations described below are associated with sediments that can be traced back to mining sources.

Geochemical Trends. Low concentrations of carbonate minerals were found in channel sediments at the control sites above mining influence. Uncontaminated channel sediment tends to contain silicate minerals such as feldspar and chert. However, sediments affected by mining inputs usually contains relatively high fractions of dolomite ($CaMg(CO_3)_2$) released from ore processing of the Bonne Terre Dolomite host rock (Pavlowsky et al., 2010). Calcium concentrations in the control area are less than 8,015 ppm with an average of 3,185 ppm. Below mining inputs, Ca peaks at 164,338 ppm at R-km 147 and has an average of 89,490 ppm. Concentrations decrease with distance from the mining area. Calcium concentrations are highest between R-km 160 to 140 (Figure 29 and Figure 30). Standard deviation bars shown in Figure 29 indicate that the variability of Ca concentrations are very low in control sites, suggesting little dolomite composition in those samples and confirming previous studies.

Sediment Pb content also has a strong correlation with distance from mining sites (Figure 31 and Figure 32). Lead concentrations in <2 mm size fractions in control sites range from below the detectable level (15 ppm) to 47 ppm. Below mining Pb concentrations are as high as 2,322 ppm at R-km 158, more than 18 times the PEC. Only one of 86 below-mining samples is below the PEC, which occurs at R-km 115. This appears to be an anomaly, however, as the site average is 327 ppm. Variability was highest at R-km 146.9, ranging from 771 ppm to 2,244 ppm. This site is below the tributary input of Flat River Creek, which transported tailings from the Federal,

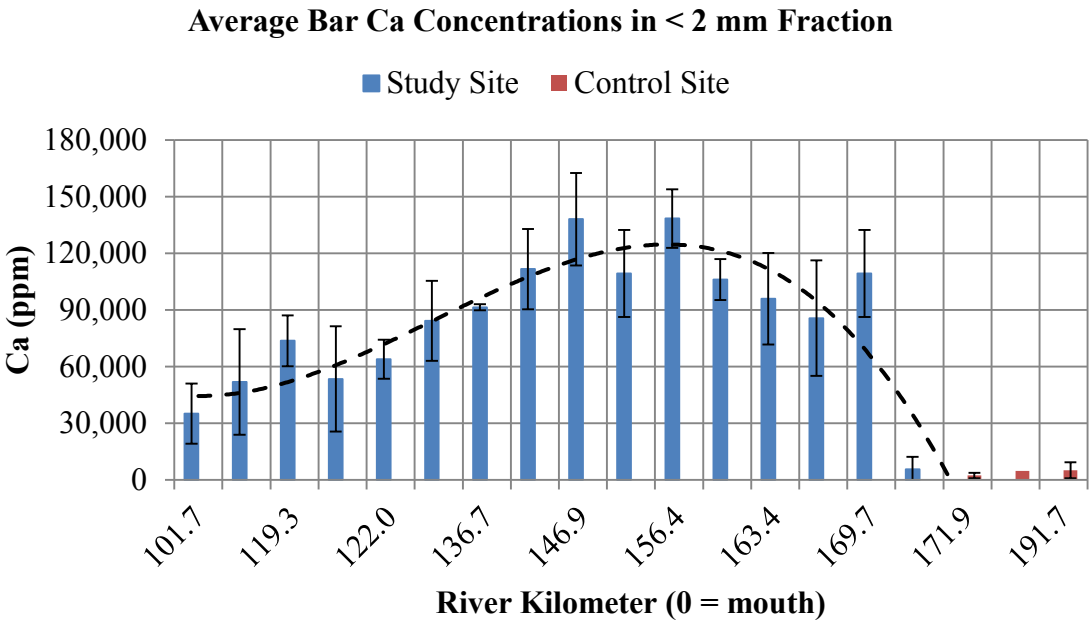

Figure 29. Bar Ca concentrations in the sand-sized (<2 mm) fraction by site average.

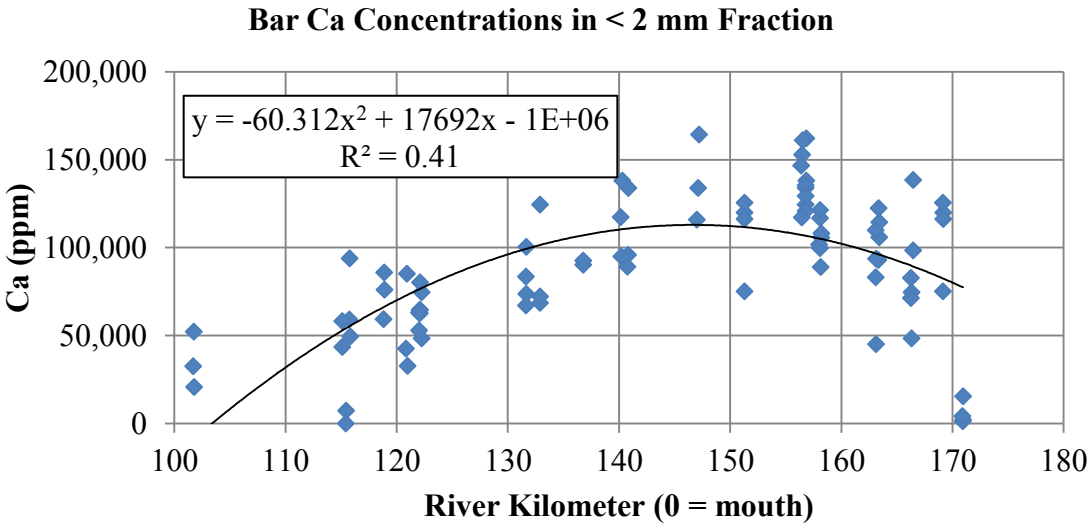

Figure 30. Scatter plot of bar Ca concentrations in the fine size fraction

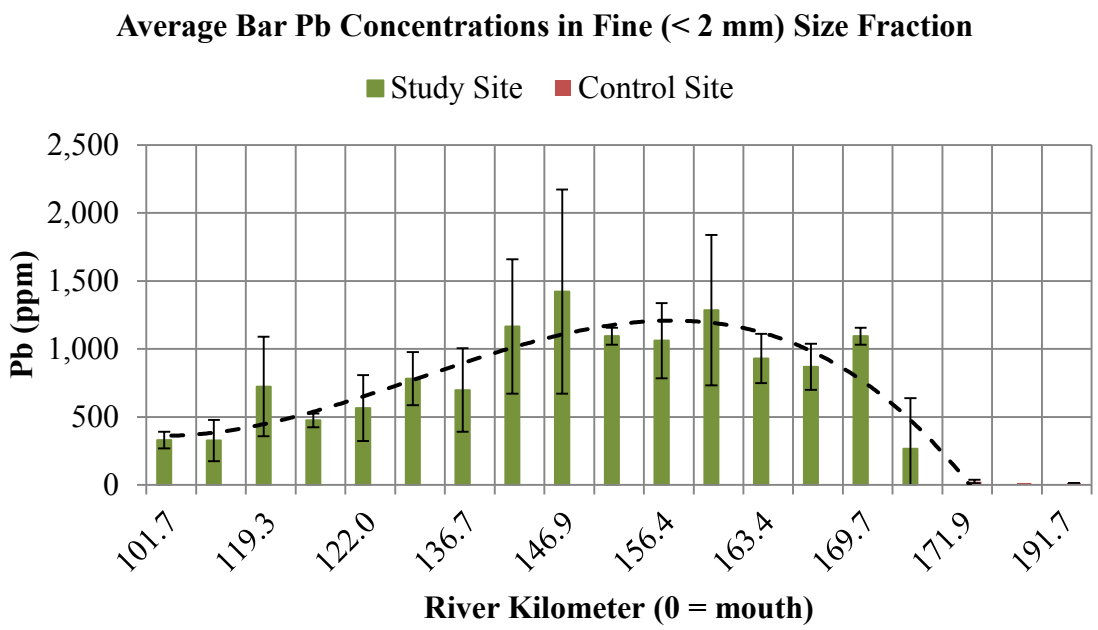

Figure 31. Bar Pb concentrations in the fine size fraction by site average.

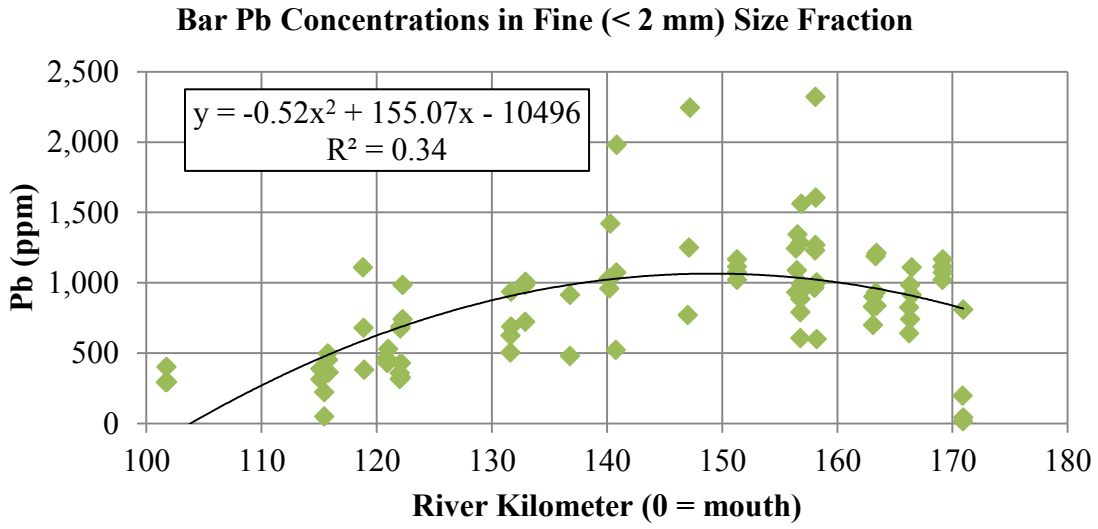

Figure 32. Scatter plot of bar Pb concentrations in the fine size fraction.

Elvins/Rivermines, and National tailings piles (Pavlowsky et al., 2010). Lead concentrations decrease to an average of less than 500 ppm by R-km 115. Although Pb levels drop of rapidly below R-km 140, previous studies including Pavlowsky et al. (2010), and Roberts et al. (2009) found samples above the probable effects limit of 128 ppm Pb throughout the entire Big River to its confluence with the Meramec River at R-km 0.

Bar Zn concentrations in the < 2 mm size fraction are also closely related to mining sediments. While control site Zn concentrations ranged from 9 to 72 ppm with an average of 35 ppm, samples in the mining area are significantly higher, averaging 1,265 ppm in between R-km 170.5 and 133.0 (Figure 33 and Figure 34). Zinc concentrations are highest just below Leadwood (R-km 170). This correlates with findings by Pavlowsky et al. (2010) who examined tailings from the Leadwood tailings pile and noted that it contains sediment with particularly high Zn concentrations, which also result in low Pb:Zn ratio compared to other upper Big River tailings piles. In the <2 mm size fraction, the Zn concentrations decrease at a faster rate than Pb concentrations, resulting in a higher Pb:Zn ratio (Figure 35). The Pb:Zn ratio appears to stabilize below R-km 146, with an anomaly of low Pb:Zn occurring at R-km 122.

As Figure 36 indicates, Ca concentrations are closely tied to Pb concentrations with a consistent ratio over the entire length of the study area. As seen in Figure 29 and Figure 31, both Pb and Ca are present in low or undetectable concentrations in control sites, and reinforces the relationship between these chemical signals and mining sediment. This suggests that neither is related to natural sediment sources. The distance-decay is similar for both mining signals.

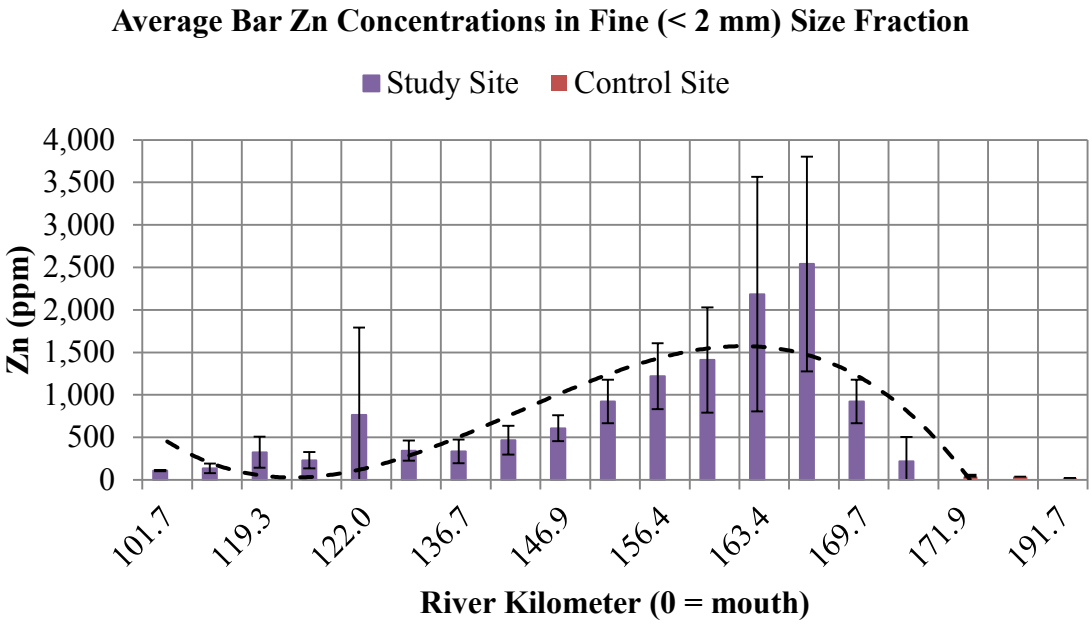

Figure 33. Bar Zn concentrations in the sand-sized (<2 mm) fraction by site average.

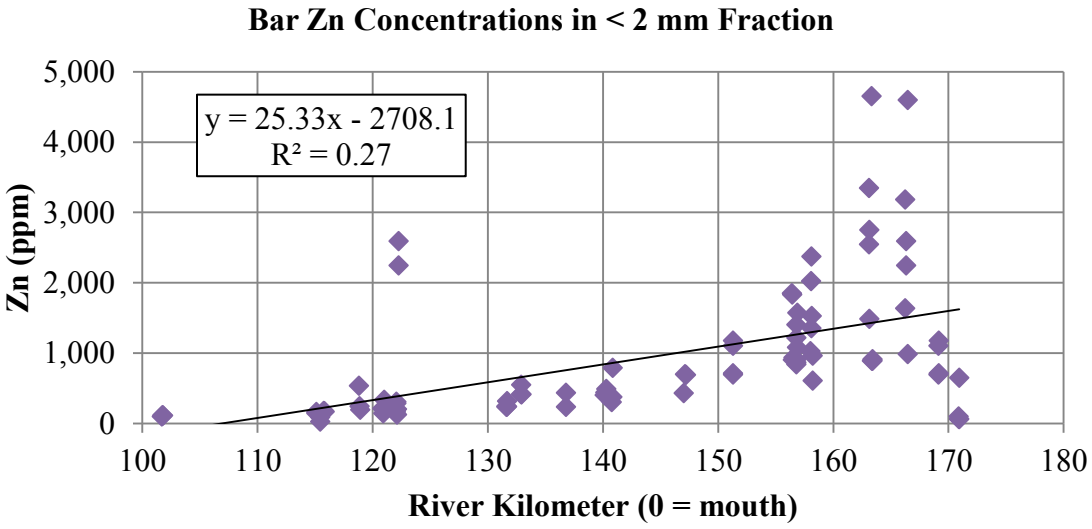

Figure 34. Scatter plot of bar Zn concentrations in the fine size fraction.

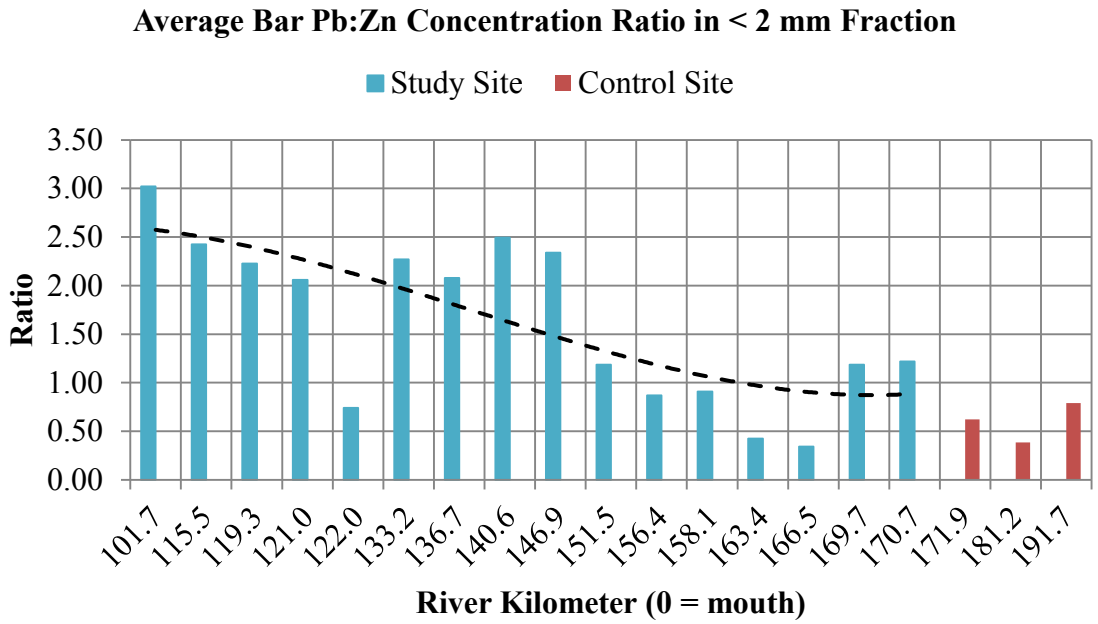

Figure 35. Pb:Zn ratio in the sand-sized fraction (<2 mm) of bars by site average.

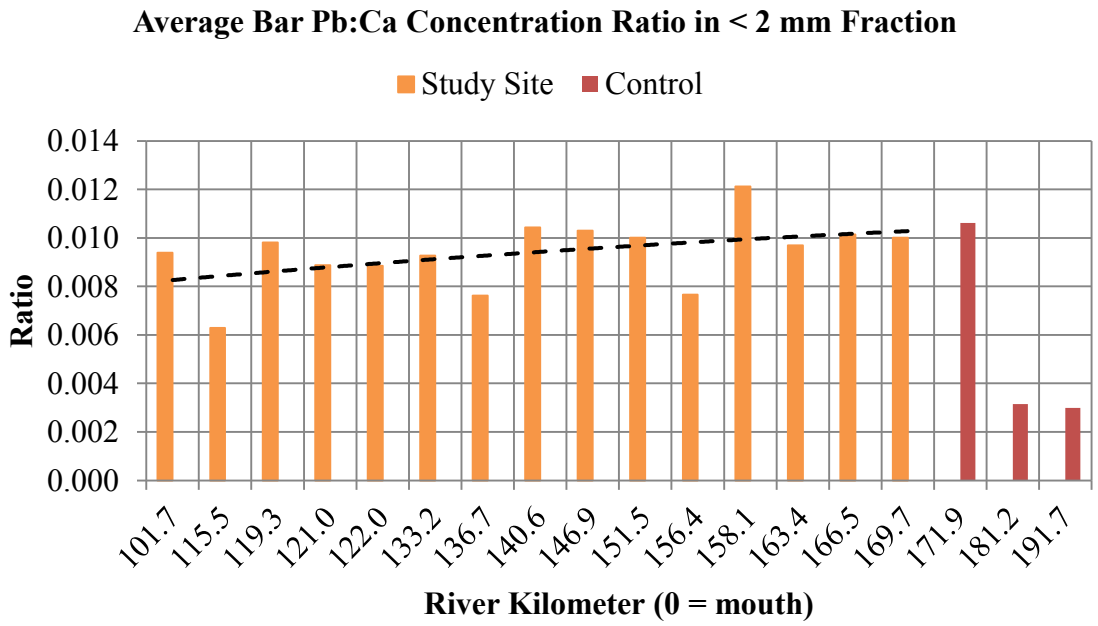

Figure 36. Pb:Ca ratio in the sand-sized fraction (<2 mm) of bars by site average.

Implications of downstream geochemical trends. Downstream trends in bar sediment and geochemistry distribution indicate a strong distance-decay relationship between mining inputs and sediment Pb contamination. While all samples contained Pb concentrations greater than the PEC of 128 ppm, average Pb ppm falls from a peak of 1,422 ppm at R-km 146.9 to a site average of 329 ppm at R-km 107.9 in Washington State Park near the St. Francois/Jefferson County line. As shown in this analysis, both Pb and Ca are good indicators of mining sediment, and Zn is a tracer of tailings specifically tied to the Leadwood tailings pile. The Pb:Zn ratio increases with distance from Leadwood, likely due to limited downstream transport or attenuation of the sediment as well as dilution by inputs from other mining and natural sources below Flat River Creek.

This study examined only the geochemistry of the less than 2 mm size fraction because it has been found to be representative of the overall sediment geochemistry (Pavlowsky et al., 2010). Despite finding high levels of Pb, Zn, and Ca throughout the study area, Pavlowsky et al (2010) found that chat-sized fragments of dolomite are not found downstream of R-km 120. This indicates that Pb contamination downstream is from fine sediments, which are more mobile than chat. Further, Young (2011) found that floodplains as far as the mouth of the Big River at R-km 0 are also contaminated with Pb, showing that Pb contamination is stored throughout the main stem of the Big River and not just in channel bars.

Particle Size Trends. As with geochemistry, particle size varies in relation to distance from mining. Bar grab samples were analyzed to determine the percent of the total sample mass in several size fractions: <2 mm or “fines”, 4-16 mm or “chat sized”, and >32 mm or “very coarse” (Figure 37). The percent of fine sediment in samples

increases with distance downstream. This may be due to mining contributions of sand-sized tailings, such as below Flat River Creek at site R-km 151.5. In general it is expected that fines would increase with distance downstream as fines are more mobile and transported at lower flow velocities than larger size fractions (Hjulström, 1939). However, Leopold et al. (1964) point out that while this trend may be true at the segment scale, tributary inputs complicate this trend at the basin scale by introducing new sediment loads throughout a river system.

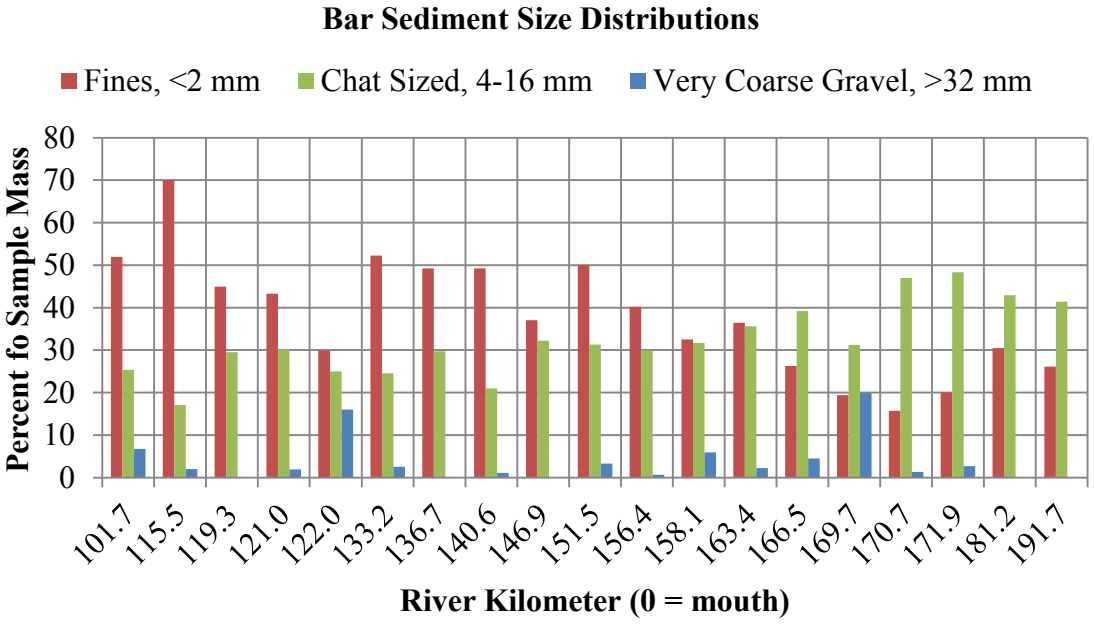

Figure 37. Distribution of sediment size fractions as a percent of total sample mass.

Chat sized sediment is most concentrated above and through the mining area and decreases slightly after R-km 150. While mine tailings fall into this size fraction, as discussed earlier natural sediment in the Big River also commonly occur in this size

fraction (Pavlowsky et al., 2010). This indicates that chat-sized sediment isn't necessarily sourced from mining, and some could be natural sediment of the same size.

Very coarse gravel of greater than 32 mm in size is highly variable and is not common in bar samples. Only one control sample contained very coarse gravel, indicating that it is variable in both upper and lower reaches. One possible explanation is that hand sorting of the samples off the shovel during grab sample collection may introduce sample error and result in this size fraction being under represented in grab samples.

Within-Bar Texture and Geochemical Variability

Sediment size variability by bar position. To better understand reach-scale variability of Pb content and sediment size it is helpful to also investigate bar composition at the sub-bar scale (Bunte and Abt, 2001). Samples from the bar head, middle, and tail were compared for variations in sediment size and geochemistry. Bar tails have the highest concentrations of fines by percent of total sample mass compared to other bar positions (Figure 38). Percent chat-sized sediment (Figure 39) is more evently distributed between the three bar positions, with bar head and middle having a slightly higher average than bar tail, although the difference is not statistically significant. Very coarse gravel does not make up a large percent of the mass of any sample for any bar position and varies greatly across bar positions (Figure 40). When present at all three bar positions, the very coarse gravel fraction is smallest in the bar tail.

An analysis of variance (ANOVA) was run using Microsoft Excel® for fine and chat-sized sediment size fractions to determine if a statistical difference exists between

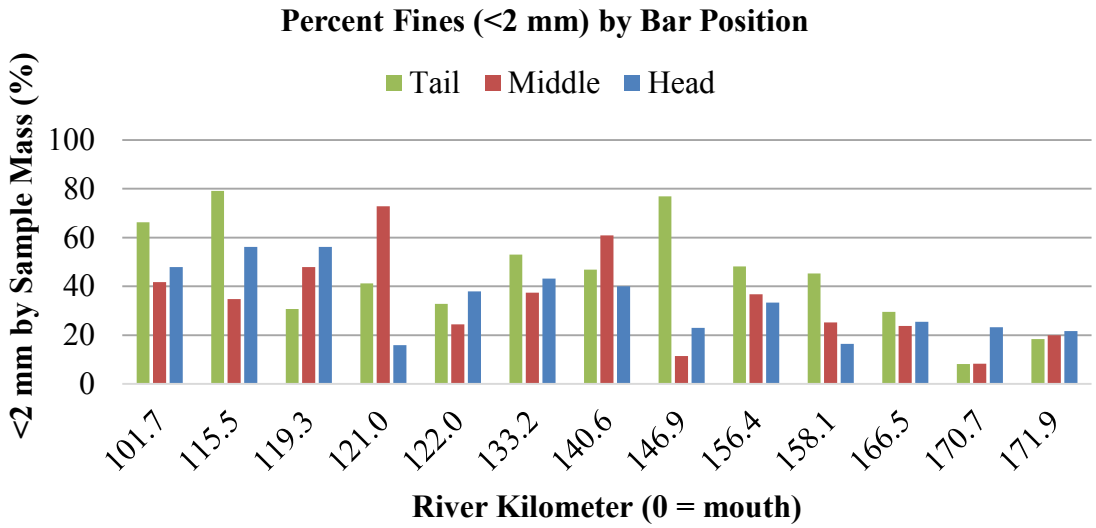

Figure 38. Distribution of fines by bar position.

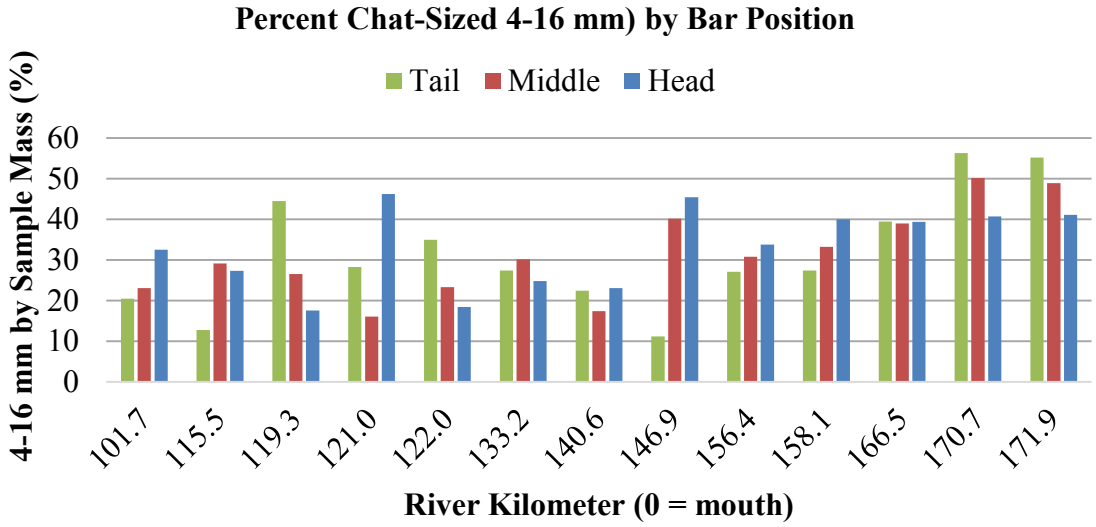

Figure 39. Chat-sized sediment (4-16 mm) as a percent of sample mass.

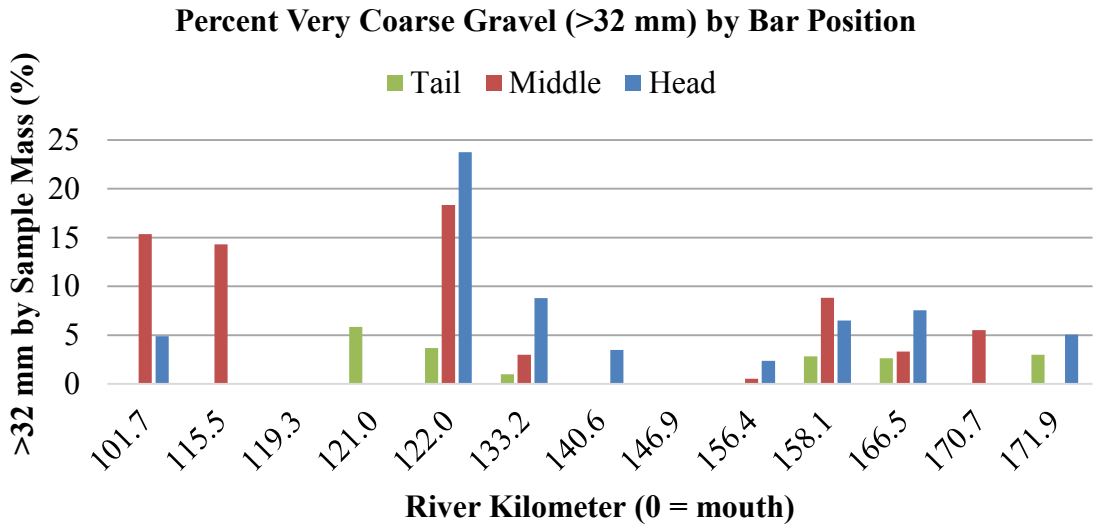

Figure 40. Coarse gravel (>32 mm) as a percent of sample mass.

bar head, middle, or tail. All samples were normally distributed in both size fractions. The ANOVA analysis indicated that a statistical significance exists only for fine sediments, with significance factor of 0.005, F_{crit} of 3.11, and F value of 6.60. The avearge bar tail percent of sample mass is 47.5 percent, while bar head and bar middle average percent fines are 35.2 and 31.2 percent, respectively. There was no statistical significance in bar position for percent chat-sized sediment, and the analysis was not run for the very coarse gravel size fraction due to low occurance of sediment in this fraction.

Implications of bar head, middle, and tail sediment size variation. The results of the bar head, middle, and tail sediment analysis were grouped by broad segment to better identify patterns related to mining inputs (Table 9). The bar tail below Flat River Creek has the highest average percent of fines in a sample, with 66 percent of the sample mass composed of fines. The coefficient of variation (% CV) for these samples is also the lowest of the three segments at 27.6 percent. This increase in bar tail fines may be due to

fine mine tailings inputs from Flat River Creek. These results expand on but are similar to those found by Pavlowsky et al (2010). In all segments, bar head and middle are comparable in percent fines by sample mass, although the bar middle is more variable with higher % CV overall. Sub-bar variation of chat sized sediment was also examined by broad segment, however no clear variations exist (Table 9). Bar tail between Eaton Branch (R-km 171) and Flat River Creek (R-km 155) is lower than others for chat content, but this may be due to the high concentration of fines in this segment as noted above. As with fines, chat-sized sediment is most variable in the bar middle, peaking in the below Flat River Creek segment with a % CV of 63.5. Overall, bar tail tends to be significantly different in percent fines than other bar positions, while chat-sized sediment content does not vary significantly. These findings are consistent with expectations based on accepted sediment transport principals.

Table 9. Channel bar sediment sample size distribution by segment (mean percent of sample and %CV).

Bar Position	Below Eaton Branch (R-km 171)		Below Flat River Creek (R-km 155)		Below Hwy E (R-km 133)	
	<2 mm	4-8 mm	<2 mm	4-8 mm	<2 mm	4-8 mm
Head	26 – 30.8%	38 – 17.7%	34 – 29.0%	31 – 46.4%	44 – 39.2%	27 – 38.0%
Middle	27 – 44.4%	34 – 29.5%	34 – 74.1%	36 – 63.5%	37 – 46.9%	25 – 24.5%
Tail	39 – 43.6%	33 – 37.5%	66 – 27.6%	15 – 57.1%	52 – 45.7%	27 – 56.3%

Pebble count sediment size variability by bar position. The Wolman pebble count was another method used to determine variability of surface texture (Wolman, 1954). Pebble counts were performed at the bar head, mid, and tail at one bar in each study reach. Figure 41 shows the 16th percentile (D_{16}) sediment size for bar head, middle, and tail at each study reach. The trend in D_{16} sizes is quite variable across study sites but tends to decrease with distance downstream. An anomaly occurs at R-km 122, where the D16 becomes larger at the bar tail and middle. This location is just downstream of Hill Creek, which may bring a coarser sediment load into the Big River. A low water bridge also exists just below R-km 122, possibly causing a change in the sediment transport regime. The D_{16} size fraction is highest at the bar head and becomes smaller overall with distance downstream. The average D_{16} in study sites for bar head is 5.0 mm, for bar middle is 5.4 mm, and for bar tail is 2.6 mm, although bar middle appears to be disproportionately skewed due to the exceptionally high D_{50} at R-km 122. As with the grab sample analysis, bar tail is the finest overall.

Average sediment size (D_{50}) increases in bar middle over distance while it remains relatively uniform for bar head or tail (Figure 42). Overall bar middle D_{50} was the coarsest, with an average of 13.4 mm in below-mining sites. As with grab samples, the bar tail has the smallest average grain size at 7.4 mm, while the bar head average is 12.6 mm. Control samples are generally coarser than downstream samples.

When comparing the 84th percentile size fraction (D_{84}) it is notable that there is no clear downstream trend for any bar position (Figure 43). In this size fraction, below mining bar head samples have the coarsest D_{84} at 26.4 mm average, while bar middle is 24.9 mm and bar tail is 17.5 mm. Control samples are on the coarser end of the gradient.

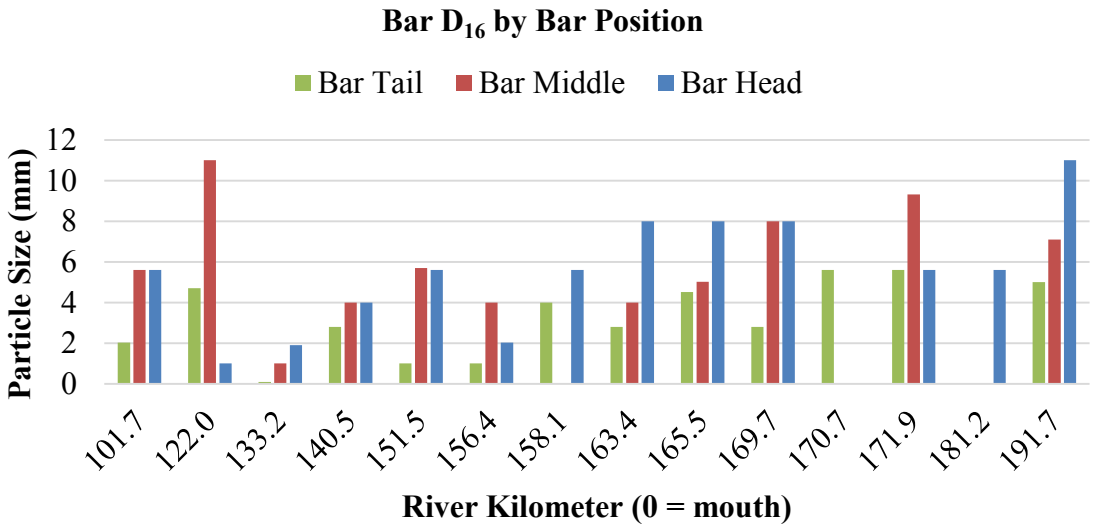

Figure 41. Average D_{16} distribution by bar position in pebble county surveys.

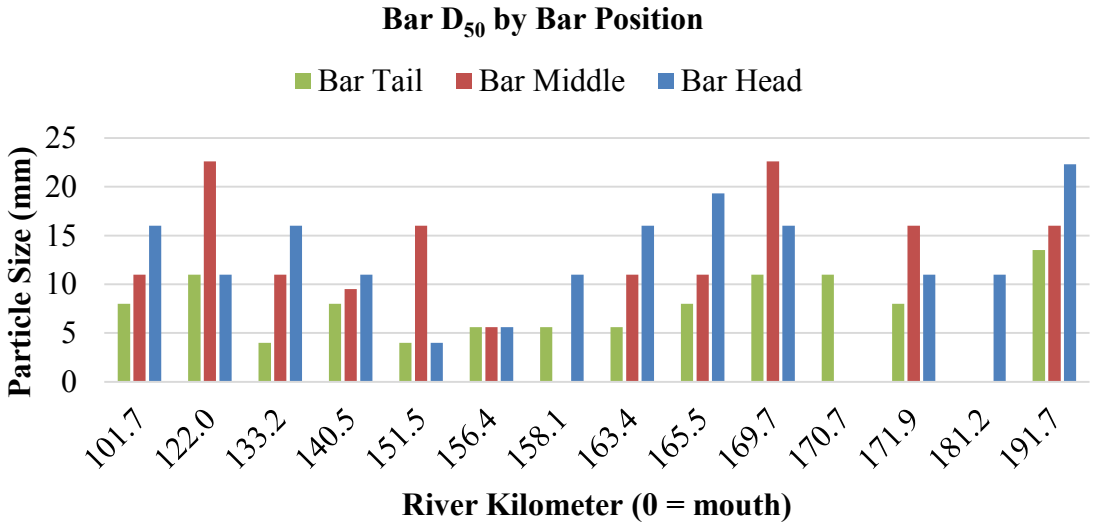

Figure 42. Average D_{50} distribution by bar position in pebble county surveys.

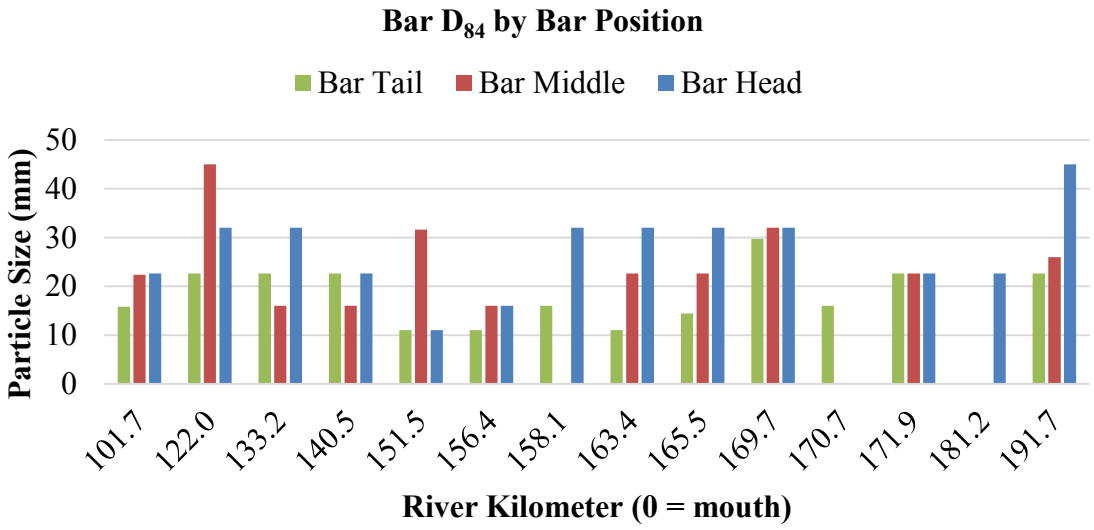

Figure 43. Average D_{84} distribution by bar position in pebble county surveys.

As noted by Leopold et al (1964), the D_{84} is important to note because the sediment size at which 84 percent of sediment is finer correlates with the hydraulic resistance of the stream, which is interrelated with channel slope, sediment gradation, channel morphology and sinuosity, and other variables.

Implications of pebble count analysis. Overall the results of the grab sample texture analysis and the pebble count analysis by bar position are comparable. In both analyses, bar middle and head positions have coarser sediment, while bar tail is the finest and overall fining occurs with distance downstream. Bar head is most variable for all positions with a % CV ranging from 51.3 percent for D_{16} to 56.9 percent for D_{84}. Percent CV ranges only from 32.1 to 39.3 percent for all other size fractions and bar positions.

Sediment size variability by sample depth. Bar surface and subsurface samples were compared to determine the vertical variability of sediment size by sample depth. Fines make up a higher percentage of subsurface sample mass than of surface mass, with

an increasing trend downstream (Figure 44). Fines as a percent of mass peak at site 151.5 in surface samples, while subsurface fines peak one site downstream at site R-km 133.2. Overall, the average for fines in surface samples is 30 percent of sample mass, while in subsurface samples the average is 44 percent. Fines are also less variable in subsurface samples, with a % CV of 49 percent, as opposed to 65 percent in surface samples.

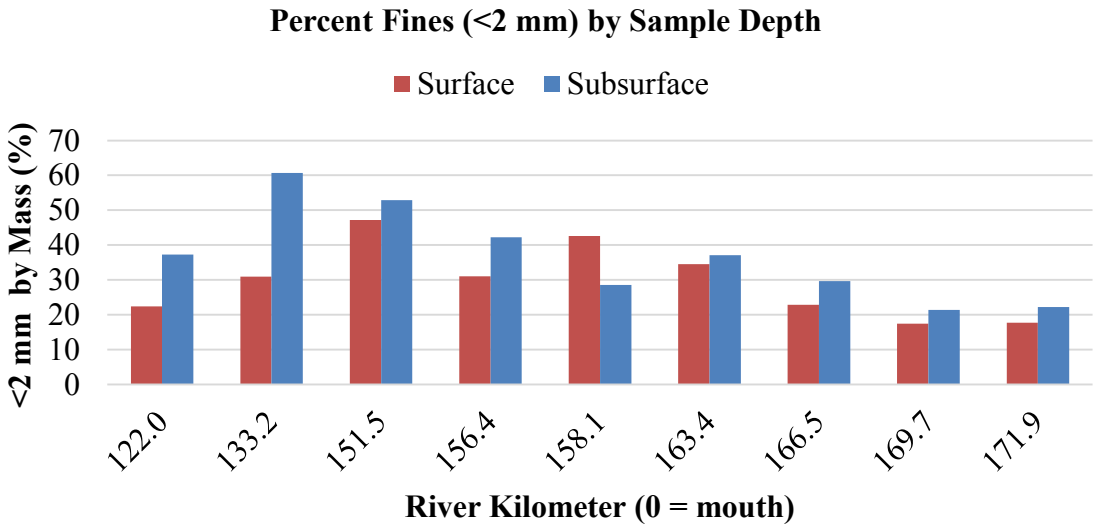

Figure 44. Percent fines (<2 mm) in surface and subsurface samples.

Percent of samples in the chat sized sediment is higher in subsurface samples in the upper mining segment, but makes up a smaller percent of sample mass in downstream reaches (Figure 45). Percent of sample mass in the chat-sized fraction decreases in both surface and subsurface with distance downstream. Very coarse gravel makes up a greater percent of surface samples than of subsurface samples at most sites (Figure 46). In both surface and subsurface samples very coarse gravel makes up a higher percentage of

control samples than samples in the mining segments. There is a sharp increase in sediment of this size at both depths are R-km 122.0.

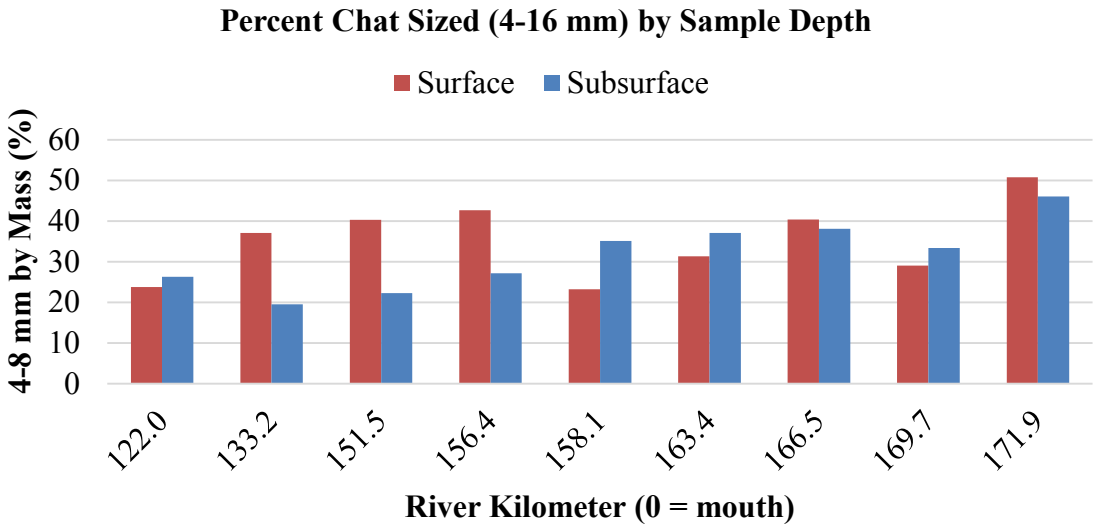

Figure 45. Percent chat-sized sediment (4-16 mm) in surface and subsurface samples.

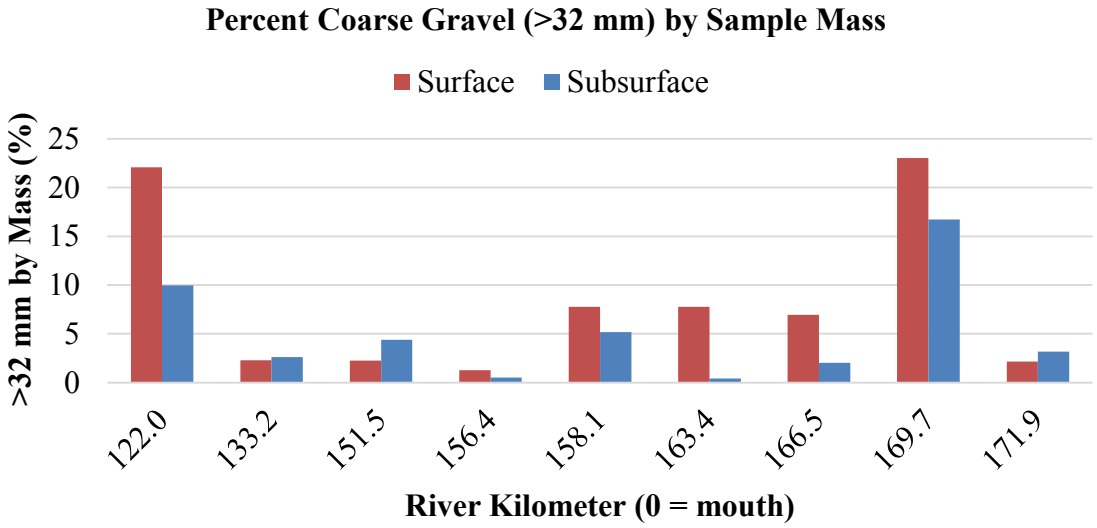

Figure 46. Percent coarse sediment (>32 mm) in surface and subsurface samples.

Implications of sediment variability by sample depth. Surface and subsurface samples are well mixed in all segments of the Big River. Table 10 shows the distribution Hwy E, however, so additional data is needed to confirm this result at this scale. Below Hwy E, where no additional mining inputs occur, surface samples have only about half of fines by sample depth. Fine content in surface and subsurface samples in the upper, central, and middle mining area (R-km 171-133) are nearly equal, suggesting a well-mixed bar form. Only two surface samples were collected between Flat River Creek and the fines as subsurface samples. This is more in line with what would be expected for a bar form, where fines are embedded at depth and surface texture tends to be coarser (Bunte and Abt, 2001). In all segments, fines exceed 20 percent, indicating a matrix supported deposit. In these types of deposits, fines fill the voids of larger particles to an extent that the larger particles do not touch (Bunte and Abt, 2001).

Table 10. Distribution of fine (<2 mm) sediment by sample depth (mean percent of sample and %CV).

Location	Surface	Subsurface
Below Eaton Branch (R-km 171)	29 – 57.2%	32 – 43.5%
Below Flat River Creek (R-km 155)	47 – N/A	47 – 41.1%
Below Hwy E (R-km 133)	25 – 37.8%	55 – 41.8%

Geochemical variability by bar position. Bar head, mid, and tail and surface and subsurface samples were also compared for variability in geochemistry. Lead concentrations were lowest in bar tail samples (Figure 47). Head samples showed the most variability in Pb content with a % CV of 70 percent, while middle samples were

more consistent with a % CV of 41 percent. Tail samples were slightly less variable with a % CV of 39 percent. Lead content decreased with distance downstream consistently across all bar positions. The data area normally distributed for all positions except bar middle, which can be made normally distributed by removing the sample with the highest Pb content. An ANOVA analysis of Pb content by bar position reveals that there is no statistical significance between samples by bar position when comparing all samples except control sites. However, when only the upper, middle, and lower, mining segments are compared (R-km 170.5 to R-km 133.0), the variance between samples is statistically significant with a significance factor of 0.05. The mean Pb content at the bar head in the mining segments is 1,303 ppm with a % CV of 48. Bar middle has an average of 1,048 ppm with smaller % CV of 15. Bar tail contains the least amount of Pb with an average of 890 ppm and % CV of 23.

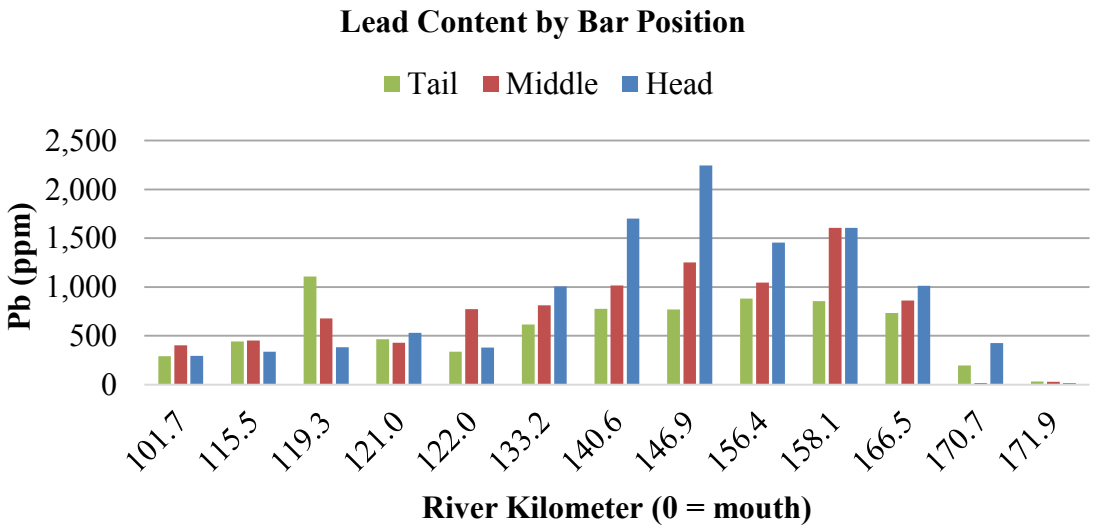

Figure 47. Distribution of lead (ppm) by sample bar position.

Zinc concentrations peak just below Leadwood, where mine tailings were much higher in Zn content than other mining sites (Pavlowsky et al., 2010) and decreased with distance downstream across all bar positions (Figure 48). This occurred at a more rapid rate than for Pb concentrations. Some bar middle samples remained elevated at around R-km 120, although these are an anomaly compared to other samples in that region. Calcium concentrations follow the same pattern as Pb and Zn concentrations and decrease with distance downstream, peaking at R-km 146.9 (Figure 49).

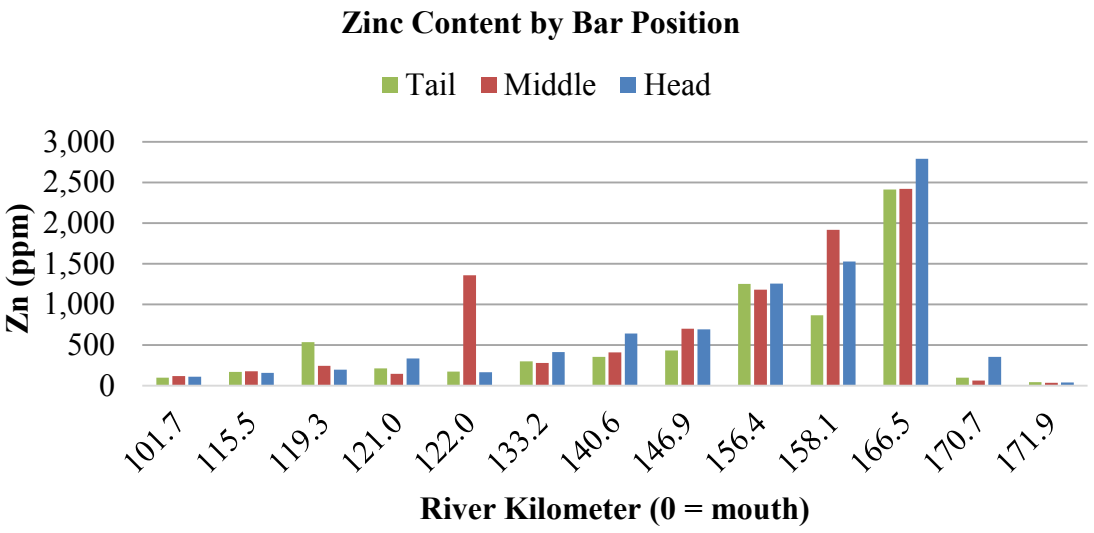

Figure 48. Distribution of zinc (ppm) by sample bar position.

Implications of geochemical variability by bar position. The ANOVA analysis of Pb content by bar position revealed that there is a statistical difference in mean Pb content between bar head, middle, and tail within the mining segments (R-km 170.5 – R-km 133). The bar tail within the mining segments contains a lower average Pb concentration than bar middle or head, suggesting that the Pb containing sediment tends

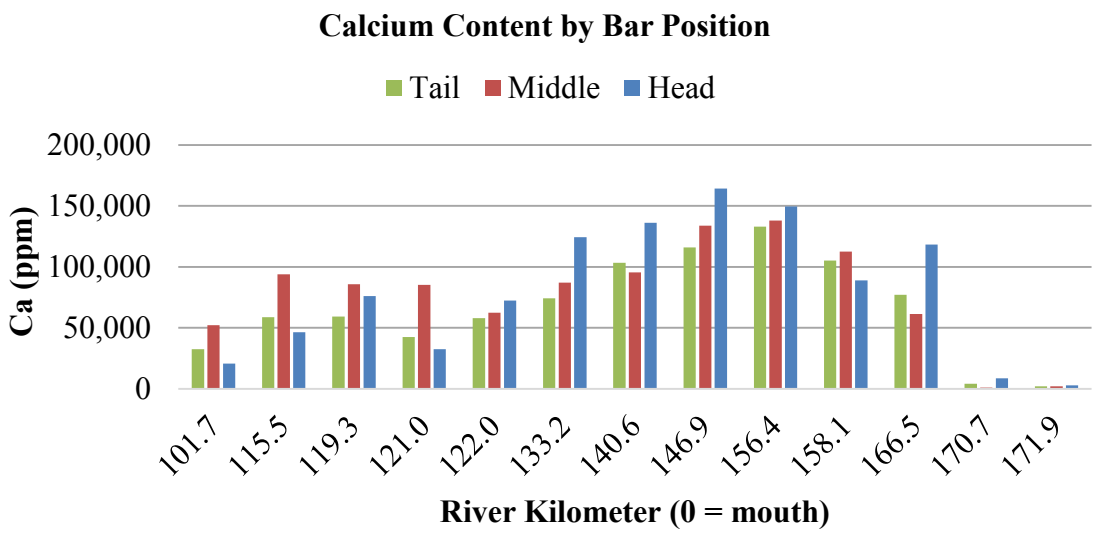

Figure 49. Distribution of calcium (ppm) by sample bar position.

to be transported and deposited with coarser sediment fractions also found more commonly at the bar head and middle. This trend is further broken down by broad segment, with bar head between Flat River Creek and Highway E (central and lower mining) experiencing the highest Pb concentration (Table 11). While elevated levels of Pb content are found throughout bar forms, they tend to be concentrated in the bar head within the central and lower mining segments. This trend is supported by Ca concentrations, which are also concentrated in the bar head in all mining segments. Below Hwy E and downstream of mining inputs, Pb content averages higher in the bar middle and tail than in the bar head. Recall that Pavlowsky et al (2010) found no dolomite chips downstream of R-km 120. This indicates that the change in Pb content from bar head, where sediment is coarser, toward the bar tail, is from fine mining particulates which are more mobile than the chat-sized grains.

Table 11. Channel bar variation of Pb by broad segment (mean (ppm) and %CV).

Sample Location	Below Eaton Branch (R-km 171)	Below Flat River Creek (R-km 155)	Below Hwy E (R-km 133)
Surface (0-15 cm)	935 – 20.8%	1,094 – N/A	630 – 33.6%
Subsurface (15-30 cm)	981 – 46.8%	1,141 – 44.4%	523 – 51.8%
Bar Head	1,224 – 27.3%	1,883 – 22.3%	1,883 – 22.3%
Bar Middle	1,112 – 32.7 %	1,105 – 10.0%	1,105 – 10.0%
Bar Tail	890 – 23.0%	892 – 27.3%	892 – 27.3%

Geochemical variability by sample depth. Lead concentrations in surface and subsurface samples decrease at a similar rate with distance downstream (Figure 50). Subsurface samples have a slightly higher variability in Pb levels than surface samples, with a % CV of 46 percent. Comparatively, surface samples have a % CV of 42 percent. Average Pb content was 795 ppm in surface samples and 876 ppm in subsurface samples. Zinc concentrations follow a pattern similar to Pb, with both surface and subsurface samples decreasing at a comparable rate (Figure 51). While Zn is higher in subsurface samples at most study reaches, the opposite is true at R-km 163.4. When comparing only sites for which both surface and subsurface samples are available, surface Zn concentrations in below-mining sites averaged 1,002 ppm and subsurface samples averaged 1,289 ppm and. Surface samples were slightly more variable in Zn concentrations with a % CV of 79 percent, while the subsurface % CV was 76 percent in below-mining sites. As with Pb and Zn, Ca concentrations also decreases similarly for both surface and subsurface samples with distance downstream (Figure 52). The surface

and subsurface concentrations of Ca are well mixed: average concentration of Ca in surface below-mining samples is 86,488 ppm with a % CV of 46 percent, while average Ca concentration in subsurface samples is 88,085 ppm with a % CV of 43 percent.

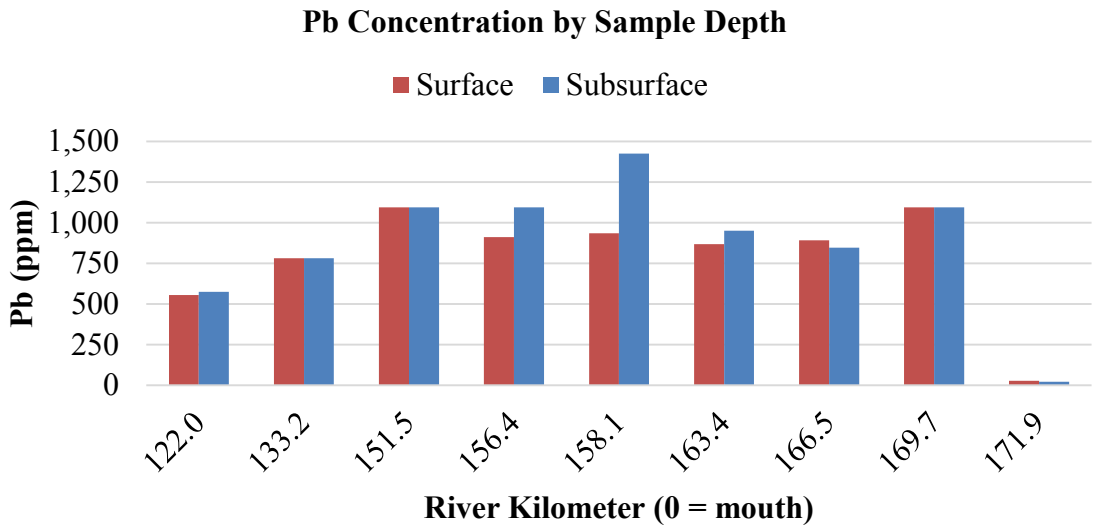

Figure 50. Lead content (ppm) in surface and subsurface samples.

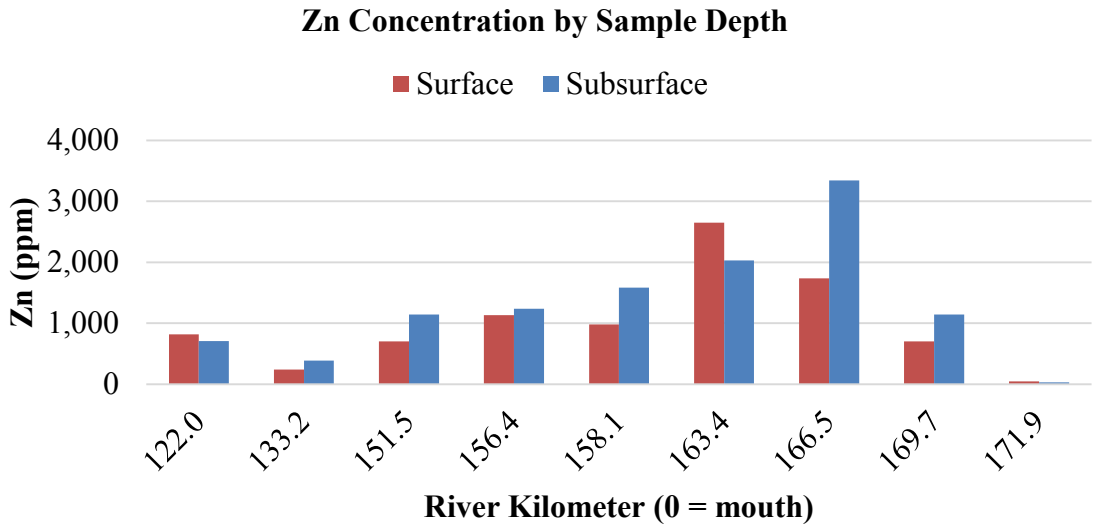

Figure 51. Zinc content (ppm) in surface and subsurface samples.

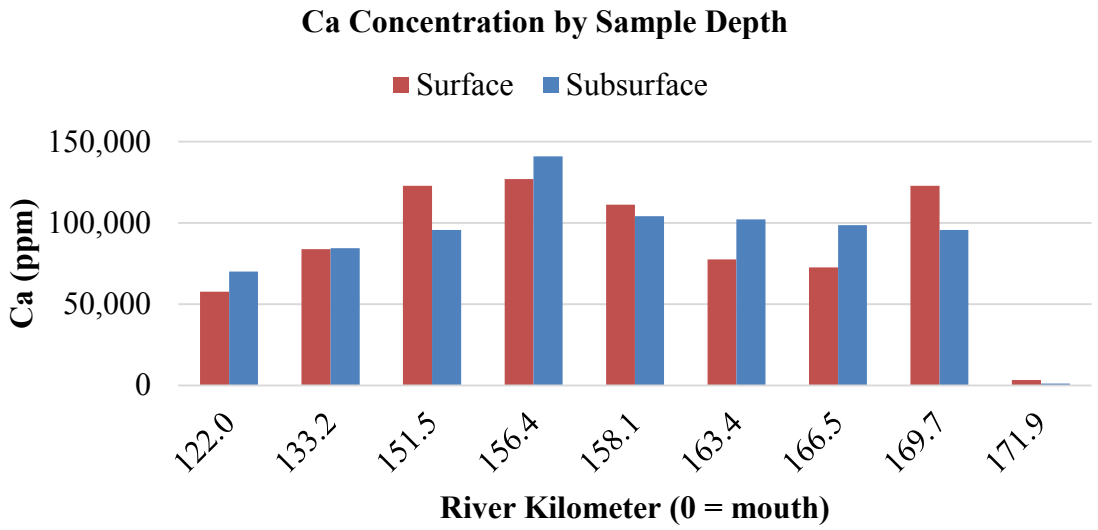

Figure 52. Calcium content (ppm) in surface and subsurface samples.

Implications of geochemical variability by sample depth. Overall, subsurface samples are slightly higher in Pb, Zn, and Ca, though the difference is not great. These samples were compared at the broader segment scale (Table 11). In mining areas above Hwy E, Pb content is well distributed. Below Highway E the average Pb content is higher in surface samples than in subsurface samples by just over 100 ppm. Recall that the fine sediment percent of sample mass in surface and subsurface samples was well-mixed within the mining segments, while it is more than twice as high in subsurface samples below Highway E (Table 10). This is contradictory to what one would expect knowing that sediment carrying Pb below R-km 120 is likely by fine grained sediment. One possible explanation for this result is that fine sediment from mining in bars below Hwy E has not been well mixed, and is instead stored near the surface of gravel bars and more mobile than the subsurface, natural fine sediment.

Evidence of Geomorphic Recovery

The results of this research indicate that basin, reach, and local geomorphic and hydrologic variables should be taken into consideration in managing contaminated sediment in riverine systems. As a river adjusts to disturbance due to excess sediment, channel planform adjusts and redevelopment of floodplains occurs (Schumm et al., 1984). This study concludes by examining the potential and stage of geomorphic recovery from disturbance due to mining in the Big River watershed. Geomorphic recovery was assessed using customized rapid channel recovery assessments described earlier (Appendix D). These assessments were performed every 50 m at nine sites with an average of 10 recordings per site. The purpose of the rapid assessments is to quantify indicators of recovery such as evidence for lateral widening, bank recession, and floodplain characteristics to identify patterns of geomorphic recovery relative to mining sites.

Aggradation occurs when excess sediment is input into a river channel and is also an indicator of recovery as a channel adjusts to increased bed load (Schumm et al., 1984; Simon, 1989). To identify where recent bed aggradation has occurred, a tile probe was used to establish the thickness of loose, unconsolidated sediment over the historical channel, which is indicated by a hard-lag surface (Bunte and Abt, 2001). This difference in texture and consolidation can be felt as a resistance layer when inserting the tile probe. The maximum recordable depth was 2.5 m. Two probes yielded no refusal and were recorded as "> 2.5" due to equipment limitation. In Figure 53 the > 2.5 m probe depths are recorded as 2.5 m, since the actual depth the refusal is greater but it is unknown by how much. Probe depths were greatest in the mining area between R-km 140.5 and 158.1.

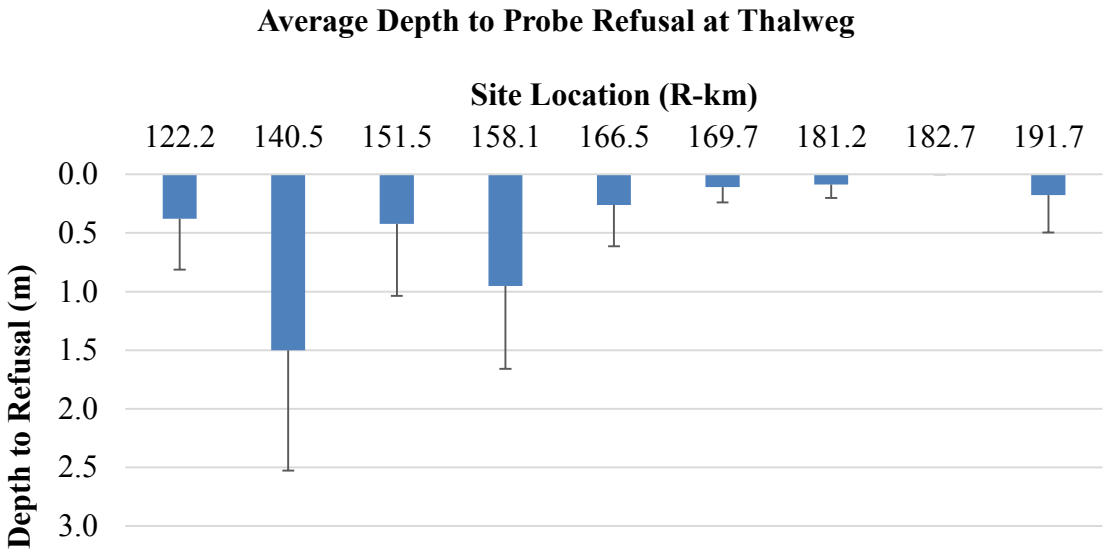

Figure 53. Depth to probe refusal at thalweg with one standard deviation shown.

Probe depth varied between samples at each study site, but in general for sites with 1 m or more of depth, % CV was 70 percent, while for averages of 0.4 or less, % CV can be greater than 100 percent. The sites with the highest variability are concentrated in upper mining and the control, R-km 181.2 to 166.5. The lowest average probe depth occurs at site 166.5, where bluff and bedrock control the channel morphology. Sites 140.5 and 158.1, which are within the lower and central mining segments, have the two highest probe depths and the lowest coefficient of variation. These statistics suggests that these sites are consistently storing more unconsolidated sediment over top of the historical channel bed than other segments.

Average depth to probe refusal is highest in riffle and run forms when examined by channel position (Figure 54). These depths are highly variable, with % CV between 138 and 157 percent for all channel positions. The standard deviation is shown as the error bars on the graph. Glide positions had the lowest average probe depth, possibly

indicating an old riffle cobble layer. Depth to probe refusal was also compared to bar type associated with the probe location (Figure 55). While probe depth was taken at the thalweg, adjacent bar form gives insight into the geomorphology and storage characteristics of the sample reach. Sites with no bar or side bars tended to have the greatest average probe depth, while areas with "mega" bar complexes had the lowest. Variability is quite high, ranging between a % CV of 139 and 165 percent for all bar types. The standard deviation is shown on the error bars in the graph.

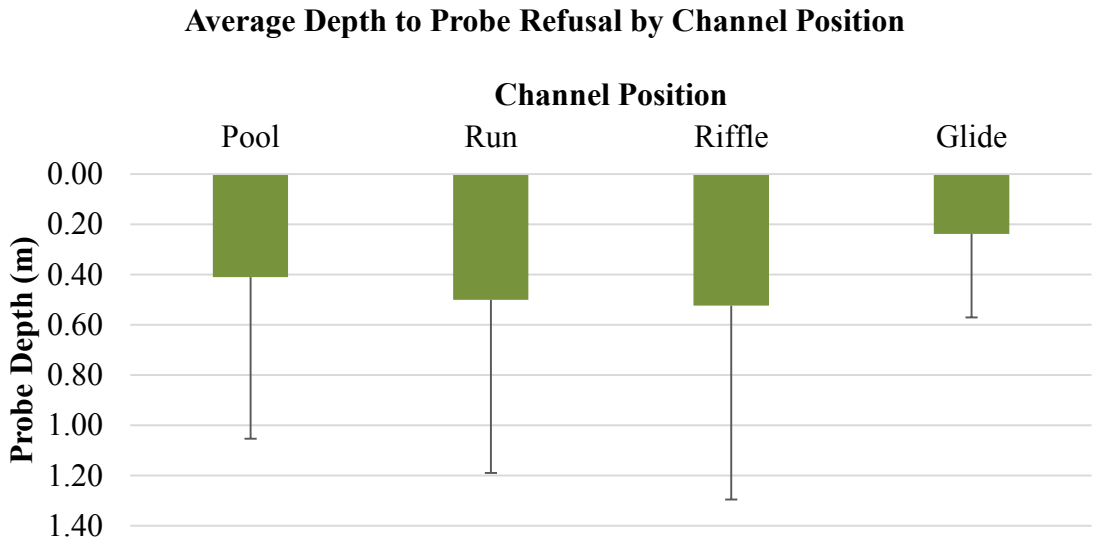

Figure 54. Average depth to probe refusal by channel position with one standard deviation shown.

Evidence for overall channel recovery is variable within the study area. Figure 56 shows the distribution of recovery factors. Site 158.1 is located within the upper mining segment and shows the highest indication of recovery over all, while control sites (171.9-191.7) have floodplain recovery but lower indication of lateral widening or bank

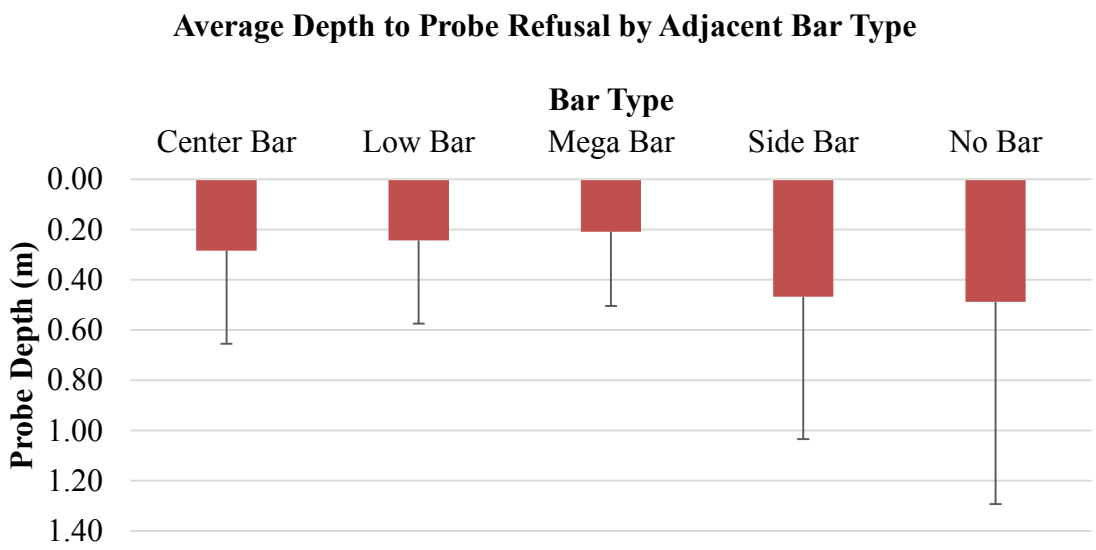

Figure 55. Depth to probe refusal at thalweg compared to adjacent bar type with one standard deviation shown.

recession. Middle and lower mining sites have the least floodplain recovery, but are exhibiting bank recessions, which may lead to floodplain recovery in the future (Simon,1989). A notable correlation also exists between large woody debris presence and bank recession. For example, at R-km 140.5 where presence of bank recession is relatively high, over 6 units of LWD are present, the highest of any other site by twice as much. This corresponds with research by Martin et al (2016), who identified that the primary wood recruitment mechanism in the Big River is bank erosion.

Implications of Recovery Factors. Figure 57 shows characteristics of Big River channel morphology derived from the air photo analysis described earlier. Bars can form the basis of new floodplains (Hooke and Yorke, 2011), and a correlation between areas of high bar area in the channel and new floodplain formation is noticeable. Recovery, particularly in the control segment, may also be tied to an aggradation phase occurring now as the channel recovers for historical overbank legacy sediments. These sediments

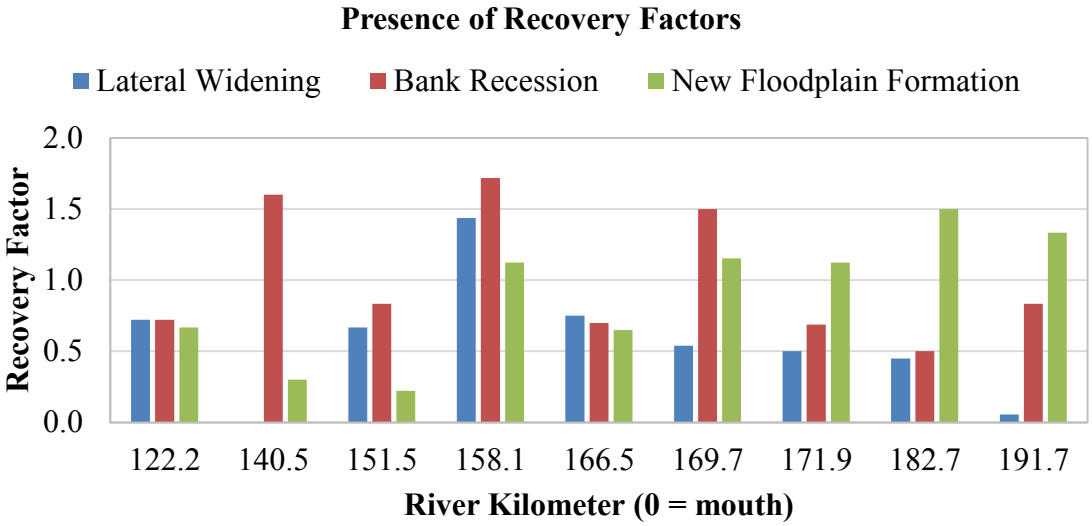

Figure 56. Presence of recovery factors at rapid channel recovery assessment sites.

came from settlement and early land use disturbance, and resulted in increased bank heights (James, 2013). During this period, the Big River would have responded by aggrading and widening, following the channel evolution outlined by Schumm et al, 1984. Downstream of the first mining input at R-km 171.5 there is additional evidence of aggradation through large percentage bar area and deeper probe depths. Bars can also indicate disturbance due to over sediment supply, variable flood and sediment pulses, change in ambient sediment texture, and channel disturbance leading to uneven erosion and deposition. These characteristics may be related to mining sediment or they may be related to early land use disturbance and response to legacy sediment. Given the results of this research and that of others, the answer is that most likely both sources are affecting channel recovery.

While the large sediment influx from historical land use disturbances may have moved downstream or attenuated in the channel bed and floodplains since initial

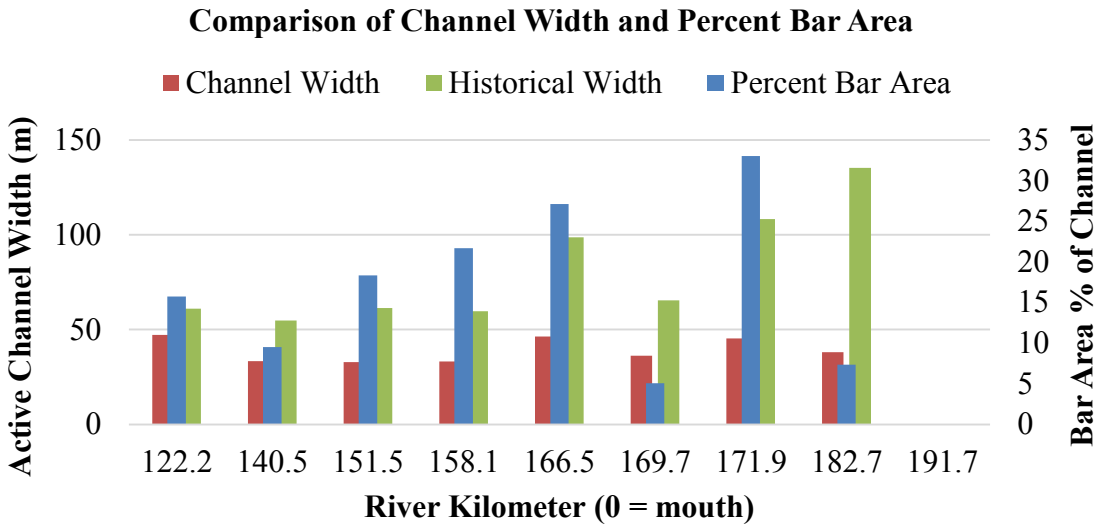

Figure 57. Comparison of current and historical channel width and percent bar area.

disturbance, floodplain recovery takes place on a longer scale (Jacobson, 1995). Signs of geomorphic recovery indicate that the channel is in the process of returning to equilibrium now that the supply of excess sediment has been eliminated. In addition to geomorphic channel indicators, it is important to understand sediment size, storage, and transport characteristics in a river, as this research has described. Solely relying on bed level and geomorphic conditions can cause misinterpretation of channel and sediment recovery, particularly when bar and floodplain storage is extensive (James, 2010). Complicating matters, a positive correlation exists between bar area increases and more frequent flood events in the Big River watershed over the past 20 years. This suggests evidence for increased bank erosion, reactivation of stored floodplain sediment, and remobilization of channel bar sediment, resulting in ongoing downstream sediment transport.

CHAPTER 6: CONCLUSIONS

This study examined the distribution and variability of contaminated mining sediment in bar deposits of the Big River, St. Francois County, Missouri. Bar form, distribution, and area were assessed for present day and historical trends using a GIS analysis. Geochemistry and particle size trends of bar deposits were analyzed at the reach and bar-unit scale. Finally, rapid geomorphic assessments were used to identify indicators of geomorphic recovery in the Big River. The influences of geomorphic factors at the valley, segment, and reach scale on bar distribution were also assessed. This information has led to a greater understanding of the geomorphic response and recovery evolution of the Big River at the sub-reach, reach, and segment scale following intense Pb mining in the watershed. The following conclusions can be drawn from this research:

1. Side bars are the most common bar type in the Big River, occurring at an average spacing of 1.8 km with average area of 3,184 m^2. Point bars, which occur along meander bends in areas of instability, are most concentrated within the core mining area between R-km 170-140 and decrease in frequency with distance downstream. Delta bars are found at tributary inputs and have the largest average unit size at 5,298 m^2. Center bars are distributed uniformly through the study area and have the smallest average bar area at 920 m^2. Bars are spaced about 8-12 channel widths apart. Center bar occurrence indicates aggradation is actively occurring in the Big River

2. Gravel bar area peaked in 1937, around the same time that new mining techniques stopped the production of chat-sized sediment. Bar area decreased from 1937-1972, before increasing again in the 1990s. A large tailings dam breach in 1977 and flood events in the 1980s may have mobilized bed sediment that had attenuated prior to the mid-1970s. By 2007 bar area was decreasing again everywhere except below the mining region, suggesting the sediment wave may be beginning to move downstream again.

3. While fine sediment quantity increases with distance downstream, the geochemical signals of mining sediment, Pb, Zn and Ca, decrease with distance downstream. This may due to dilution and storage of the contaminated sediment wave. Lead concentration decreases from a site average high of nearly 1,500 ppm

at R-km 146.0 to below 500 ppm by R-km 100, or the St. Francois and Jefferson County line. The negative relationship between fine sediment quantity and contamination indicate that the ratio of natural to mining sediment increases with distance from mining. Further, previous studies have indicated that chat-sized mining sediment has not moved further downstream than R-km 120, meaning contamination below that location is due to fines.

4. Chat sized grains are well distributed throughout bar positions but are most variable at the bar tail, where % CV is 50 percent. Chat grain content of samples peaks at 56 percent in a tail sample at R-km 170.7, the first mining input site. Distribution of chat sediment does not vary in a statistically significant manner and this size fraction is just as commonly found in control sites as in below-mining sites, indicating that its source can be both mining and natural. Fines are statistically more concentrated in bar tails and make up as much as 81 percent of sample mass in the middle mining segment. This trend is in line with traditional sediment transport models. Very coarse gravel tends to be highest in the bar middle, peaking at 36 percent at R-km 169.7, but was not found at every sample site. The % CV for very coarse gravel is high, ranging from 143 percent at bar middle to 174 percent in bar tail samples.

5. Fines are more concentrated in subsurface samples, averaging 44 percent of sample mass versus 30 percent for surface samples. Very coarse gravel is uncommon in subsurface samples. Chat sized sediments are relatively uniform between surface and subsurface samples averaging 33 and 29 percent, respectively, with a % CV at 49 and 43 percent. In the mining area, percent of fines in surface and subsurface samples are equal, while subsurface samples have twice the fine content as surface samples below Highway E. This suggests that bar sediment in the mining area may be actively mixed and transported as the channel adjusts to disturbance.

6. Lead content averages higher at the bar head and middle within mining segments, but is higher and more variable (% CV from 29-51) in the bar tail below Highway E. This indicates that the change in Pb content from bar head, where sediment is coarser, toward the bar tail, is from fine mining particulates which are more mobile than the chat-sized grains. Lead concentration in bar head samples peaked at R-km 146.9 with a site average bar head Pb concentration of 2,244 ppm.

7. Concentrations of Pb, Zn, and Ca are slightly higher in subsurface samples than in surface samples, however variability is greater in subsurface samples, ranging from a % CV of 44 to 52 percent. Average Pb content is 1,094 ppm in the central and lower mining segment surface samples and 1,141 ppm in subsurface samples of the same segments. Surface samples contain more Pb than subsurface samples below Highway E, suggesting that Pb contaminated sediment is more transient, newer, and less embedded in bar deposits than in mining area sites.

8. Recovery indicators are present to varying degrees in the study area. While upstream of the initial sediment input sites (R-km 171) is showing evidence of floodplain recovery, downstream recovery indicators are more intermittent. The channel is in the process of geomorphic recovery, though other variables such as land use and flood events will affect the time frame for recovery. Probe depth is highest around R-km 140, which also coincides with wide valley and large bar area and frequency. These factors along with geochemical analysis indicate that this zone is acting as a sediment sink and storage of excess mining sediment, preventing the sediment wave from moving downstream at a consistent rate under normal conditions.

9. Parts of the Big River appear to be in stage V of Simon's 1989 channel evolution model, the aggradation phase. This recovery stage follows a period of degradation and narrowing and is characterized by channel widening and the presence of a slough line along banks, formation of new floodplain at a lower elevation that original, and reestablishing woody vegetation on banks. These reaches are also characterized by large woody debris presence, an occurrence related to bank recession in the Big River.

This study focused on the distribution and geochemistry of bar forms in the Big River. The Big River Watershed is the site of a large superfund site, and many studies have been conducted to date to understand the extent of Pb contamination in the channel and watershed. These include an assessment of floodplain contaminant storage (Pavlowsky et al., 2010; Young, 2011; Huggins, 2016), effects of mining on major tributaries (Hill, 2016), remediation through dredging (Owen et al., 2011), and the effects of sediment fining and Pb contamination on aquatic macroinvertebrates (Roberts et al., 2009), among many others. Additional research into the locations of major disturbance zones would increase understanding of the potential for bed and bank erosion and contamination remobilization. Further studies into the role of flooding on sediment remobilization and transport would also be beneficial to the long-term restoration efforts in this watershed.

Channel bars in the Big River contain the history of lead mining sediment in the Old Lead Belt and are a valuable resource for evaluating the distribution of contamination in the Big River. This study represents an important step in understanding the distribution and geochemistry of bar forms and how they have been affected by mining in the Big River. The results of this study can be used to improve understanding of the potential effects of future remobilization of channel bar sediment, identify sampling locations, and evaluate changes in sediment transport and storage over time. The findings of this study could also be used by resource managers to evaluate remediation plan effectiveness and assess sediment distribution patterns in comparable mined watersheds. The mining sediment wave in the Big River appears to be moving in an asymmetrical manner, being variably stored and released based on factors of hydrology, channel morphology, and land use. Ultimately geomorphic channel recovery is an ongoing process, and contaminated channel and floodplain deposits along the entire main stem of the Big River will continue to store and remobilize contaminated sediments to the river system for centuries.

LITERATURE CITED

Asberry, K., 1997. Big River mine tailings/St. Joe Minerals corporation site. United States Environmental Protection Agency Region 7, EPA ID# MOD981126899.

Ashmore, P., Bertoldi, W., Gardner, J.T., 2011. Active width of gravel-bed braided rivers. Earth Surface Processes and Landforms, 3 6(11), 1510-1521.

Bartley, R., Rutherfurd, I., 2005. Re-evaluation of the wave model as a tool for quantifying the geomorphic recovery potential of streams disturbed by sediment slugs. Geomorphology 64, 221-242.

Brierley, G.J., Fryirs, K., 2009. Don't fight the site: three geomorphic considerations in catchment-scale river rehabilitation planning. Environmental Management 43, 1201-1218.

Brown, B.L., 1981. Soil Survey of St. Francois County, Missouri. USDA-SCS. U.S. Gov. Print Office, Washington, D.C.

Bunte, K., Abt, S.R., 2001. Sampling surface and subsurface particle-size distributions in wadable gravel- and cobble-bed streams for analyses in sediment transport, hydraulics, and streambed monitoring. Gen. Tech. Rep. RMRS-GTR-74. Fort Collins, CO: U.S. Department of Agriculture, Forest Service, Rocky Mountain Research Station, 428 p.

Chang, H.H., 1984. Modeling of river channel changes. Journal of Hydraulic Engineering 110, 157-172.

Charlton, R., 2008. Fundamentals of fluvial geomorphology. Routledge, New York, New York.

De Rose, R.C., Basher, L.R., 2010. Measurement of river bank and cliff erosion from sequential LIDAR and historical aerial photography. Geomorphology 126, 132-147.

Downs, P.W., Thorne, C.R., 1996. A geomorphological justification of river channel reconnaissance surveys. Transactions of the Institute of British Geographers, New Series 21 (3), 455-468.

Downward, S.R., Gurnell, A.M., Brookes, A., 1994. A methodology for quantifying river channel planform change using GIS. IAHS Publications-Series of Proceedings and Reports-Intern Assoc. Hydrological Sciences 224, 449-456.

Doyle, M.W., Shields, F.D. Jr., 2000. Incorporation of bed texture into a channel evolution model. Geomorphology 34, 291-309.

Gale, N.L., Adams, C.D., Wixson, B.G., Loftin, K.A., Huang, Y., 2004. Lead, zinc, copper, and cadmium in fish and sediments from the Big River and Flat River Creek of Missouri's Old Lead Belt. Environmental Geochemistry and Health 26, 37-49.

Gilbert, G.K., 1917. Hydraulic-mining debris in the Sierra Nevada. U.S. Geological Survey Professional Paper 105, 1-154.

Gunter, J.A., 2011. Big River mine tailings superfund site OU-1 St. Francois County, Missouri. US EPA Region 7, Kansas City, Kansas, 48 pp.

Hjulström, F. 1939. Transportation of detritus by moving water. In Trask, P.D. (ed) Recent Marine Sediments, a Symposium. American Association of Petroleum Geologists, Tulsa, Oklahoma, 5–31.

Hooke J.M., Yorke, L., 2011. Channel bar dynamics on multi-decadal timescales in an active meandering river. Earth Surface Processes and Landforms 36, 1910-1928.

Hughes, M.L., McDowell, P.F., Marcus, W.A., 2006. Accuracy assessment of georectified aerial photographs: implications for measuring lateral channel movement in a GIS. Geomorphology 74, 1-16.

Hupp, C.R., 1992. Riparian vegetation recovery patterns following stream channelization: a geomorphic perspective. Ecology 73, 1209-1226.

Hupp, C.R., Simon, A., 1991. Bank accretion and the development of vegetated depositional surfaces along modified alluvial channels. Geomorphology 4, 111-124.

Jacobson, R. B., Primm, A.T., 1997. Historical land-use changes and potential effects on stream disturbance in the Ozark plateaus, Missouri. United States Geological Survey Water-Supply Paper 2484.

Jacobson, R.B., 1995. Spatial controls on patterns of land-use induced stream disturbance at the drainage-basin scale--an example from gravel-bed streams of the Ozark Plateaus, Missouri. Geophysical Monograph 89, 219-239.

Jacobson, R.B., Gran, K.B., 1999. Gravel sediment routing from widespread, low-intensity landscape disturbance, Current River Basin, Missouri. Earth Surface Processes and Landforms, Vol. 24, 897-917.

James, L.A., 1989. Sustained storage and transport of hydraulic gold mining sediment in the Bear River, California. Annals of the Association of American Geographers 79 (4), 570-592.

James, L.A., 2006. Bed waves at the basin scale: implications for river management and restoration. Earth Surface Processes and Landforms 31, 1692-1706.

James, L.A., 2010. Secular sediment waves, channel bed waves, and legacy sediment. Geography Compass, 4 (6), 576-598.

James, L.A., 2013. Legacy sediment: definitions and processes of episodically produced anthropogenic sediment. Anthropocene 2, 16-26.

Kellerhals, R., Church, M., 1989. The morphology of large rivers: Characterization and management. Proceedings of the International Large River Symposium. Canadian Special Publication of Fisheries and Aquatic Sciences, 31-48.

Knighton, A.D., 1989. River adjustment to changes in sediment load: the effects of tin mining on the Ringarooma River, Tasmania, 1875-1984. Earth Surface Processes and Landforms 14 (4), 333-359.

Lane, E.W., 1955. The importance of fluvial morphology in hydraulic engineering. Proceedings from the American Society of Civil Engineering 81, paper 75, 1-17.

Langedal, M., 1997. The influence of a large anthropogenic sediment source on the fluvial geomorphology of the Knabeåna-Kvina Rivers, Norway. Geomorphology, 19 (1-2), 117-132.

Leopold, L.B., Wolman, M.G., Miller, J.P., 1964. Fluvial processes in geomorphology. San Francisco, California, W. H. Freeman and Sons, 522 p.

Lisle, T.E., Pizzuto, J.E., Ikeda, H., Iseya, F., Kodama, Y., 1997. Evolution of a sediment wave in an experimental channel. Water Resources Research 33 (8), 1971-1981.

MacDonald, D.D., Ingersoll, C.G., Berger, T.A., 2000. Development and evaluation of consensus-based sediment quality guidelines for freshwater ecosystems. Archives of Environmental Contamination and Toxicology 39 (1), 20-31.

Macklin, M.G., Brewer, P.A., Hudson-Edwards, K.A., Bird, G., Coulthard, T.J., Dennis, I.A., Lechler, P.J., Miller, J.R., Turner, J.N., 2006. A geomorphological approach to the management of rivers contaminated by metal mining. Geomorphology 79 (3-4), 423-447.

Mallakpour, I., Villarini, G., 2015. The changing nature of flooding across the central United States. Nature Climate Change 5, 250-254.

Martin, D.J., Pavlowsky, R.T., 2011. Spatial patterns of channel instability along an Ozark river, southwest Missouri. Physical Geography 32 (5), 445-468.

Martin, D.J., Pavlowsky, R.T., Harden, C.P., 2016. Reach-scale characterization of large woody debris in a low-gradient, Midwestern U.S.A. river system. Geomorphology 262, 91-100.

MDNR, 2004. Biological assessment and fine sediment study: Big River (lower): Irondale to Washington State Park, St. Francois, Washington, and Jefferson

Counties, Missouri, 2002-2003. Prepared by the Water Quality Monitoring Section, Environmental Services Program, Air and Land Protection Division of the Missouri Department of Natural Resources, 60 p.

MDNR, 2007. The estimated volume of mine-related benthic sediment in Big River at two point bars in St. Francois State Park using ground penetrating radar and x-ray florescence. Prepared by the Water Quality Monitoring Unit, Environmental Services Program, Air and Land Protection Division of the Missouri Department of Natural Resources, 118 p.

MDNR, 2011. MO 2011 Bedrock 500K (SHP). MDNR Division of Geology and Land Survey, Geological Survey Program, Rolla, Missouri. Retrieved 02/19/2013 from ftp://msdis.missouri.edu/pub/metadata_gos/MO_2011_Bedrock_500K_shp.xml.

Meneau, K.J., 1997. Big River watershed inventory and assessment. Missouri Department of Conservation, St. Charles, Missouri, 106 p.

Missouri Spatial Data Information Service. Retrieved 2009 from the University of Missouri Department of Geography, Geographic Resources Center Web site at http://msdis.missouri.edu/datasearch/ThemeList.jsp.

Morisawa, M., 1985. Rivers: forms and processes. Longman Group Limited, New York, New York.

Mount, N.J., Louis, J., 2005. Estimation and propagation of error in measurements of river channel movement from aerial imagery. Earth Surface Processes and Landforms 30, 635-643.

Natural Resources Conservation Service, 2011. Soil Survey Staff, United States Department of Agriculture. Soil Survey Geographic (SSURGO) Database. Available online at http://sdmdataaccess.nrcs.usda.gov/, accessed 05/05/2011.

NewFields, 2006. Hydrogeology and groundwater quality of mill waste piles: St. Francois County, Missouri. Report submitted on November 30, 2006 as an addendum to the March 2006 “Focused Remedial Investigation of Mined Areas in St. Francois County, Missouri” by NewFields, 730 17th Street, Suite 925, Denver, CO 80202.

NewFields, 2007. Volume of sediment in Big River, Flat River Creek, and Owl Creek-St. Francois County mined areas, Missouri. Report submitted on June 29, 2007 as an addendum to the March 2006 “Focused remedial investigation of mined areas in St. Francois County, Missouri” by Newfields, 730 17th Street, Suite 925, Denver, CO 80202.

Owen, M.R., Pavlowsky, R.T., Martin, D.J., 2012. Big River borrow pit monitoring project: final report. Big River Mining Sediment Assessment Project, OEWRI EDR 10-003.

Owen, M.R., Pavlowsky, R.T., Womble, P.J., 2011. Historical disturbance and contemporary floodplain development along an Ozark river, southwest Missouri. Physical Geography 32 (5), 423-444.

Ozarks Environmental and Water Resources Institute, 2007. Standard operating procedure for: X-MET3000TXS+ handheld XRF analyzer. Missouri State University, Springfield, Missouri.

Panfil, M.S., Jacobson, R.B., 2001. Relations among geology, physiography, land use, and stream habitat conditions in the Buffalo and Current river systems, Missouri and Arkansas: USGS/BRD/BSR- 2001-0005, 111 p.

Pavlowsky, R.T., Owen, M. R., Martin, D.J., 2010. Channel and floodplain deposits of the Big River system in St. Francois, Washington, and Jefferson Counties, Missouri. OEWRI EDR-10-002.

Rafferty, M.D., 1980. The Ozarks, land and life. University of Arkansas Press. Vancouver.

Rice, S.P., Church, M., Wooldridge, C.L., Hickin, E.J., 2009. Morphology and evolution of bars in a wandering gravel-bed river; lower Fraser river, British Columbia, Canada. Sedimentology 56 (3), 709-736.

Roberts, A.D., Mosby, D.E., Weber, J.S., Besser, J., Hundley, J., McMurray, S., Faiman, S., 2009. An assessment of freshwater mussel (Bivalvia Margaritiferidae and Unionidae) populations and heavy metal sediment contamination in the Big River, Missouri. Report Prepared for U.S. Department of the Interior, 109 p.

Rosgen, D.L., 1996. Applied river morphology. Wildland Hydrology, Pagosa Springs, Colorado.

Saucier, R.T., 1983. Historic changes in the Current River meander regime. Proceedings of the Rivers '83 Conference, American Society of Civil Engineers, 180–190.

Schmitt, C.J., and S.E. Finger, 1982. The dynamics of metals from past and present mining activities in the Big and Black River watersheds, southeastern Missouri. Final report to the U.S. Army Corps of Engineers, St. Louis District, project no. DACW43-80-A-0109.

Schumm, S.A., 1977. The fluvial system. John Wiley and Sons, New York, New York.

Schumm, S.A., 1985. Patterns of alluvial rivers. Annual Review of Earth and Planetary Sciences, 13 (1), 5-27.

Schumm, S.A., Darby, S.E., Watson, C.C., 1984. Incised channels: morphology dynamics and control. Water Resources Publications, Littleton, Colorado.

Simon, A., 1989. A model of channel response in disturbed alluvial channels, Earth Surface Processes and Landforms 14, 11-26.

Simon, A., Hupp, C.R., 1986. Channel evolution in modified Tennessee channels. Proceedings of the Fourth Federal Interagency Sedimentation Conference, March 24-27, 1986, Las Vegas, NV.

Simon, A., Hupp, C.R., 1987. Geomorphic and vegetative recovery processes along modified Tennessee streams: an interdisciplinary approach to distributed fluvial systems. Forest Hydrology and Watershed Management. Proceedings of the Vancouver Symposium. IAHS-AISH Publ. No. 167, 251-262.

Simons, Li and Associates, 1982. Engineering analysis of fluvial systems. Simons, Li and Associates, Fort Collins, Colorado.

Skaer, D.M., 2000. Soil Survey of Jefferson County, Missouri. USDA-NRCS. U.S. Gov. Print Office, Washington, D.C.

Smith, B.J., Schumacher, J.G., 1991. Hydrochemical and sediment data for the old lead belt, Southeastern Missouri – 1988–89. USGS Open File Report 91–211 (98 pp.).

Smith, B.J., Schumacher, J.G., 1993. Surface-water and sediment quality in the Old Lead Belt, southeastern Missouri – 1988-89. USGS Water-Resources Investigations Report 93-4012, 92 p.

Stephenson, R.A., 1970. On the use of grain size analysis in geomorphological studies. The Professional Geographer 22 (4), 200-203.

Taggart, A.F., 1945. Handbook of mineral dressing: ores and industrial minerals. John Wiley and Sons Inc., New York.

Thorne, C.R., Allen, R.G., Simon, A., 1996. Geomorphological river channel reconnaissance for river analysis, engineering, and management. Transactions of the Institute of British Geographers, New Series 21 (3), 469-483.

U.S. Geological Survey, 2012a. Water-resources data for the United States, Water Year 2011: U.S. Geological Survey Water -Data Report WDR-US-2011, site 07018100.

U.S. Geological Survey, 2012b. Water-resources data for the United States, Water Year 2011: U.S. Geological Survey Water -Data Report WDR-US-2011, site 07017200.

U.S. Geological Survey, 2012c. Water-resources data for the United States, Water Year 2011: U.S. Geological Survey Water -Data Report WDR-US-2011, site 07018500.

Watson, C.C., Biedenharn, D.S., Bledsoe, B.P., 2002. Use of incised channel evolution models in understanding rehabilitation alternatives. Journal of the American Water Resources Association 38 (1), 151-160.

Wilcock, P.; Pitlick, J.; Cui, Y., 2009. Sediment transport primer: estimating bed-material transport in gravel-bed rivers. Gen. Tech. Rep. RMRS-GTR-226. Fort Collins, CO: U.S. Department of Agriculture, Forest Service, Rocky Mountain Research Station. 78 p.

Winkler, J.A., Arritt, R.W., Pryor, S.C., 2012: Climate projections for the Midwest: availability, interpretation and synthesis. U.S. National Climate Assessment Midwest Technical Input Report, 24 p.

Wolman, M.G., 1954. A method of sampling coarse river-bed material. Transactions of the American Geophysical Union 35 (6), 951-956.

Young, B.M., 2011. Historical channel change and mining-contaminated sediment remobilization in the lower Big River, eastern Missouri. Master's Thesis, Missouri State University, USA.

APPENDICES

Appendix A: Field Site Details

R-km (at center)	Coordinates		Area of Drainage (km^2)	Description
	Latitude	Longitude		
101.7	38.08735	-90.68187	1,363.1	Washington State Park
115.5	38.04165	-90.62119	1,282.3	Hwy CC at Blackwell
119.3	38.01378	-90.61571	1,142.2	Upstream of Mill Creek
121.0	38.00683	-90.62269	1,139.1	Dickinson Rd.
122.0	38.00377	-90.61084	1,136.2	Upstream of Dickinson Rd.
133.2	37.96771	-90.57524	1,049.5	Hwy E below Bonne Terre
136.7	37.95501	-90.55166	1,020.7	Cherokee Landing
140.6	37.95624	-90.54184	1,007.4	St. Francois State Park
146.9	37.92583	-90.49898	820.8	Hwy K below Flat River Creek
151.5	37.90752	-90.49350	809.2	River's Bend Rd.
156.4	37.89026	-90.51478	678.1	Hwy 67 above Flat River Creek
158.1	37.88860	-90.52759	675.0	Desloge
163.4	37.88858	-90.56024	662.8	Bar Site
165.5	37.87546	-90.55113	658.9	Bone Hole
166.5	37.87507	-90.56051	645.7	Upstream of Bone Hole
169.7	37.86531	-90.57747	640.8	Downstream of Leadwood
170.7	37.86996	-90.58581	637.7	Leadwood Access
171.9	37.87867	-90.58296	625.4	Upstream of Leadwood
181.2	37.86778	-90.63986	572.4	Highway 8
182.7	37.86938	-90.65283	569.1	Upstream of Highway 8
191.7	37.83025	-90.69137	456.6	Irondale Gage

Appendix B. Bar Sediment Sample Descriptions

Appendix B. Bar and sediment sample descriptions.

Sample No.	Coordinates		River Kilometer (0=mouth)	Collection Date	Type	Position	Depth (cm)
	Latitude	Longitude					
1	37.83021	-90.69112	191.64	11/23/2008	T	15-30	1
2	37.83021	-90.69112	191.64	11/23/2008	T	15-30	2
3	37.86776	-90.63961	181.17	1/19/2009	M	15-30	3
4	37.88044	-90.58304	172.17	9/23/2011	H	0-15	4
5	37.88044	-90.58304	172.17	9/23/2011	H	15-30	5
6	37.88044	-90.58304	172.15	9/23/2011	M	0-15	6
7	37.88044	-90.58304	172.15	9/23/2011	M	15-30	7
8	37.87992	-90.58307	172.09	9/23/2011	T	0-15	8
9	37.87992	-90.58307	172.09	9/23/2011	T	15-30	9
10	37.87206	-90.58791	170.94	10/1/2008	H	15-30	10
11	37.87206	-90.58798	170.94	10/1/2008	H	15-30	11
12	37.87194	-90.58785	170.91	10/1/2008	M	15-30	12
13	37.87182	-90.58777	170.89	10/1/2008	T	15-30	13
14	37.86540	-90.57151	169.16	7/1/2011	M	0-15	14
15	37.86540	-90.57151	169.16	7/1/2011	M	15-30	15
16	37.86548	-90.57140	169.14	7/1/2011	T	0-15	16
17	37.86548	-90.57140	169.14	7/1/2011	T	15-30	17
18	37.87537	-90.56057	166.45	9/23/2011	H	0-15	18
19	37.87537	-90.56057	166.45	9/23/2011	H	15-30	19
20	37.87409	-90.56030	166.31	9/23/2011	M	0-15	20
21	37.87409	-90.56030	166.31	9/23/2011	M	15-30	21
22	37.87347	-90.56042	166.25	9/23/2011	T	0-15	22
23	37.87347	-90.56042	166.25	9/23/2011	T	15-30	23
24	37.88838	-90.56005	163.40	9/16/2009	M	10-20	24
25	37.88844	-90.55992	163.40	9/16/2009	M	10-20	25
26	37.88877	-90.56039	163.35	9/16/2009	T	10-20	26
27	37.88895	-90.56011	163.33	9/16/2009	T	10-20	27
28	37.89069	-90.55914	163.12	6/30/2011	M	0-15	28
29	37.89069	-90.55914	163.12	6/30/2011	M	15-30	29
30	37.89078	-90.55907	163.10	6/30/2011	T	0-15	30
31	37.89078	-90.55907	163.10	6/30/2011	T	15-30	31
32	37.88780	-90.52773	158.20	12/9/2011	T	0-15	32
33	37.88780	-90.52773	158.20	12/9/2011	T	15-30	33
34	37.88844	-90.52753	158.13	1/19/2009	H	15-30	34

Appendix B. Bar and sediment sample descriptions.

Sample No.	Coordinates		River Kilometer (0=mouth)	Collection Date	Type	Position	Depth (cm)
	Latitude	Longitude					
35	37.88879	-90.52755	158.09	12/9/2011	M	0-15	35
36	37.88879	-90.52755	158.09	12/9/2011	M	15-30	36
37	37.88883	-90.52756	158.08	1/19/2009	M	15-30	37
38	37.88951	-90.52743	158.00	1/19/2009	T	15-30	38
39	37.89057	-90.51861	156.86	10/2/2008	H	15-30	39
40	37.89048	-90.51836	156.84	10/2/2008	M	15-30	40
41	37.89052	-90.51813	156.80	6/30/2011	M	0-15	41
42	37.89052	-90.51813	156.80	6/30/2011	M	15-30	42
43	37.89043	-90.51786	156.79	10/2/2008	T	15-30	43
44	37.89048	-90.51786	156.79	6/30/2011	T	0-15	44
45	37.89048	-90.51786	156.79	6/30/2011	T	15-30	45
46	37.89015	-90.51506	156.54	10/2/2008	H	15-30	46
47	37.89016	-90.51443	156.48	10/2/2008	M	15-30	47
48	37.89026	-90.51394	156.44	10/2/2008	M	15-30	48
49	37.89037	-90.51339	156.39	10/2/2008	T	15-30	49
50	37.90747	-90.49361	151.29	7/1/2011	M	0-15	50
51	37.90747	-90.49361	151.29	7/1/2011	M	15-30	51
52	37.90756	-90.49354	151.28	7/1/2011	T	0-15	52
53	37.90756	-90.49354	151.28	7/1/2011	T	15-30	53
54	37.92537	-90.49831	147.21	11/24/2008	H	15-30	54
55	37.92592	-90.49898	147.12	11/24/2008	M	15-30	55
56	37.92629	-90.50006	147.01	11/24/2008	T	15-30	56
57	37.95434	-90.53916	140.85	11/24/2008	H	15-30	57
58	37.95443	-90.53958	140.81	11/24/2008	M	15-30	58
59	37.95465	-90.54009	140.75	11/24/2008	T	15-30	59
60	37.95848	-90.54144	140.28	11/24/2008	H	15-30	60
61	37.95905	-90.54110	140.21	11/24/2008	M	15-30	61
62	37.95947	-90.54065	140.15	11/24/2008	T	15-30	62
63	37.95516	-90.55039	136.79	10/3/2008	M	15-30	63
64	37.95512	-90.55063	136.77	10/3/2008	M	15-30	64
65	37.96763	-90.57503	132.91	11/24/2008	H	15-30	65
66	37.96769	-90.57525	132.90	11/24/2008	H	15-30	66
67	37.96777	-90.57512	132.89	11/24/2008	T	15-30	67
68	37.96755	-90.58382	131.66	7/2/2011	M	0-15	68
69	37.96755	-90.58382	131.66	7/2/2011	M	15-30	69
70	37.96723	-90.58379	131.62	7/2/2011	T	0-15	70

Appendix B. Bar and sediment sample descriptions.

Sample No.	Coordinates		River Kilometer (0=mouth)	Collection Date	Type	Position	Depth (cm)
	Latitude	Longitude					
71	37.96723	-90.58379	131.62	7/2/2011	T	15-30	71
72	38.00273	-90.60974	122.24	9/21/2011	M	0-15	72
73	38.00273	-90.60974	122.24	9/21/2011	M	15-30	73
74	38.00359	-90.61064	122.11	9/21/2011	H	0-15	74
75	38.00359	-90.61064	122.11	9/21/2011	H	15-30	75
76	38.00368	-90.61116	122.06	9/21/2011	M	0-15	76
77	38.00368	-90.61116	122.06	9/21/2011	M	15-30	77
78	38.00385	-90.61172	122.01	9/21/2011	T	0-15	78
79	38.00385	-90.61172	122.01	9/21/2011	T	15-30	79
80	38.00729	-90.62201	120.99	1/21/2009	H	15-30	80
81	38.00700	-90.62248	120.93	1/21/2009	M	15-30	81
82	38.00684	-90.62345	120.84	1/21/2009	T	15-30	82
83	38.01354	-90.61610	118.91	1/21/2009	H	15-30	83
84	38.01364	-90.61565	118.87	1/21/2009	M	15-30	84
85	38.01386	-90.61506	118.81	1/21/2009	T	15-30	85
86	38.03867	-90.62063	115.82	11/24/2008	H	15-30	86
87	38.03893	-90.62079	115.78	11/24/2008	M	15-30	87
88	38.03914	-90.62076	115.75	11/24/2008	T	15-30	88
89	38.04193	-90.62103	115.44	11/24/2008	H	15-30	89
90	38.04209	-90.62090	115.43	11/24/2008	T	15-30	90
91	38.04457	-90.62096	115.10	1/21/2009	H	15-30	91
92	38.04472	-90.62108	115.10	1/21/2009	T	15-30	92
93	38.08752	-90.68167	101.79	1/22/2009	H	15-30	93
94	38.08733	-90.68226	101.74	1/22/2009	M	15-30	94
95	38.08715	-90.68261	101.69	1/22/2009	T	15-30	95

Appendix C. Pebble Count Data

Site	Riffle			Glide			Riffle & Glide			Bar Head			Bar Mid			Bar Tail		
	D16	D50	D84	D16	D50	D84	D16	D50	D84	D16	D50	D84	D16	D50	D84	D16	D50	D84
191.7	n/a	n/a	n/a	3.6	22.3	36.7	n/a	n/a	n/a	11.0	22.3	45.0	7.1	16.0	26.0	5.0	13.5	22.6
182.7	16.0	90.0	217.6	4.7	22.6	128.0	11.0	64.0	154.8	n/a	n/a	n/a	n/a	n/a	n/a	n/a	n/a	n/a
181.2	11.0	22.6	45.0	16.0	32.0	45.0	11.0	32.0	45.0	5.6	11.0	22.6	n/a	n/a	n/a	n/a	n/a	n/a
171.9	8.0	22.6	32.0	1.2	16.0	32.0	4.0	22.6	32.0	5.6	11.0	22.6	9.3	16.0	22.6	5.6	8.0	22.6
170.7	22.6	45.0	64.0	5.6	11.0	22.6	8.0	22.6	64.0	n/a	n/a	n/a	n/a	n/a	n/a	5.6	11.0	16.0
169.7	8.7	22.6	45.0	4.0	11.0	22.6	5.6	22.6	45.0	8.0	16.0	32.0	8.0	22.6	32.0	2.8	11.0	29.7
165.5	5.6	16.0	22.6	5.6	13.5	26.0	5.6	16.0	22.6	8.0	19.3	32.0	5.0	11.0	22.6	4.5	8.0	14.4
163.4	5.6	11.0	22.6	1.0	5.6	16.0	2.0	8.0	22.6	8.0	16.0	32.0	4.0	11.0	22.6	2.8	5.6	11.0
158.1	8.0	11.0	19.7	8.0	16.0	22.6	8.0	16.0	22.6	5.6	11.0	32.0	n/a	n/a	n/a	4.0	5.6	16.0
156.4	3.0	11.0	32.0	1.0	5.6	16.0	1.0	5.6	22.6	2.0	5.6	16.0	4.0	5.6	16.0	1.0	5.6	11.0
151.5	4.0	16.0	22.6	1.0	5.6	16.0	1.0	8.0	22.6	5.6	4.0	11.0	5.7	16.0	31.6	1.0	4.0	11.0
140.5	5.6	11.0	22.6	1.0	5.6	16.0	1.0	11.0	22.6	4.0	11.0	22.6	4.0	9.5	16.0	2.8	8.0	22.6
133.2	11.0	22.6	45.0	2.8	11.0	22.6	4.0	16.0	32.0	1.9	16.0	32.0	1.0	11.0	16.0	0.1	4.0	22.6
122.0	11.0	32.0	64.0	2.0	22.6	64.0	2.7	32.0	64.0	1.0	11.0	32.0	11.0	22.6	45.0	4.7	11.0	22.6
101.7	n/a	n/a	n/a	n/a	n/a	n/a	n/a	n/a	n/a	5.6	16.0	22.6	5.6	11.0	22.3	2.0	8.0	15.8

Appendix D. Channel Recovery Assessments

Appendix D-1: Key to channel recovery assessments.

Category	Notes Code	Description
Riffle (R-)	RR	Regime
	RH	Bar Head
	RT	Bar Tail
	RD	Delta
	RB	Bedrock
	RO	Other
	RA	Artificial
	RC	Riffle Crest
Glide (G-)	GC	Center
	GL	Lateral
	GS	Short, < 1 channel width wide
Pool (P-)	PC	Center
	PL	Lateral
	PB	Bluff
	PS	Scour
	PO	Other
	PA	Artificial
Run (N-)	NR	Below Riffle
	NP	Below Pool
Gravel Bar Type	X	None
	L	Low/subaqueous
	S	Side/alternating
	T	Transverse/diagonal
	D	Delta
	P	Point
	C	Center/mid-channel
	M	Mega bar
Age of Disturbance	R	Recent
	P	Past
Floodplain Type	X	None
	B	Bench
	S	Shelf
	L	Low/subaqueous
	H	High
	T	Terrace

Appendix D-1: Key to channel recovery assessments.

Category	Notes Code	Description
	BR	Bedrock
Bank Angle	1	Low (<45 deg.)
	2	Medium (45-75 deg.)
	3	Steep (70-85 deg.)
	4	Vertical (<85 deg.)
Bank Vegetation	a	Raw
	b	Grass
	c	Shrubs
	d	Young trees
	e	Legacy trees
Recovery Indicators	0	Not present
	1	Some evidence
	2	Present
	r	Right side only
	l	Left side only
Other	% AC	Percent of active channel

Appendix D-2. Channel recovery assessments: channel bedform, gravel bars, islands, and LWD.

Site	R-km	Date	Channel Bedform			Gravel Bars			Island	LWD
			Channel Unit	Water Depth	Probe Refusal	Primary Type	Surface Area		(R or L)	Trees
							Total	High	(FP or LT)	(count)
			(code)	(m)	(m)	(code)	(% AC)	(% AC)		
C1	191.87	12/10/2011	PC	1.0	0.1	X				0
C1	191.80	12/11/2011	PC	1.1	0	X				1
C1	191.75	12/12/2011	PB	1.4	0.1	X				0
C1	191.67	12/13/2011	GL	1.1	0	X				0
C1	191.55	12/14/2011	GL	1.1	1	X				1
C1	191.45	12/15/2011	NR	1.1	0	C	80	70		0
C1	191.34	12/16/2011	NR	0.5	0.2	C	90	85		6
C1	191.29	12/17/2011	GL	0.5	0	C	90	85		3
C1	191.23	12/18/2011	NR	0.6	0.2	C	90	85		0
C2	183.50	3/9/2012	GL	0.9	0	S	20	0		3
C2	183.45	3/9/2012	RB	0.8	0	X				0
C2	183.37	3/9/2012	NR	0.8	0	X				0
C2	183.31	3/9/2012	PO	1.0	0	X				2
C2	183.25	3/9/2012	PO	1.1	0	X				2
C2	183.20	3/9/2012	GC	0.8	0	X				0
C2	183.14	3/9/2012	GC	0.9	0	X				0
C2	183.10	3/9/2012	RB	0.8	0	S	5	0		0
C2	183.06	3/9/2012	RB	0.7	0	X				3
C2	183.00	3/9/2012	RB	0.7	0	L	10	0		0
C4	172.18	12/9/2011	PL	1.5	0	S	10	0		2
C4	172.12	12/9/2011	GL	1.1	0.2	S	50	15		2

Appendix D-2. Channel recovery assessments: channel bedform, gravel bars, islands, and LWD.

Site	R-km	Date	Channel Bedform			Gravel Bars			Island	LWD
			Channel Unit	Water Depth	Probe Refusal	Primary Type	Surface Area		(R or L)	Trees
							Total	High	(FP or LT)	(count)
			(code)	(m)	(m)	(code)	(% AC)	(% AC)		
C4	172.03	12/9/2011	GL	1.0	0.3	S	25	20		0
C4	171.96	12/9/2011	RNR	0.9	0	S	70	85		2
C4	171.84	12/9/2011	PL	1.5	0	S	90	85		3
C4	171.74	12/9/2011	PB	1.2	0.1	S	20	18		0
C4	171.64	12/9/2011	GC	1.2	0.1	X				0
C4	171.52	12/9/2011	NR	0.8	0	X				0
M2	169.11	12/9/2011	NR	1.5	0	L	10	0		0
M2	169.22	12/9/2011	RH	1.1	0	S	20	5		1
M2	169.30	12/9/2011	PC	1.9	0	X				1
M2	169.39	12/9/2011	PC	1.9	0	X				1
M2	169.50	12/9/2011	NR	1.2	0.1	L	5	0		2
M2	169.64	12/9/2011	NR	1.1	0.3	L	5	0		1
M2	169.74	12/9/2011	NR	1.0	0.1	M	80	60		3
M2	169.83	12/9/2011	GC	0.7	0	X				0
M2	169.96	12/9/2011	GC	0.7	0.2	X				0
M2	170.08	12/9/2011	NR	1.0	0.2	S	5	3		1
M2	170.19	12/9/2011	RH	0.6	0	S	70	40		0
M2	170.26	12/9/2011	RH	0.4	0.4	S	70	30		0
M2	170.31	12/9/2011	GC	0.9	0.1	X				0
M3	166.59	12/10/2011	PB	1.8	0	X				4
M3	166.49	12/10/2011	GC	0.9	0.3	X				2

Appendix D-2. Channel recovery assessments: channel bedform, gravel bars, islands, and LWD.

Site	R-km	Date	Channel Bedform			Gravel Bars			Island	LWD
			Channel Unit	Water Depth	Probe Refusal	Primary Type	Surface Area		(R or L)	Trees
							Total	High	(FP or LT)	(count)
			(code)	(m)	(m)	(code)	(% AC)	(% AC)		
M3	166.43	12/10/2011	NR	1.1	0.1	M	70	5		2
M3	166.35	12/10/2011	PL	1.6	0.1	M	85	40		2
M3	166.29	12/10/2011	NP	1.2	1	M	90	10		3
M3	166.25	12/10/2011	NP	1.4	0.2	M	80	10		1
M3	166.18	12/10/2011	PB	1.7	0	M	PB	0		2
M3	166.11	12/10/2011	PB	1.7	0.1	M	10	8		0
M3	166.04	12/10/2011	PB	>2.5	0	X				0
M3	165.57	12/10/2011	GC	1.5	0.8	X				0
M6	157.64	12/9/2011	NP	0.5	0.4	L	20	0		5
M6	157.69	12/9/2011	NP	0.3	1.5	S	5	0		3
M6	157.73	12/9/2011	PL	1.2	1.1	S	20	0		0
M6	157.79	12/9/2011	PB	1.2	1.4	S	50	20		0
M6	157.84	12/9/2011	RH	0.2	1.6	S	20			1
M6	157.92	12/9/2011	PL	1.3	0	S	70	0		3
M6	157.97	12/9/2011	GL	0.8	0.9	S	50	0		0
M6	156.93	12/8/2011	PL	1.6	0.9	L	<5	0		3
M6	156.87	12/8/2011	PC	1.4	1.2	X				3
M6	156.82	12/8/2011	GL	1.6	0	S	50	25		2
M6	156.74	12/8/2011	PB	1.3	0	S	20	5		1
M6	156.67	12/8/2011	GC	1.1	1.1	S	40	0		4
M6	156.61	12/8/2011	RT	0.4	2.2					

Appendix D-2. Channel recovery assessments: channel bedform, gravel bars, islands, and LWD.

Site	R-km	Date	Channel Bedform			Gravel Bars			Island	LWD
			Channel Unit	Water Depth	Probe Refusal	Primary Type	Surface Area		(R or L)	Trees
							Total	High	(FP or LT)	(count)
			(code)	(m)	(m)	(code)	(% AC)	(% AC)		
M6	156.56	12/8/2011	NR	0.6	2.3	X				1
M6	156.50	12/8/2011	PL	1.4	0.5	S	40	5		3
M6	156.44	12/8/2011	RT	1.0	0.5	S	65	20		1
M6	156.38	12/8/2011	NR	0.8	0.6	S	25	15		0
M8	151.63	3/10/2012	GC	0.9	0	L, P	10	0		1
M8	151.58	3/10/2012	NR	0.7	0.1	S	40	0		1
M8	151.52	3/10/2012	PL	0.9	0.1	S	50	0		1
M8	151.46	3/10/2012	RH	0.7	0.5	M	80	60		0
M8	151.41	3/10/2012	NR	0.6	0.1	M	50	40		5
M8	151.38	3/10/2012	PL	1.0	0.3	X				2
M8	151.32	3/10/2012	RH	0.5	2	S	70	0		2
M8	151.26	3/10/2012	NR	0.5	0.4	S	5	0		0
M8	151.20	3/10/2012	PS	1.0	0.3	C	40	0		7
M10	140.74	3/12/2012	GC	0.25	>2.5	X				5
M10	140.84	3/12/2012	NR	0.45	1	C	70	20	R, FP	8
M10	140.96	3/12/2012	NR	0.45	1.4	X				5
M10	141.10	3/12/2012	NR	0.18	>2.5	X				6
M10	141.19	3/12/2012	PB	0.9	0.1	S	5	0		8
M13	122.29	3/10/2012	GL	0.55	0.1	X				3
M13	122.20	3/10/2012	NR	1.7	0.1	S	10	0		10
M13	122.09	3/10/2012	PL	2.2	0	M	50	5		4

Appendix D-2. Channel recovery assessments: channel bedform, gravel bars, islands, and LWD.

Site	R-km	Date	Channel Bedform			Gravel Bars			Island	LWD
			Channel Unit	Water Depth	Probe Refusal	Primary Type	Surface Area		(R or L)	Trees
							Total	High	(FP or LT)	(count)
			(code)	(m)	(m)	(code)	(% AC)	(% AC)		
M13	122.00	3/10/2012	RT	0.15	0.1	M	70	0		1
M13	121.89	3/10/2012	NR	0.4	0.8	S	20	0		1
M13	121.75	3/10/2012	PB	1.35	0.8	X				4
M13	121.64	3/10/2012	PB	1.3	0.1	X				5
M13	121.54	3/10/2012	GC	0.6	0.2	S	50	0		2
M13	121.42	3/10/2012	NP	0.8	1.2	S	5	0		4

Appendix D-3. Channel recovery assessments: floodplain characteristics and bank condition.

Site	R-km	Floodplain Characteristics				Bank Condition					
		Right		Left		Right			Left		
		Type (code)	Width (m)	Type (code)	Width (m)	Angle (code)	Und Cut (% length)	Slumps (% length)	Angle (code)	Und Cut (% length)	Slumps (% length)
C1	191.87	H	1	S	30	2a		30	1d		
C1	191.80	H	1	S	5	2a		15	1d		
C1	191.75	BR		L	2	2d			1d		
C1	191.67	BR		S	15	3c			1d		
C1	191.55	H	10	L	15	2e		20	2d		
C1	191.45	BR		L	1	2d			2d		
C1	191.34	S		S	30	2c			1d		
C1	191.29	S	40	LT		2a			2d		
C1	191.23	S	60	L	3	1d			2d		
C2	183.50	L	30+	BR	2	1d			1d		
C2	183.45	L	15	S	15	2c			1d		
C2	183.37	B	3	S	20	1d			1d		
C2	183.31	X	0	S	20	3b		20	1d		
C2	183.25	L	10	S	10	3c	30		1d		
C2	183.20	L	10	H	10	3c	20	10	2d		
C2	183.14	L	8	S	6	2c			1d		
C2	183.10	B	1	L	10	10			1d		
C2	183.06	L	6	X	0	10			2d		
C2	183.00	L	5	X	0	10			1d		
C4	172.18	L	5	H		1d			4a		
C4	172.12	L	30	L	15	1d			4a		

Appendix D-3. Channel recovery assessments: floodplain characteristics and bank condition.

Site	R-km	Floodplain Characteristics				Bank Condition					
		Right		Left		Right			Left		
		Type (code)	Width (m)	Type (code)	Width (m)	Angle (code)	Und Cut (% length)	Slumps (% length)	Angle (code)	Und Cut (% length)	Slumps (% length)
C4	172.03	L	30	L	15	2d		10	3d		
C4	171.96	L	10	L	50	2d			1d		
C4	171.84	H		L	50	3d		20	1d		
C4	171.74	H		BR		4c		20	4d		
C4	171.64	H		BR		3d		30	2d		
C4	171.52	B	3	BR		2d		30	2d		
M2	169.11	BR		H		2d			2d		30
M2	169.22	BR		H					2d		20
M2	169.30	FILL		H					2d		30
M2	169.39	FILL		L	1				2d		10
M2	169.50	FILL		H	10				2d		30
M2	169.64	FILL		L	10	2d			2d		10
M2	169.74	BR		H		2d			3a		
M2	169.83	BR		L	10	2d			2d		10
M2	169.96	BR		L	10	2d			2d		80
M2	170.08	H		L	10	2d	10	5	1d		
M2	170.19	H	20	L	10	3b		70	1d		
M2	170.26	H	20	L	1.5	3b		70	2d		20
M2	170.31	H	20	L	1	2d			2d	10	20
M3	166.59	H	2	BR		3d		30			
M3	166.49	H		L	2	3d		30	3b		

Appendix D-3. Channel recovery assessments: floodplain characteristics and bank condition.

Site	R-km	Floodplain Characteristics				Bank Condition					
		Right		Left		Right			Left		
		Type (code)	Width (m)	Type (code)	Width (m)	Angle (code)	Und Cut (% length)	Slumps (% length)	Angle (code)	Und Cut (% length)	Slumps (% length)
M3	166.43	H	2	H		2d		30	2d		
M3	166.35	L	1	X		2d		70	1b		
M3	166.29	H		S		2e		20	1b		
M3	166.25	H		S		2			1b		
M3	166.18	BR		S		4			1a		
M3	166.11	BR		L	5	4			2a		
M3	166.04	BR		H		4			3c		
M3	165.57	BR		L	5	2d	20		2d		
M6	157.64	L	5	H		2d		50	2d		50
M6	157.69	L	10	L	2	3b		30	2d		70
M6	157.73	L	8	L	2	4a		15	1d		70
M6	157.79	BR		H	10	3b			1d		
M6	157.84	BR/H		H	10	3d	5		2d		20
M6	157.92	H/BR		LT		2d		20	2d		60
M6	157.97	H/BR		LT		2c			2d		60
M6	156.93	H		L	15	2c	0	50	2d	0	0
M6	156.87	H		H	0	3c	0	50	3d	0	20
M6	156.82	L	2	BR	0	4a	0	0	1d	0	0
M6	156.74	X	0	H	0	4a	0	0	2d	0	0
M6	156.67	H		BR	5	1d	0	0	2d	0	0
M6	156.61										

Appendix D-3. Channel recovery assessments: floodplain characteristics and bank condition.

Site	R-km	Floodplain Characteristics				Bank Condition					
		Right		Left		Right			Left		
		Type (code)	Width (m)	Type (code)	Width (m)	Angle (code)	Und Cut (% length)	Slumps (% length)	Angle (code)	Und Cut (% length)	Slumps (% length)
M6	156.56	H		L	5	3c	0	40	1d	0	0
M6	156.50	H		L	10	2b	0	70	2d	0	0
M6	156.44	H	5	L	15	2d	50	0	1d	0	0
M6	156.38	L	10	L	15	2d	0	0	2d	0	0
M8	151.63	B	1.5	X	0	2d			1d		
M8	151.58	S	0	H	30+	2d			1d		
M8	151.52	S	0	L	30+	2d			1d		
M8	151.46	S	0	X	0	3d			4a		10
M8	151.41	S	0	X	0	3d			4a		40
M8	151.38	B	2	H	20+	2e			1s		
M8	151.32	H	10	H	20+	2d		10	2s/l		10
M8	151.26	T	15	H	20+	2d		30	1d		
M8	151.20	T	20	L	2	3a		50	1d		
M10	140.74	H	100+	T	100+	2d			2d		
M10	140.84	H	100+	T	2	2b			2a/b		100
M10	140.96	L	8	T	20	1d			2c		80
M10	141.10	T	100+	T	15	1c		15	2c		
M10	141.19	T	100+	X	0	1c			4a		
M13	122.29	H	10	T	100	4a			3d		
M13	122.20	H	10	T	100	1d			2d		30
M13	122.09	H	10	S	10	1d			1d		

Appendix D-3. Channel recovery assessments: floodplain characteristics and bank condition.

Site	R-km	Floodplain Characteristics				Bank Condition					
		Right		Left		Right			Left		
		Type (code)	Width (m)	Type (code)	Width (m)	Angle (code)	Und Cut (% length)	Slumps (% length)	Angle (code)	Und Cut (% length)	Slumps (% length)
M13	122.00	L	5	T	100	1d			3c		
M13	121.89	L	50	T	100	1d			2d		
M13	121.75	L	20+	T	100	3b			4a		
M13	121.64	H	20+	T	100	2d			4a		
M13	121.54	H	30	T	100	1d			3c		10
M13	121.42	H	30	T	100	3b			1d		

Appendix D-4. Channel recovery assessments: recovery indicators.

Site	R-km	Recovery Indicators Present? 0 = no 1 = maybe 2 = yes		
		Lateral Widening	Bank Recession	Floodplain Recovery
C1	191.87	0	1.5	1.5
C1	191.80	0.5	0	1.5
C1	191.75	0	0	1.5
C1	191.67	0	0	1.5
C1	191.55	0	1.5	1.5
C1	191.45	0	0	1.5
C1	191.34	0	1.5	1.5
C1	191.29	0	1.5	0
C1	191.23	0	1.5	1.5
C2	183.50	0	1	2
C2	183.45	1	1	2
C2	183.37	0	0.5	2
C2	183.31	0	2	0
C2	183.25	0.5	0.5	1.5
C2	183.20	1.5	0	1.5
C2	183.14	0.5	0	2
C2	183.10	1	0	2
C2	183.06	0	0	0.5
C2	183.00	0	0	1.5
C4	172.18	2	1.5	1.5
C4	172.12	0	1.5	1.5
C4	172.03	0	0	2
C4	171.96	0.5	0	2
C4	171.84	1	0.5	1.5
C4	171.74	0.5	0	0.5
C4	171.64	0	0.5	0
C4	171.52	0	1.5	0
M2	169.11	0	0.5	1l
M2	169.22	0	1.5	1l
M2	169.30	0	1.5	0
M2	169.39	0	1.5	1.5
M2	169.50	0	2	0.5
M2	169.64	0	2	2
M2	169.74	2	0	0
M2	169.83	0	1.5	1.5

Appendix D-4. Channel recovery assessments: recovery indicators.

Site	R-km	Recovery Indicators Present? 0 = no 1 = maybe 2 = yes		
		Lateral Widening	Bank Recession	Floodplain Recovery
M2	169.96	0	1.5	1.5
M2	170.08	1.5	2	2
M2	170.19	2	2	2
M2	170.26	1.5	1.5	1.5
M2	170.31	0	2	1.5
M3	166.59	0	0.5	0
M3	166.49	1.5	0	1.5
M3	166.43	2	1.5	1.5
M3	166.35	2	2	0
M3	166.29	0	0	0
M3	166.25	0	0.5	0.5
M3	166.18	0	0	0
M3	166.11	0	0	1.5
M3	166.04	0	0.5	0
M3	165.57	2	2	1.5
M6	157.64	1.5	2	2
M6	157.69	2	2	2
M6	157.73	2	2	2
M6	157.79	2	2	1
M6	157.84	2	2	1.5
M6	157.92	2	2	0
M6	157.97	2	2	0
M6	156.93	1	1.5	1.5
M6	156.87	1	1.5	0.5
M6	156.82	2	1.5	0.5
M6	156.74	0	0	0
M6	156.67	1	1.5	0
M6	156.56	2	1.5	1.5
M6	156.50	2	2	1.5
M6	156.44	0.5	2	2
M6	156.38	0	2	2
M8	151.63	0	0.5	0
M8	151.58	0	0.5	0
M8	151.52	0	0.5	0.5
M8	151.46	2	0	0

Appendix D-4. Channel recovery assessments: recovery indicators.

Site	R-km	Recovery Indicators Present? 0 = no 1 = maybe 2 = yes		
		Lateral Widening	Bank Recession	Floodplain Recovery
M8	151.41	2	0	0
M8	151.38	1	0.5	1.5
M8	151.32	0	2	0
M8	151.26	1	2	0
M8	151.20	0	1.5	0
M10	140.74	0	0.5	0
M10	140.84	0	2	0
M10	140.96	0	2	1.5
M10	141.10	0	2	0
M10	141.19	0	1.5	0
M13	122.29	2	0	0
M13	122.20	0	2	1.5
M13	122.09	0	1.5	1.5
M13	122.00	2l	0	1.5
M13	121.89	0	0	1.5
M13	121.75	0	0	0
M13	121.64	0	0	0
M13	121.54	1.5	1.5	0
M13	121.42	1.5	1.5	0

Appendix E. Bar Sediment Sample Analysis

Appendix E. Bar sediment sample analysis.

Sample No.	Size Distribution by Mass (% of sample)							XRF Analysis (<2 mm fraction)		
	Fines (<2 mm)	VFG (2-4 mm)	FG (4-8 mm)	MG (8-16 mm)	CG (16-32 mm)	VCG (32-64 mm)	Chat (4-16mm)	Pb (ppm)	Zn (ppm)	Ca (ppm)
1	31	18	23	16	12	0	39	ND	21	2,037
2	22	18	21	22	17	0	43	ND	17	8,015
3	30	21	26	17	6	0	43	ND	39	4,766
4	26	14	19	19	16	7	38	ND	49	4,589
5	18	10	17	27	25	4	44	ND	32	1,138
6	17	15	22	29	17	0	51	20	22	3,207
7	23	18	24	22	12	0	46	35	44	969
8	11	19	31	32	7	0	63	47	72	2,428
9	26	14	22	26	7	6	47	ND	17	1,515
10	18	11	22	23	26	0	45	810	649	15,420
11	29	29	22	14	6	0	36	42	60	1,862
12	8	10	22	28	26	6	50	ND	64	1,128
13	8	14	23	34	22	0	56	196	99	4,126
14	10	6	6	9	22	40	15	1,167	712	119,972
15	19	9	10	12	18	31	23	1,073	1,179	116,249
16	25	12	22	22	14	6	44	1,020	693	125,554
17	24	12	20	24	18	2	44	1,115	1,106	75,120
18	22	12	15	18	18	15	33	1,109	985	98,333
19	28	15	21	25	10	0	46	913	4,598	138,465
20	24	12	16	23	20	5	39	740	2,594	48,269

Appendix E. Bar sediment sample analysis.

Sample No.	Size Distribution by Mass (% of sample)							XRF Analysis (<2 mm fraction)		
	Fines (<2 mm)	VFG (2-4 mm)	FG (4-8 mm)	MG (8-16 mm)	CG (16-32 mm)	VCG (32-64 mm)	Chat (4-16mm)	Pb (ppm)	Zn (ppm)	Ca (ppm)
21	23	12	17	22	24	2	39	985	2,246	74,639
22	22	15	22	27	13	1	49	826	1,635	71,345
23	37	10	14	16	20	4	29	640	3,186	82,781
24	22	25	25	24	4	0	49	1,212	912	105,812
25	20	12	22	28	18	0	50	837	892	114,483
26	43	12	17	16	12	0	33	933	891	122,363
27	40	20	20	15	5	0	35	1,190	4,653	92,961
28	28	13	21	15	14	9	36	903	2,752	45,025
29	44	14	17	15	8	2	32	828	1,488	93,696
30	41	16	16	10	10	6	27	832	2,549	109,848
31	53	21	16	7	3	0	23	699	3,349	83,139
32	72	15	9	3	1	0	12	601	610	105,616
33	40	21	21	11	7	0	32	1,003	961	108,076
34	16	27	23	17	11	6	40	1,606	1,527	89,036
35	13	7	14	20	30	16	35	1,269	1,354	116,783
36	20	14	19	18	17	11	37	2,322	2,372	99,760
37	42	27	20	8	2	0	28	1,230	2,023	121,391
38	24	26	26	12	3	8	39	963	1,027	101,721
39	27	21	25	15	11	0	40	1,563	1,572	138,086
40	45	29	16	7	4	0	23	992	1,082	162,097
41	29	18	23	18	10	3	41	935	866	124,395

Appendix E. Bar sediment sample analysis.

Sample No.	Size Distribution by Mass (% of sample)							XRF Analysis (<2 mm fraction)		
	Fines (<2 mm)	VFG (2-4 mm)	FG (4-8 mm)	MG (8-16 mm)	CG (16-32 mm)	VCG (32-64 mm)	Chat (4-16mm)	Pb (ppm)	Zn (ppm)	Ca (ppm)
42	34	25	23	14	3	0	38	1,283	1,216	134,006
43	70	17	9	4	0	0	13	790	910	135,317
44	33	17	29	15	5	0	45	885	1,403	129,304
45	42	17	15	12	13	0	28	606	841	120,729
46	40	21	16	11	7	5	27	1,345	936	161,131
47	45	18	14	11	12	0	25	1,088	904	152,898
48	31	24	17	11	17	0	28	933	1,831	117,199
49	47	27	16	7	4	0	23	1,245	1,852	146,701
50	10	4	65	8	9	5	73	1,167	712	119,972
51	29	11	18	15	18	9	32	1,073	1,179	116,249
52	85	7	5	3	1	0	7	1,020	693	125,554
53	77	7	7	5	4	0	12	1,115	1,106	75,120
54	23	23	28	18	9	0	45	2,244	691	164,338
55	11	18	25	15	31	0	40	1,251	701	133,858
56	77	11	8	4	1	0	11	771	432	115,870
57	39	21	18	11	4	7	29	1,982	791	133,997
58	63	19	11	5	3	0	16	1,073	374	95,943
59	44	20	17	12	6	0	30	522	305	89,204
60	41	39	16	1	2	0	17	1,422	488	138,114
61	59	18	12	7	4	0	19	959	441	94,978
62	50	25	11	4	10	0	15	1,031	402	117,398

Appendix E. Bar sediment sample analysis.

Sample No.	Size Distribution by Mass (% of sample)							XRF Analysis (<2 mm fraction)		
	Fines (<2 mm)	VFG (2-4 mm)	FG (4-8 mm)	MG (8-16 mm)	CG (16-32 mm)	VCG (32-64 mm)	Chat (4-16mm)	Pb (ppm)	Zn (ppm)	Ca (ppm)
63	47	17	16	16	4	0	32	914	434	90,289
64	51	15	16	12	6	0	28	480	236	92,502
65	43	12	11	14	12	9	25	1,007	411	124,390
66	89	6	3	2	1	0	5	984	550	68,481
67	82	9	1	4	4	0	4	723	417	72,264
68	28	9	11	20	28	5	30	937	239	100,477
69	47	10	13	17	12	1	30	688	315	73,580
70	34	16	22	22	6	0	44	625	242	67,031
71	43	13	18	16	7	3	34	504	236	83,450
72	26	6	10	14	33	11	24	740	2,594	48,269
73	40	6	11	17	22	5	28	985	2,246	74,639
74	20	4	6	13	21	36	19	430	204	64,532
75	56	6	7	10	9	11	18	327	126	80,273
76	9	4	5	8	21	39	13	689	307	64,496
77	22	7	10	19	24	18	29	674	283	62,581
78	34	10	15	24	15	1	39	358	164	52,989
79	31	8	12	19	24	6	31	315	181	63,086
80	16	28	30	16	10	0	46	530	335	32,660
81	73	9	8	8	2	0	16	430	145	85,173
82	41	10	12	16	14	6	28	464	211	42,524
83	56	9	10	8	17	0	18	382	196	75,961

Appendix E. Bar sediment sample analysis.

Sample No.	Size Distribution by Mass (% of sample)							XRF Analysis (<2 mm fraction)		
	Fines (<2 mm)	VFG (2-4 mm)	FG (4-8 mm)	MG (8-16 mm)	CG (16-32 mm)	VCG (32-64 mm)	Chat (4-16mm)	Pb (ppm)	Zn (ppm)	Ca (ppm)
84	48	16	15	11	10	0	27	679	244	85,861
85	31	11	18	27	14	0	44	1,109	534	59,234
86	49	7	12	21	10	0	33	363	167	49,470
87	35	7	12	17	15	14	29	452	175	93,833
88	59	10	12	13	5	0	25	497	177	59,148
89	85	4	8	3	0	0	11	223	91	7,267
90	100	0	0	0	0	0	0	50	24	ND
91	63	9	12	9	7	0	21	313	146	43,371
92	99	1	0	0	0	0	0	388	163	58,163
93	48	11	14	18	4	5	33	295	111	20,607
94	42	8	11	12	11	15	23	401	117	52,109
95	66	13	17	4	0	0	20	292	99	32,493

Appendix F. GIS 500 m Channel Cell Analysis

Appendix F. GIS 500 m channel cell analysis

R-km (at center)	Historical Area (m2)	Historical Width (m)	Bar Area (m^2)	Active Channel Area (m^2)	Centerline Length (m)	Mean Bar Width (m)	Mean Active Channel Width (m)	Mean Wetted Width (m)	Bar Area (% of Channel)	Segment Number
99.25	30,690	61.4	2,296.29	21,894.23	509.05	4.51	43.79	39.28	10.49	6
99.75	24,475	48.9	0.00	16,437.79	497.30	0.00	32.88	32.88	0.00	6
100.25	29,538	59.1	0.00	14,990.81	494.96	0.00	29.98	29.98	0.00	6
100.75	27,603	55.2	2,914.42	20,256.96	511.94	5.69	40.51	34.82	14.39	6
101.25	32,318	64.6	1,127.58	18,275.18	514.56	2.19	36.55	34.36	6.17	6
101.75	33,793	67.6	8,457.99	22,456.39	563.24	15.02	44.91	29.90	37.66	6
102.25	29,312	58.6	0.00	16,391.74	508.54	0.00	32.78	32.78	0.00	6
102.75	42,867	85.7	14,211.89	29,398.02	539.70	26.33	58.80	32.46	48.34	6
103.25	39,253	78.5	8,462.57	24,968.32	541.85	15.62	49.94	34.32	33.89	6
103.75	48,880	97.8	5,161.86	19,760.59	514.00	10.04	39.52	29.48	26.12	6
104.25	46,725	93.4	2,512.92	17,717.78	514.59	4.88	35.44	30.55	14.18	6
104.75	33,924	67.8	1,507.29	20,020.88	529.58	2.85	40.04	37.20	7.53	6
105.25	31,896	63.8	249.67	18,630.51	503.85	0.50	37.26	36.77	1.34	6
105.75	36,435	72.9	1,318.07	17,919.84	517.72	2.55	35.84	33.29	7.36	6
106.25	41,872	83.7	7,174.72	24,956.46	520.14	13.79	49.91	36.12	28.75	6
106.75	32,280	64.6	1,292.11	21,985.86	512.96	2.52	43.97	41.45	5.88	6
107.25	21,280	42.6	374.25	18,879.31	502.15	0.75	37.76	37.01	1.98	6
107.75	24,549	49.1	2,501.55	20,621.71	510.59	4.90	41.24	36.34	12.13	6
108.25	24,251	48.5	957.81	17,206.44	514.72	1.86	34.41	32.55	5.57	6

Appendix F. GIS 500 m channel cell analysis

R-km (at center)	Historical Area (m2)	Historical Width (m)	Bar Area (m^2)	Active Channel Area (m^2)	Centerline Length (m)	Mean Bar Width (m)	Mean Active Channel Width (m)	Mean Wetted Width (m)	Bar Area (% of Channel)	Segment Number
108.75	26,107	52.2	2,266.17	21,165.93	507.88	4.46	42.33	37.87	10.71	6
109.25	29,028	58.1	0.00	20,486.90	505.43	0.00	40.97	40.97	0.00	6
109.75	31,272	62.5	11,567.73	25,777.22	514.50	22.48	51.55	29.07	44.88	6
110.25	29,647	59.3	9,691.78	27,296.02	516.46	18.77	54.59	35.83	35.51	6
110.75	27,842	55.7	1,043.61	19,904.03	511.05	2.04	39.81	37.77	5.24	6
111.25	26,367	52.7	2,104.00	18,288.59	492.67	4.27	36.58	32.31	11.50	6
111.75	37,192	74.4	3,687.50	19,672.67	521.46	7.07	39.35	32.27	18.74	6
112.25	33,792	67.6	706.77	19,127.13	511.75	1.38	38.25	36.87	3.70	6
112.75	41,922	83.8	5,621.80	20,305.37	518.95	10.83	40.61	29.78	27.69	6
113.25	27,881	55.8	0.00	19,755.21	505.03	0.00	39.51	39.51	0.00	6
113.75	34,470	68.9	0.00	21,054.99	492.65	0.00	42.11	42.11	0.00	6
114.25	37,906	75.8	0.00	23,416.82	498.22	0.00	46.83	46.83	0.00	6
114.75	30,696	61.4	0.00	21,324.44	504.46	0.00	42.65	42.65	0.00	6
115.25	24,757	49.5	2,124.08	18,943.83	522.33	4.07	37.89	33.82	11.21	6
115.75	22,840	45.7	976.89	19,834.96	514.96	1.90	39.67	37.77	4.93	7
116.25	25,568	51.1	3,004.65	24,768.32	509.92	5.89	49.54	43.64	12.13	7
116.75	25,322	50.6	2,484.01	22,040.86	520.34	4.77	44.08	39.31	11.27	7
117.25	25,197	50.4	0.00	22,028.75	501.49	0.00	44.06	44.06	0.00	7
117.75	23,104	46.2	0.00	20,518.86	502.61	0.00	41.04	41.04	0.00	7
118.25	30,701	61.4	1,024.38	20,027.46	513.27	2.00	40.05	38.06	5.11	7
118.75	43,653	87.3	2,313.18	20,107.34	511.00	4.53	40.21	35.69	11.50	7

Appendix F. GIS 500 m channel cell analysis

R-km (at center)	Historical Area (m2)	Historical Width (m)	Bar Area (m^2)	Active Channel Area (m^2)	Centerline Length (m)	Mean Bar Width (m)	Mean Active Channel Width (m)	Mean Wetted Width (m)	Bar Area (% of Channel)	Segment Number
119.25	38,666	77.3	3,105.71	22,250.84	508.65	6.11	44.50	38.40	13.96	7
119.75	39,664	79.3	1,993.23	23,535.34	518.12	3.85	47.07	43.22	8.47	7
120.25	35,643	71.3	1,004.15	20,070.03	523.71	1.92	40.14	38.22	5.00	7
120.75	34,418	68.8	13,263.43	28,077.39	508.59	26.08	56.15	30.08	47.24	7
121.25	28,633	57.3	4,471.53	22,805.84	511.51	8.74	45.61	36.87	19.61	7
121.75	27,822	55.6	1,900.91	20,175.13	515.39	3.69	40.35	36.66	9.42	7
122.25	34,091	68.2	8,180.22	26,459.18	509.37	16.06	52.92	36.86	30.92	7
122.75	29,727	59.5	1,316.95	24,257.66	509.16	2.59	48.52	45.93	5.43	7
123.25	34,840	69.7	12,306.37	28,550.00	523.22	23.52	57.10	33.58	43.10	7
123.75	30,128	60.3	1,253.11	21,509.30	536.75	2.33	43.02	40.68	5.83	7
124.25	29,343	58.7	9,294.34	23,842.72	520.73	17.85	47.69	29.84	38.98	7
124.75	27,816	55.6	759.10	17,630.70	512.90	1.48	35.26	33.78	4.31	7
125.25	30,943	61.9	5,508.14	21,744.74	515.09	10.69	43.49	32.80	25.33	7
125.75	26,744	53.5	1,129.51	23,148.22	511.44	2.21	46.30	44.09	4.88	7
126.25	27,054	54.1	1,084.66	21,811.16	508.35	2.13	43.62	41.49	4.97	7
126.75	22,404	44.8	2,343.76	20,411.17	521.88	4.49	40.82	36.33	11.48	7
127.25	25,302	50.6	4,706.42	21,912.15	487.19	9.66	43.82	34.16	21.48	7
127.75	24,077	48.2	2,983.43	19,935.62	504.72	5.91	39.87	33.96	14.97	7
128.25	24,260	48.5	2,979.41	18,776.52	507.77	5.87	37.55	31.69	15.87	7
128.75	30,688	61.4	3,853.55	20,258.96	535.14	7.20	40.52	33.32	19.02	7
129.25	31,507	63.0	0.00	17,957.55	496.55	0.00	35.92	35.92	0.00	7

Appendix F. GIS 500 m channel cell analysis

R-km (at center)	Historical Area (m2)	Historical Width (m)	Bar Area (m^2)	Active Channel Area (m^2)	Centerline Length (m)	Mean Bar Width (m)	Mean Active Channel Width (m)	Mean Wetted Width (m)	Bar Area (% of Channel)	Segment Number
129.75	35,503	71.0	880.85	17,225.16	508.22	1.73	34.45	32.72	5.11	7
130.25	39,530	79.1	3,119.94	19,232.31	510.65	6.11	38.46	32.35	16.22	7
130.75	43,079	86.2	2,269.14	19,522.09	503.90	4.50	39.04	34.54	11.62	7
131.25	33,248	66.5	1,380.26	13,786.47	488.24	2.83	27.57	24.75	10.01	7
131.75	26,335	52.7	3,148.54	14,549.78	514.38	6.12	29.10	22.98	21.64	7
132.25	34,132	68.3	5,432.64	19,650.45	550.89	9.86	39.30	29.44	27.65	7
132.75	24,548	49.1	4,528.33	16,393.41	506.73	8.94	32.79	23.85	27.62	7
133.25	31,743	63.5	10,863.55	24,800.92	554.09	19.61	49.60	30.00	43.80	8
133.75	63,042	126.1	7,910.59	22,183.68	570.94	13.86	44.37	30.51	35.66	8
134.25	44,681	89.4	21,519.45	36,589.90	542.49	39.67	73.18	33.51	58.81	8
134.75	35,171	70.3	11,081.89	23,266.60	537.16	20.63	46.53	25.90	47.63	8
135.25	20,964	41.9	872.91	17,375.13	498.43	1.75	34.75	33.00	5.02	8
135.75	24,641	49.3	0.00	17,156.14	507.42	0.00	34.31	34.31	0.00	8
136.25	28,644	57.3	2,638.23	20,195.66	559.67	4.71	40.39	35.68	13.06	8
136.75	25,410	50.8	147.12	15,429.15	501.48	0.29	30.86	30.56	0.95	8
137.25	26,212	52.4	5,112.36	21,455.93	524.28	9.75	42.91	33.16	23.83	8
137.75	19,891	39.8	0.00	16,497.88	506.30	0.00	33.00	33.00	0.00	8
138.25	35,465	70.9	4,757.43	17,805.49	517.19	9.20	35.61	26.41	26.72	8
138.75	24,629	49.3	942.38	15,796.73	520.61	1.81	31.59	29.78	5.97	8
139.25	25,127	50.3	4,375.38	18,482.04	523.19	8.36	36.96	28.60	23.67	8
139.75	26,086	52.2	794.42	15,957.23	504.29	1.58	31.91	30.34	4.98	8

Appendix F. GIS 500 m channel cell analysis

R-km (at center)	Historical Area (m2)	Historical Width (m)	Bar Area (m^2)	Active Channel Area (m^2)	Centerline Length (m)	Mean Bar Width (m)	Mean Active Channel Width (m)	Mean Wetted Width (m)	Bar Area (% of Channel)	Segment Number
140.25	25,259	50.5	2,946.80	16,754.94	519.43	5.67	33.51	27.84	17.59	8
140.75	27,174	54.3	0.00	14,199.10	506.66	0.00	28.40	28.40	0.00	8
141.25	29,618	59.2	1,932.42	19,111.78	503.71	3.84	38.22	34.39	10.11	8
141.75	23,876	47.8	0.00	13,597.92	507.94	0.00	27.20	27.20	0.00	8
142.25	32,624	65.2	11,529.57	22,978.07	532.32	21.66	45.96	24.30	50.18	8
142.75	25,468	50.9	6,779.45	20,710.46	509.30	13.31	41.42	28.11	32.73	8
143.25	25,158	50.3	6,030.81	19,350.44	540.23	11.16	38.70	27.54	31.17	8
143.75	20,340	40.7	748.88	15,192.52	512.48	1.46	30.39	28.92	4.93	8
144.25	34,864	69.7	5,511.35	18,799.44	509.43	10.82	37.60	26.78	29.32	8
144.75	22,788	45.6	3,910.47	16,639.94	516.53	7.57	33.28	25.71	23.50	9
145.25	19,563	39.1	2,292.38	16,262.52	503.81	4.55	32.53	27.97	14.10	9
145.75	18,407	36.8	1,521.64	14,618.99	505.48	3.01	29.24	26.23	10.41	9
146.25	24,915	49.8	1,148.42	15,661.68	510.81	2.25	31.32	29.08	7.33	9
146.75	27,270	54.5	2,295.70	16,785.33	523.27	4.39	33.57	29.18	13.68	9
147.25	30,781	61.6	1,105.02	13,940.96	505.09	2.19	27.88	25.69	7.93	9
147.75	27,995	56.0	3,869.28	17,839.75	534.08	7.24	35.68	28.43	21.69	9
148.25	34,413	68.8	2,184.93	14,544.29	504.23	4.33	29.09	24.76	15.02	9
148.75	38,597	77.2	3,822.95	16,169.24	521.46	7.33	32.34	25.01	23.64	9
149.25	24,392	48.8	1,540.91	14,894.13	496.30	3.10	29.79	26.68	10.35	9
149.75	40,795	81.6	1,573.00	15,802.87	534.77	2.94	31.61	28.66	9.95	9
150.25	43,205	86.4	9,303.75	22,128.10	555.01	16.76	44.26	27.49	42.04	9

Appendix F. GIS 500 m channel cell analysis

R-km (at center)	Historical Area (m2)	Historical Width (m)	Bar Area (m^2)	Active Channel Area (m^2)	Centerline Length (m)	Mean Bar Width (m)	Mean Active Channel Width (m)	Mean Wetted Width (m)	Bar Area (% of Channel)	Segment Number
150.75	26,721	53.4	1,657.76	15,069.59	522.83	3.17	30.14	26.97	11.00	9
151.25	38,610	77.2	2,906.46	16,427.05	523.11	5.56	32.85	27.30	17.69	9
151.75	28,727	57.5	3,534.17	17,996.96	529.21	6.68	35.99	29.32	19.64	9
152.25	24,682	49.4	2,957.68	14,909.79	504.71	5.86	29.82	23.96	19.84	9
152.75	28,134	56.3	6,555.96	18,273.03	541.44	12.11	36.55	24.44	35.88	9
153.25	23,331	46.7	3,764.21	20,068.13	523.72	7.19	40.14	32.95	18.76	9
153.75	23,771	47.5	794.76	12,898.16	519.78	1.53	25.80	24.27	6.16	9
154.25	22,353	44.7	396.36	14,036.18	509.20	0.78	28.07	27.29	2.82	9
154.75	28,042	56.1	3,506.03	16,074.80	526.40	6.66	32.15	25.49	21.81	9
155.25	30,906	61.8	8,510.58	20,372.17	543.83	15.65	40.74	25.09	41.78	10
155.75	24,354	48.7	2,933.61	19,019.46	504.42	5.82	38.04	32.22	15.42	10
156.25	22,777	45.6	2,303.44	15,991.76	502.33	4.59	31.98	27.40	14.40	10
156.75	31,997	64.0	6,869.56	18,578.50	519.09	13.23	37.16	23.92	36.98	10
157.25	29,879	59.8	2,717.91	16,307.19	512.36	5.30	32.61	27.31	16.67	10
157.75	31,947	63.9	4,853.77	16,914.58	510.12	9.51	33.83	24.31	28.70	10
158.25	26,202	52.4	4,677.58	17,551.70	517.99	9.03	35.10	26.07	26.65	10
158.75	31,399	62.8	1,632.58	15,404.47	528.87	3.09	30.81	27.72	10.60	10
159.25	29,821	59.6	3,184.98	19,168.22	513.07	6.21	38.34	32.13	16.62	10
159.75	38,293	76.6	15,326.00	27,996.76	541.66	28.29	55.99	27.70	54.74	10
160.25	29,380	58.8	3,196.19	14,588.42	515.74	6.20	29.18	22.98	21.91	10
160.75	20,291	40.6	2,755.73	14,042.43	512.17	5.38	28.08	22.70	19.62	10

Appendix F. GIS 500 m channel cell analysis

R-km (at center)	Historical Area (m2)	Historical Width (m)	Bar Area (m^2)	Active Channel Area (m^2)	Centerline Length (m)	Mean Bar Width (m)	Mean Active Channel Width (m)	Mean Wetted Width (m)	Bar Area (% of Channel)	Segment Number
161.25	40,739	81.5	1,603.85	17,639.25	530.92	3.02	35.28	32.26	9.09	10
161.75	44,359	88.7	12,878.64	24,542.97	507.21	25.39	49.09	23.70	52.47	10
162.25	28,378	56.8	1,024.12	18,077.46	519.66	1.97	36.15	34.18	5.67	10
162.75	31,614	63.2	928.90	16,827.56	509.63	1.82	33.66	31.83	5.52	10
163.25	35,944	71.9	7,033.30	18,973.18	513.99	13.68	37.95	24.26	37.07	10
163.75	27,569	55.1	5,727.80	19,832.71	531.71	10.77	39.67	28.89	28.88	10
164.25	27,213	54.4	4,403.19	18,146.33	589.46	7.47	36.29	28.82	24.26	10
164.75	25,453	50.9	2,279.52	16,881.53	520.81	4.38	33.76	29.39	13.50	10
165.25	31,358	62.7	7,633.73	23,625.88	534.60	14.28	47.25	32.97	32.31	10
165.75	33,107	66.2	197.68	22,897.95	499.88	0.40	45.80	45.40	0.86	10
166.25	55,877	111.8	11,980.34	31,393.50	572.73	20.92	62.79	41.87	38.16	10
166.75	49,669	99.3	4,407.37	20,119.03	545.19	8.08	40.24	32.15	21.91	10
167.25	42,317	84.6	4,640.28	18,062.27	533.31	8.70	36.12	27.42	25.69	10
167.75	32,878	65.8	2,477.02	16,532.60	503.55	4.92	33.07	28.15	14.98	10
168.25	37,181	74.4	650.69	19,456.46	575.41	1.13	38.91	37.78	3.34	10
168.75	32,304	64.6	737.21	16,741.24	512.84	1.44	33.48	32.04	4.40	10
169.25	28,743	57.5	1,434.56	17,655.76	530.62	2.70	35.31	32.61	8.13	10
169.75	37,434	74.9	1,048.55	19,177.94	513.41	2.04	38.36	36.31	5.47	10
170.25	31,956	63.9	372.04	17,440.90	507.74	0.73	34.88	34.15	2.13	10
170.75	39,572	79.1	1,118.96	22,907.76	508.01	2.20	45.82	43.61	4.88	11
171.25	38,947	77.9	696.87	25,949.32	522.88	1.33	51.90	50.57	2.69	11

Appendix F. GIS 500 m channel cell analysis

R-km (at center)	Historical Area (m2)	Historical Width (m)	Bar Area (m^2)	Active Channel Area (m^2)	Centerline Length (m)	Mean Bar Width (m)	Mean Active Channel Width (m)	Mean Wetted Width (m)	Bar Area (% of Channel)	Segment Number
171.75	25,052	50.1	2,058.97	19,473.05	509.36	4.04	38.95	34.90	10.57	11
172.25	41,480	83.0	13,534.89	27,940.60	538.22	25.15	55.88	30.73	48.44	11
172.75	95,748	191.5	8,103.52	20,538.38	517.27	15.67	41.08	25.41	39.46	11
173.25	41,477	83.0	7,105.64	23,691.70	521.10	13.64	47.38	33.75	29.99	11
173.75	37,742	75.5	537.72	20,180.26	544.94	0.99	40.36	39.37	2.66	11
174.25	29,497	59.0	2,006.44	16,827.68	501.51	4.00	33.66	29.65	11.92	11
174.75	36,982	74.0	7,202.73	22,314.68	518.10	13.90	44.63	30.73	32.28	11
175.25	26,505	53.0	0.00	18,828.45	512.69	0.00	37.66	37.66	0.00	11
175.75	47,167	94.3	714.11	18,257.40	496.44	1.44	36.51	35.08	3.91	11
176.25	38,035	76.1	0.00	20,803.14	513.28	0.00	41.61	41.61	0.00	11
176.75	40,009	80.0	160.55	15,407.25	490.53	0.33	30.81	30.49	1.04	11
177.25	49,293	98.6	13,616.50	29,719.22	605.68	22.48	59.44	36.96	45.82	11
177.75	37,388	74.8	320.53	16,618.84	495.24	0.65	33.24	32.59	1.93	11
178.25	41,740	83.5	2,766.85	21,249.52	511.34	5.41	42.50	37.09	13.02	11
178.75	45,885	91.8	5,937.32	18,490.84	529.17	11.22	36.98	25.76	32.11	11
179.25	37,887	75.8	9,846.23	25,834.36	510.12	19.30	51.67	32.37	38.11	11
179.75	29,397	58.8	78.41	18,599.20	518.70	0.15	37.20	37.05	0.42	11
180.25	34,093	68.2	10,699.80	28,767.88	545.93	19.60	57.54	37.94	37.19	11
180.75	56,650	113.3	22,909.43	37,373.68	533.27	42.96	74.75	31.79	61.30	11
181.25	40,416	80.8	7,916.92	29,428.90	521.64	15.18	58.86	43.68	26.90	11
181.75	22,407	44.8	0.00	17,080.03	503.03	0.00	34.16	34.16	0.00	11

Appendix F. GIS 500 m channel cell analysis

R-km (at center)	Historical Area (m2)	Historical Width (m)	Bar Area (m^2)	Active Channel Area (m^2)	Centerline Length (m)	Mean Bar Width (m)	Mean Active Channel Width (m)	Mean Wetted Width (m)	Bar Area (% of Channel)	Segment Number
182.25	75,745	151.5	2,186.32	16,795.45	537.24	4.07	33.59	29.52	13.02	11
182.75	95,306	190.6	2,156.85	21,156.83	569.49	3.79	42.31	38.53	10.19	11
183.25	31,931	63.9	260.80	19,044.85	515.89	0.51	38.09	37.58	1.37	11

Appendix G. GIS 500 m Valley Cell Analysis

Appendix G. GIS 500 m valley cell analysis

R-km (at center)	Valley Area (m^2)	Valley Width (m)	Sinuosity	Bar Area (m^2)	Bar Width (m)
99.4	372,845	746	1.08	0.01	0.00
100.0	354,928	710	1.78	1,110.57	2.22
101.0	297,354	595	1.57	1,803.85	3.61
101.9	170,906	342	1.85	9,585.57	19.17
102.4	175,259	351	1.03	0.00	0.00
102.9	162,267	325	1.19	16,753.61	33.51
103.5	189,452	379	1.20	11,063.43	22.13
104.1	280,628	561	1.71	2,670.43	5.34
105.1	381,767	764	1.66	1,618.72	3.24
105.9	356,961	714	1.81	4,755.73	9.51
106.5	193,586	387	1.06	3,918.64	7.84
107.1	236,503	473	1.13	1,484.77	2.97
107.6	141,177	282	1.09	2,501.55	5.00
108.2	288,842	578	1.00	803.75	1.61
108.7	172,451	345	1.08	2,420.23	4.84
109.2	218,263	437	1.02	0.00	0.00
109.7	188,897	378	1.16	11,743.64	23.49
110.3	318,971	638	1.19	10,064.59	20.13
110.8	212,171	424	1.19	494.89	0.99
111.3	285,767	572	0.95	2,104.00	4.21
111.9	284,383	569	1.28	4,394.28	8.79
112.5	201,210	402	1.16	1,923.88	3.85
113.1	265,909	532	1.10	3,697.92	7.40
113.6	263,295	527	1.04	0.00	0.00
114.1	158,747	317	1.05	0.00	0.00
114.6	134,679	269	1.01	0.00	0.00
115.1	224,628	449	1.03	1,426.21	2.85
115.7	215,140	430	1.11	1,668.04	3.34
116.1	227,385	455	0.77	1,815.02	3.63
116.5	137,195	274	0.99	3,680.36	7.36
117.0	119,203	238	1.06	0.00	0.00
117.5	134,267	269	1.04	0.00	0.00
118.1	163,037	326	1.20	1,024.38	2.05
118.7	205,097	410	1.33	2,313.18	4.63
119.3	96,797	194	1.09	4,381.43	8.76
119.8	83,241	166	1.10	717.51	1.44
120.4	149,144	298	1.27	3,836.37	7.67
121.0	158,657	317	1.07	14,129.43	28.26

Appendix G. GIS 500 m valley cell analysis

R-km (at center)	Valley Area (m^2)	Valley Width (m)	Sinuosity	Bar Area (m^2)	Bar Width (m)
121.5	166,217	332	1.13	2,040.10	4.08
122.0	151,915	304	1.23	7,105.12	14.21
122.7	196,513	393	1.30	3,257.59	6.52
123.3	161,992	324	1.12	13,328.06	26.66
123.8	136,584	273	1.00	0.00	0.00
124.3	191,529	383	1.04	9,316.73	18.63
124.8	245,047	490	1.01	736.71	1.47
125.4	236,016	472	1.29	6,637.65	13.28
126.0	174,784	350	1.27	209.22	0.42
127.0	336,807	674	2.79	7,925.62	15.85
127.9	129,605	259	1.16	3,860.88	7.72
128.5	234,824	470	1.18	5,955.50	11.91
129.0	208,776	418	1.04	0.00	0.00
129.5	210,006	420	1.01	0.00	0.00
130.0	221,112	442	1.10	2,887.07	5.77
130.6	208,908	418	1.56	3,386.36	6.77
131.4	135,659	271	1.26	2,373.31	4.75
131.9	100,726	201	1.18	6,173.74	12.35
132.4	141,710	283	1.01	3,996.29	7.99
132.9	299,003	598	1.09	11,659.11	23.32
133.5	202,017	404	1.37	5,546.57	11.09
134.1	266,651	533	1.04	20,913.59	41.83
134.7	373,302	747	1.67	15,658.83	31.32
135.4	349,462	699	1.29	413.21	0.83
136.2	342,146	684	1.93	2,785.35	5.57
137.0	289,713	579	1.55	5,029.05	10.06
137.6	213,534	427	0.87	83.32	0.17
138.2	255,622	511	1.39	4,959.67	9.92
139.1	384,279	769	2.48	5,909.94	11.82
139.9	181,812	364	1.06	2,946.80	5.89
140.5	92,773	186	1.15	0.00	0.00
141.0	159,191	318	1.05	1,932.42	3.86
141.5	192,054	384	1.05	0.00	0.00
142.0	116,461	233	1.07	9,399.89	18.80
142.6	105,438	211	1.08	8,839.18	17.68
143.2	99,267	199	1.17	6,100.77	12.20
143.6	121,838	244	1.00	748.88	1.50
144.1	149,243	298	1.09	5,522.13	11.04
144.6	346,638	693	1.04	3,899.69	7.80
145.1	158,998	318	1.04	2,376.08	4.75

Appendix G. GIS 500 m valley cell analysis

R-km (at center)	Valley Area (m^2)	Valley Width (m)	Sinuosity	Bar Area (m^2)	Bar Width (m)
145.6	165,200	330	1.05	1,863.91	3.73
146.1	171,031	342	1.14	722.45	1.44
146.7	154,588	309	1.06	2,295.70	4.59
147.4	143,256	287	1.42	1,960.90	3.92
147.9	143,344	287	1.25	4,504.33	9.01
148.5	168,143	336	1.25	4,595.45	9.19
149.2	158,227	316	1.34	1,462.40	2.92
149.8	230,133	460	1.15	10,039.64	20.08
150.3	132,462	265	1.16	1,925.65	3.85
150.9	115,207	230	1.29	2,966.69	5.93
151.5	208,976	418	1.57	4,043.16	8.09
152.2	162,440	325	1.09	5,387.39	10.77
152.8	110,462	221	1.14	4,882.72	9.77
153.3	159,964	320	1.00	3,163.86	6.33
153.8	175,961	352	1.11	638.65	1.28
154.3	166,147	332	1.11	2,139.18	4.28
155.0	340,246	680	1.72	10,273.79	20.55
155.6	185,255	371	1.04	3,306.78	6.61
156.2	196,638	393	1.07	3,344.96	6.69
156.7	170,827	342	1.05	5,622.01	11.24
157.2	120,208	240	1.16	2,550.77	5.10
157.8	158,278	317	1.20	5,219.14	10.44
158.3	141,174	282	1.07	5,944.80	11.89
158.8	168,430	337	1.07	0.00	0.00
159.4	117,833	236	1.22	17,688.68	35.38
159.9	87,926	176	1.05	3,100.78	6.20
160.5	94,420	189	1.19	1,697.06	3.39
161.0	89,386	179	1.09	2,357.51	4.72
161.5	114,236	228	0.99	12,005.46	24.01
162.0	71,949	144	1.09	3,120.03	6.24
162.5	65,448	131	1.03	928.90	1.86
163.0	64,764	130	1.04	7,033.30	14.07
163.5	91,260	183	1.12	5,119.11	10.24
164.1	140,532	281	1.29	5,062.23	10.12
164.6	99,207	198	1.03	2,563.80	5.13
165.1	86,664	173	1.11	7,299.09	14.60
165.6	119,912	240	1.03	1,008.89	2.02
166.1	109,011	218	1.15	12,926.05	25.85
166.6	91,393	183	1.14	3,172.15	6.34
167.2	126,951	254	1.36	6,376.33	12.75

Appendix G. GIS 500 m valley cell analysis

R-km (at center)	Valley Area (m^2)	Valley Width (m)	Sinuosity	Bar Area (m^2)	Bar Width (m)
167.8	183,419	367	1.01	219.27	0.44
168.3	160,554	321	1.24	806.32	1.61
168.8	100,102	200	1.04	1,523.18	3.05
169.4	93,743	187	1.07	492.97	0.99
169.9	146,214	292	1.02	1,420.58	2.84
170.4	216,889	434	1.03	1,118.96	2.24
170.9	149,755	300	1.20	696.87	1.39
171.6	190,927	382	1.26	793.73	1.59
172.1	146,546	293	1.10	14,237.74	28.48
172.6	146,913	294	1.05	8,659.07	17.32
173.2	253,385	507	1.96	7,650.21	15.30
174.1	204,619	409	1.03	1,898.63	3.80
174.6	166,662	333	1.12	7,043.25	14.09
175.2	171,173	342	1.30	267.30	0.53
175.7	275,828	552	1.08	714.11	1.43
176.3	311,742	623	1.15	0.00	0.00
176.9	407,719	815	1.56	12,741.31	25.48
177.6	402,598	805	1.24	1,356.27	2.71
178.1	293,399	587	1.09	2,766.85	5.53
178.8	348,972	698	1.34	7,059.66	14.12
179.3	312,946	626	1.10	8,802.30	17.60
179.8	340,966	682	1.05	996.96	1.99
180.3	286,544	573	1.08	22,053.67	44.11
180.8	346,469	693	1.10	18,299.74	36.60
181.4	270,746	541	1.30	175.78	0.35
182.1	247,511	495	1.31	2,119.27	4.24
182.6	354,751	710	1.18	2,223.90	4.45
183.2	401,660	803	1.53	260.80	0.52
183.9	494,478	989	1.59	15,746.37	31.49
184.5	414,002	828	0.72	0.00	0.00
185.0	328,020	656	1.54	3,937.61	7.88
185.7	388,881	778			
186.3	379,438	759			
187.8	313,688	627			
187.4	374,277	749			
188.0	411,511	823			
188.5	459,722	919			
189.4	730,323	1,461			
190.6	463,179	926			
191.4	268,244	536			

Appendix G. GIS 500 m valley cell analysis

R-km (at center)	Valley Area (m^2)	Valley Width (m)	Sinuosity	Bar Area (m^2)	Bar Width (m)
192.1	286,583	573			